Novel Mesoporous Alumina Supported Alkali and Enzymatic Catalysts for Biodiesel Production

Wei Wu

Supervisor: Professor Dongke Zhang *FTSE*

This thesis is presented for the degree of Doctor of Philosophy of Chemical Engineering of the University of Western Australia

Centre for Energy

School of Mechanical and Chemical Engineering

September 2016

Declaration

To the best of my knowledge and belief this thesis contains no material previously published by any other person except where due acknowledgement has been made.

This thesis contains no material which has been accepted for the award of any other degree or diploma in any university.

Signature 

Date: 13-01-2017

To My Beloved Family

Abstract

The use of biodiesel as a substitute for or as an alternative to conventional petroleum diesel has been of great interest. Compared to currently more widely used homogeneous alkali or acid catalysts, heterogeneous catalysts are recognised for potential advantages such as easy separation of products; recovery, regeneration and reuse of the catalyst thus leading to a cheaper, simpler and more environmentally benign operation. Therefore, developing new, highly active, reliable and durable heterogeneous catalysts seems to be an attractive alternative to overcome the existing problems associated with homogeneous catalysts.

The present research was aimed to develop mesoporous alumina (MA) supported potassium (MAK) and MA immobilised lipase as the heterogeneous catalysts for biodiesel production. Facile synthesis strategies were investigated in order to realise the control of structural properties (surface area, pore volume and pore size) of MA over a broad range. The synthesised MAs with tunable structural properties were then used as supports for potassium incorporation and lipase immobilisation. A reaction kinetic study of the MAK catalysed transesterification of canola oil with methanol was performed to provide an insight into the mechanism of the transesterification process. The optimisation of enzymatic transesterification was performed using response surface methodology (RSM) to explore the impact of reaction conditions with MA supported pseudomonas fluorescens lipase as the catalyst.

A facile route for the aqueous phase synthesis of MA with tunable structural properties was demonstrated in this study. Interaction between the boehmite particulates and the template could competently direct the loose stacking of the boehmite particulates, resulting in the variations in the structural properties of MAs. By modulating the synthesis conditions, including the amount of nitric acid addition, type of template,

amount of template addition, doping of inorganic aluminium precursors and the calcination temperature, an effective means to control the structural properties of MA over wide ranges were realised.

MAK catalysts were synthesised following the one-pot synthesis pathway via self-assembly of potassium precursor KNO_3 and aluminum isopropoxide. Higher surface area, pore volume and greater pore size of the catalyst reduced the mass transfer limitation in catalysis, thus leading to the higher biodiesel yields. A high biodiesel yield of 92.2% was achieved over the MA1P20K catalyst (synthesised with 1.0 g of P123 and 20% molar fraction of K species per 20 mmol of Al). The kinetic study showed that the MAK catalysed transesterification followed the Eley–Rideal mechanism and the activation energy ranged from 20.9 to 23.4 $kJmol^{-1}$.

A process design exercise was performed on the MAK catalyst based biodiesel plants and compared with the conventional homogeneous NaOH catalyst based biodiesel plant. MAK catalyst showed similar catalytic activity and energy efficiency as compared to conventional NaOH catalyst. Owing to its heterogeneous nature, the MAK catalyst also allowed a facile catalyst recovery, thus getting rid of an extra neutralisation process to remove the catalyst while enabling potential reuse of the catalyst. Compared to the NaOH catalyst, another advantage of the heterogeneous MAK-catalysed process was the much reduced water usage required for biodiesel washing and purification. All these advantages afford the basis for the future development and commercial applications of the MAK catalyst.

Immobilised enzymatic catalysts were prepared by the adsorption of pseudomonas fluorescens lipase on MAs. Results showed that the adsorption capability of lipase on MA and the lipase activity were highly dependent on the structural properties of MA. Due to the large contact interface and pore volume, MA4P15AlN (synthesised with 4.0

g of P123 and 15% $Al(NO_3)_3$ substitution to the total 20 mmol Al) exhibited high lipase activity and superior lipase adsorption capability, resulted in higher biodiesel yield than other MAs and a reference commercial Al_2O_3. The optimisation study using RSM with MA4P15AlN supported lipase as the catalyst achieved a highest biodiesel yield of 88.9% under the following reaction conditions: temperature 41 ℃, water addition 3.9 wt% and catalyst loading ratio 5.0 wt%.

Acknowledgements

I wish to take this opportunity to thank all of the people who contributed to the completion of my PhD thesis. Of special note, I would like to express my sincere and utmost gratitude to my supervisor, Professor Dongke Zhang *FTSE*, for providing me with a precious opportunity to join the Centre for Energy at The University of Western Australia and to carry out this PhD project with him. He has inspired and guided me with his patience, experience, knowledge and invaluable advice on both academic matter and life philosophy. His passion for science has set a wonderful role model for me to follow in the future. Without his supervision, continuous support and encouragement, I would not have reached where I am.

I would also like to gratefully acknowledge the postgraduate research scholarships provided by Centre for Energy at The University of Western Australia and also the partial living stipend scholarship provided by the China Scholarship Council.

In regards to technical support, I would like to acknowledge the Australian Microscopy and Microanalysis Research Facility at the Centre for Microscopy, Characterisation and Analysis, The University of Western Australia, for their training and technical support in the SEM, TEM and XRD analyses. I would also like to show my gratitude to Professor Paul McCormick for his advice and help in the nitrogen physisorption technique operation and data interpretation.

Sincere thanks go to my friends, past and present at the Centre for Energy, especially the co-supervisor Dr Mingming Zhu, colleagues Mr Zhijian Wan, Mr Zhezi Zhang, Dr Yang Zhang, Dr Wenxu Zhou, Dr Yu Ma, Ms Yii Leng Chan and all other colleagues for the administrative or technical assistance, discussion, friendship and encouragement in various ways. Thanks to all the friends I met in Perth for your sincere friendship and support, which have made my overseas life and study enjoyable and happy.

Last but certainly not least, my deepest love goes to my parents, brother and sister-in-law for their endless love and spiritual support all the time. Otherwise, it would have been impossible to finish this work.

Publications

Journal

● Wu, W., Wan, Z.J., Chen, W., Yang, H. and Zhang, D.K., A facile Synthesis Strategy for Structural Property Control of Mesoporous Alumina and Its Effect on Catalysis for Biodiesel Production, *Advanced Powder Technology* 25 ,1220–1226, 2014

● Wu, W., Wan, Z.J., Chen, W., Zhu, M.M. and Zhang, D.K., Synthesis of Mesoporous Alumina with Tunable Structural Properties, *Microporous and Mesoporous Materials* 217, 12–20, 2015

● Wu, W., Wan, Z.J., Chen, W., Zhu, M.M. and Zhang, D.K., A Facile Route to Aqueous Phase Synthesis of Mesoporous Alumina with Controllable Structural Properties, *Microporous and Mesoporous Materials* 223, 203–212, 2016

● Wu, W., Zhu, M.M., Wan, Z.J. and Zhang, D.K., Pseudomonas Fluorescens Lipase Immobilized on Mesoporous Alumina as Trans-esterification Catalysts for Biodiesel Production, *Renewable Energy* Submitted, 2016

● Wu, W., Zhu, M.M. and Zhang, D.K., An Experimental and Kinetic Study of Canola Oil Transesterification Catalyzed by Mesoporous Alumina Supported Potassium, *Applied Catalysis A: General* In Press, 2016

Conference

● Wu, W., Chen, W., Yang, H. and Zhang, D.K., Ordered Mesoporous Alumina Supported Potassium Carbonate as Solid Base Catalysts for Biodiesel Production, *Chemeca 2012*, Sep 28th – Oct 02nd, Brisbane, Australia.

Table of Contents

List of Figures

List of Tables

Chapter 1 Introduction

1.1 Background and Motivation

The growing energy demand and the continuously fluctuating oil price impel the exploration of sustainable, stable and economically feasible source of alternative energy. Among many possible options, biodiesel has received considerable attention due to its environmental benefits and being renewable (Yusuf *et al.* 2011; Atabani *et al.* 2012). Biodiesel is a mixture of mono-alkyl esters of long chain fatty acids made by transesterification of animal fats or vegetable oils and a short chain alcohol, methanol or ethanol, with a suitable catalyst (Lin *et al.* 2011). The catalysts can be alkaline, acidic or enzymatic, either homogeneous or heterogeneous (Chouhan *et al.* 2011; Borges *et al.* 2012). Compared to conventional homogeneous catalysts, heterogeneous catalysts are believed to possess potential advantages such as easy separation of products; recovery, regeneration and reuse of the catalyst thus leading to a cheaper, simpler and more environmentally benign operation. Therefore, developing new heterogeneous catalysts has become an alternative to overcome the existing problems associated with homogeneous catalysts (Chouhan *et al.* 2011; Borges *et al.* 2012). In addition, among the enzymatic, acidic and alkaline types of catalysts, alkali catalysed transesterification process offers a higher reaction rate than the acid catalysed process while enzymatic catalysis is increasingly favoured owing to the mild reaction conditions, being free of impact of free fatty acid (FFA) and the environmentally benign nature (Gog *et al.* 2012).

In general, heterogeneous catalysts normally contain the supported alkaline active sites or the immobilised lipase on porous materials as the supports (Lee *et al.* 2009; Endalew *et al.* 2011; Semwal *et al.* 2011). In virtue of the highly porous structure, the support is capable of providing large surface area and organised internal channels for the incorporation of either alkaline active sites or lipase.

MA has been widely used as a catalyst support owing to its accessible channels and large surface area, which can be also tuned in synthesis (C Márquez‐Alvarez *et al.* 2008). However, to date, systematic work on the control of the structural properties of MA is scarce. Systematic investigation into the effect of synthesis conditions on the structural properties of MA is needed, including acid concentration, the types and addition amounts of soft templates, aluminium precursors and calcination temperature. More importantly, there has been little literature information in the public domain with regard to the use of MA as the catalytic support for biodiesel production.

1.2 Scope, Aims and Hypothesis

The present PhD thesis research was aimed to develop MA supported potassium and MA based enzymatic catalysts for biodiesel production. Within this scope, facile synthesis strategies in order to realise the control of structural properties (surface area, pore volume and pore size) of MA were investigated. The effect of synthetic conditions on the resulting structural properties of MA, including the amount of nitric acid addition, type of template, amount of template addition, doping of inorganic aluminium precursors and the calcination temperature were explored. The synthesised MAs with tunable structural properties were then used as the supports for potassium incorporation and lipase immobilisation. The effect of the structural properties of MA on the catalytic process were studied. Reaction kinetics was also investigated to provide an insight into the mechanisms of the transesterification process.

A clear statement of hypothesis is given as follows:

1. MA can be synthesised following the sol-gel self-assembly pathway with aid of a soft template while the resulting structural properties are greatly influenced by the synthesis conditions.

2. Catalytic performance of the MAK catalyst is dependent on the structural properties of the MAK catalyst. Higher surface area, pore volume and greater pore size of the catalyst can reduce the mass transfer limitation in catalysis, thus leading to higher biodiesel yields.
3. MA is a good support to immobilise lipase while the improved structural properties can enhance lipase adsorption and lipase activity, and then consequently increase the resulting biodiesel yield.

1.3 Thesis Outline

There are a total of eight chapters in this thesis, as outlined below. The structure of the thesis is schematically shown in Figure 1-1.

- **Chapter 1** defines the scope, overall aims, hypothesis and the thesis structure;
- **Chapter 2** reviews the current knowledge status in the open literature on different catalysts for biodiesel production. This finally leads to the identification of knowledge gapes in the literature, some of which naturally became the specific objectives for the present research;
- **Chapter 3** presents the research methodology, experimental approaches as well as the analytical techniques employed to achieve the research objectives of this study;
- **Chapter 4** details the synthesis, and control of the structural properties, of mesoporous alumina, by exploring the effect of synthesis conditions;
- **Chapter 5** discusses the preparation, characterisation and testing of MA supported potassium catalysts for biodiesel production;
- **Chapter 6** reports the preparation, characterisation and testing of the MA immobilised lipase as the catalysts for biodiesel production;

- **Chapter 7** provides a critical and broad-scope evaluation of the findings from the present research and discusses the implications of these findings, along with the new gaps identified for future work;
- **Chapter 8** draws the conclusions from the present research and offers a set of recommendations for further research in the future.

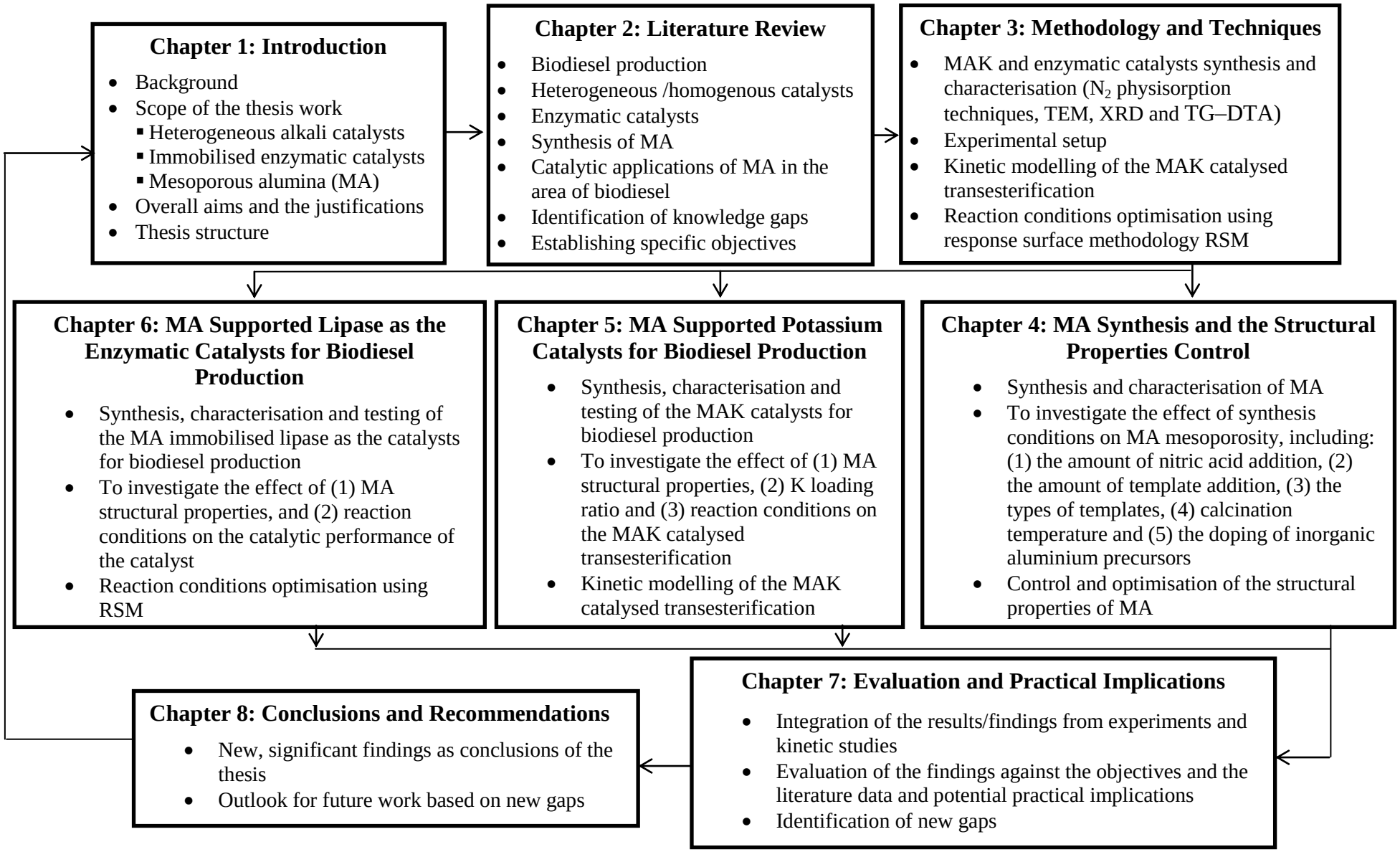

Figure 1-1 A schematic of the thesis structure

Chapter 2 Literature Review

2.1 Introduction

The purpose of this chapter is to provide a detailed account of the current state of knowledge and technology of biodiesel production and identify areas where R&D effort is needed. This chapter begins with a general overview of the fundamentals of biodiesel, followed by a discussion of the available techniques for biodiesel production. Then the current status of knowledge of involved catalysts is reviewed, which includes extensive discussions on the types and performance of different homogeneous and heterogeneous catalysts, the effect of reaction parameters on catalysis and the kinetic modelling. This review further examines the current use of lipase as the enzymatic catalyst for biodiesel production as well as the synthesis and application of mesoporous alumina as the catalyst support. This chapter finally provides conclusions based on the thorough review and defines the research gaps which assist in identifying the specific objectives of the present research.

2.2 The Fundamentals of Biodiesel

2.2.1Composition of Biodiesel

Biodiesel is chemically defined as a mixture of mono-alkyl esters (commonly methyl ethyl esters), obtained from renewable feedstocks like vegetable oils and animal fats. The composition of biodiesel depends on the fatty acids distribution of the triglycerides (TGs) in the feedstock (Lin *et al.* 2011). A variety of feedstocks can potentially be employed for biodiesel production, ranging from conventional edible oils (e.g. palm, rapeseed, canola, sunflower and soybean), animal tallows and waste cooking oil to non-edible oils (e.g. jatropha and coconut) and more recently algae and microbial oils

(Luque *et al.* 2010; Lin *et al.* 2011; Atabani *et al.* 2012). Common fatty acid components are shown in Table 2-1.

Table 2-1 Fatty acid components in common biodiesel feedstocks (Lin *et al.* 2011)

Fatty Acid	Chemical structure
C12:0 Lauric acid	$CH_3(CH_2)_{10}COOH$
C14:0 Myristic acid	$CH_3(CH_2)_{12}COOH$
C16:0 Palmitic acid	$CH_3(CH_2)_{14}COOH$
C16:1 Palmitoleic acid	$CH_3(CH_2)_5CH=CH(CH_2)_7COOH$
C18:0 Stearic acid	$CH_3(CH_2)_{16}COOH$
C18:1 Oleic acid	$CH_3(CH_2)_7CH=CH(CH_2)_7COOH$
C18:2 Linoleic acid	$CH_3(CH_2)_4CH=CHCH_2CH=CH(CH_2)_7COOH$
C18:3 Linolenic acid	$CH_3CH_2CH=CHCH_2CH=CHCH_2CH=CH(CH_2)_7COOH$
C20:0 Arachidic acid	$CH_3(CH_2)_{18}COOH$
C20:1 Eicosenoic acid	$CH_3(CH_2)_5CH=CH(CH_2)_{11}COOH$
C22:0 Behenic acid	$CH_3(CH_2)_{20}COOH$
C22:1 Erucic acid	$CH_3(CH_2)_7CH=CH(CH_2)_{11}COOH$

2.2.2Properties of Biodiesel

Biodiesel is usually characterised by its physicochemical properties, including viscosity, density, boiling point, flash point, cetane number, cloud and pour points, distillation range, acid value and oxidation stability (Demirbas 2009; Atabani *et al.* 2012). The properties are summarised in Table 2-2. It must be noted that the physical and chemical fuel properties of biodiesel are closely related to the fatty acid composition of feedstock (Atabani *et al.* 2012).

Several international biodiesel standard specifications have been established to govern the quality of biodiesel on the market. The most commonly used specifications are the American Standards for Testing Materials (ASTM 6751-3) and the European Union Standards (EN 14214). These specifications are based on a variety of factors varying from region to region, such as the accessibility of feedstock, the existing diesel fuel standards, the predominance of diesel engine type as well as the emission regulations (Sarin 2012).

Table 2-2 Physical properties of biodiesel (Yusuf *et al.* 2011)

Properties	Biodiesel
Formula range	C_{14}-C_{24} methyl esters or $C_{15\text{-}25}H_{28\text{-}48}O_2$
Kinematic viscosity range (mm^2s^{-1}, at 40 ℃)	3.3-5.2
Density range (kgm^{-3}, at 15 ℃)	860-894
Boiling-point range (℃)	>184
Flash-point range (℃)	147-177
Distillation range (℃)	197-327
Vapor pressure (mm Hg, at 22 ℃)	<5
Solubility in water	Insoluble in water
Physical appearance	Light to dark yellow, clear liquid
Odour	Light musty/soapy odor
Biodegradability	More biodegradable than petroleum diesel
Reactivity	Stable, but avoid strong oxidising agents

2.3 Biodiesel Production

2.3.1Biodiesel Production Technologies

To date, there have been many efforts to develop vegetable oil derivatives that approximate the properties and performance of conventional diesel fuels. The pathways include dilution or microemulsion, pyrolysis, supercritical methanol and transesterification. The advantages and disadvantages of the four pathways are given in Table 2-3.

Table 2-3 A comparison of main technologies for biodiesel production (Lin *et al.* 2011; Atabani *et al.* 2012)

Technologies	Advantages	Disadvantages
Dilution or microemulsion	• Simple process	• High viscosity • Low volatility • Low stability
Pyrolysis	• Simple process • No-polluting	• High temperature • Expensive equipment • Low purity
Transesterification	• Fuel properties close to diesel • High Efficiency • Low cost • Suitable for industrialised production	• Low FFA and water content are required (for alkaline catalysts) • Pollutants will be produced because the products must be neutralised and washed • Accompanied by side reactions • Difficult products separation
Supercritical methanol	• No catalyst • Short reaction Time • High Efficiency • Good adaptability	• High temperature and pressure • High equipment cost • High energy consumption

The physical methods like dilution and microemulsion do not require any chemical process and can reduce the viscosity of vegetable oils. However, they cannot solve the problems such as carbon deposits and lube pollution, which make the direct use of vegetable oils in diesel engines difficult (Lin *et al.* 2011; Atabani *et al.* 2012).

For pyrolysis, though a product that has high cetane number, low viscosity, acceptable amounts of sulfur, water and sediments contents can be produced, the ash content, carbon residue, and pour point are unacceptable (Atabani *et al.* 2012). While for the use of supercritical methanol, high temperature and pressure conditions indicate high equipment cost and intense energy input, which will increase the overall production cost. Amongst the four techniques, transesterification is deemed as the most promising solution. Due to its high conversion efficiency and relatively low cost, transesterification has been widely used for industrialised biodiesel production (Atabani *et al.* 2012).

2.3.2 Transesterification

2.3.2.1 Mechanisms

Transesterification is a chemical reaction between triglycerides and short-chain alcohols to produce mono-esters. The long- and branched-chain triglycerides are converted into mono-esters and glycerol. A typical transesterification process consists of three consecutive reversible reactions: triglyceride to be converted to diglyceride and then to monoglyceride and finally fatty esters and a glycerol (Demirbas 2009; Atabani *et al.* 2012). Figure 2-1 shows the reaction steps of transesterification of triglycerides and methanol.

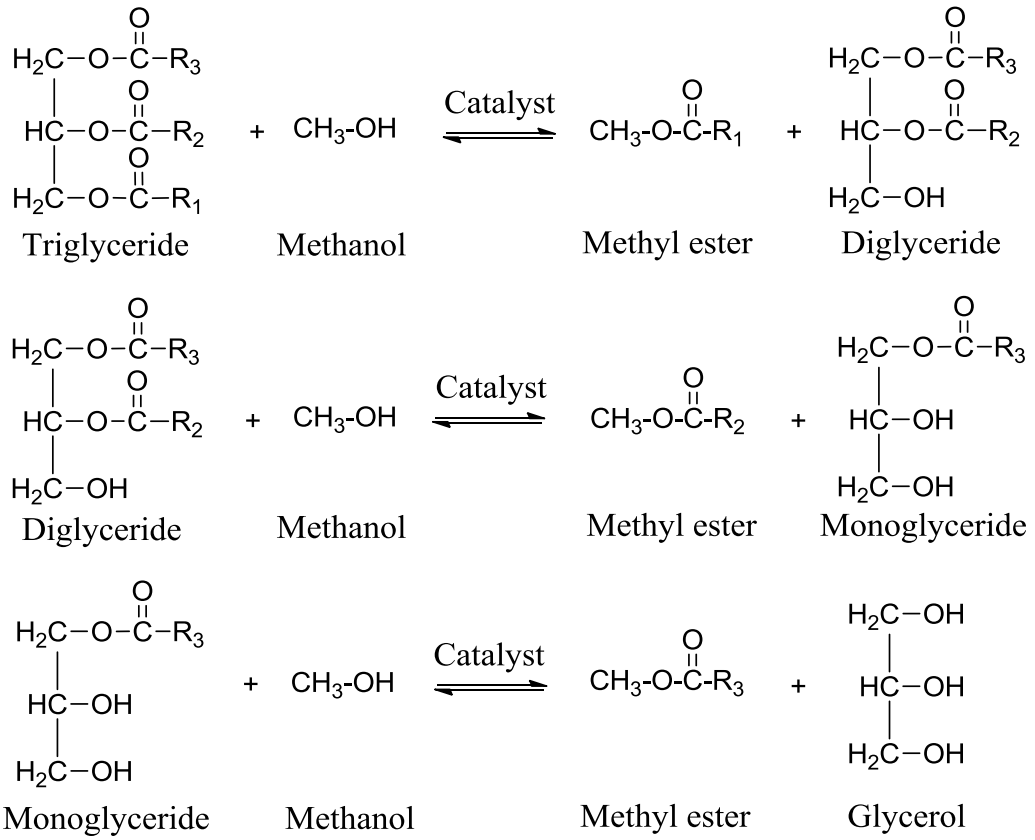

Figure 2-1 Reaction steps of transesterification (Atabani *et al.* 2012)

2.3.2.2 Effect of Reaction Parameters

The reaction parameters affecting the transesterification process are the molar ratio of alcohol to oil (M/O), temperature, water content and FFA. In order to maximise biodiesel yield, these parameters must be optimised.

2.3.2.2.1 Molar Ratio of Alcohol to Oil

Molar ratio of alcohol to oil is an important variable affecting the yield of methyl ester (Demirbas 2009; Balat *et al.* 2010). Though the stoichiometric molar ratio of alcohol to triglyceride is 3:1, biodiesel output can be facilitated by the higher density of alcohol in a shorter time. Therefore, the ratios of 6:1 and 9:1 are usually applied (Demirbas 2009). However, for enzymatic catalysts, the addition of short-chain alcohols like methanol shows a strong denaturing effect on lipase, leading to unfavourable catalyst deactivation and thus a decrease in biodiesel yield (Gog *et al.* 2012). This problem is the main

deterrent for practical industrial production of biodiesel using enzyme as the catalyst. Aiming to overcome this problem, stepwise addition of methanol (methanol is fed into the reactor in three steps of 1:1 mole ratio each) is the most common strategy and has been proved to be effective, though the cost in processing and extra complexity have been added as well (Helwani *et al.* 2009).

2.3.2.2.2 Temperature

For alkali catalysts, transesterification reaction is generally conducted close to the boiling point of methanol, between 60 ℃ and 80 ℃ at atmospheric pressure. While the enzymatic transesterification process is usually performed at a lower temperature, ranges from 30 ℃ to 55 ℃ to prevent the loss of lipase activity (Gog *et al.* 2012). In fact, for the enzymatic transesterification process, the reaction rate initially increases as the temperature increases, but decreases sharply at the onset of denaturation of the enzyme (Gog *et al.* 2012). Therefore, based on this trend, there must be a particular optimum temperature for each lipase, giving a peak value to the biodiesel yield (Gog *et al.* 2012).

2.3.2.2.3 Water Content and FFA

Water content and FFA are the key factors in determining the viability of the vegetable oil derived biodiesel, especially in the alkali-catalysed transesterification processes. The induced saponification and soap by FFA and water not only consume catalyst, but also cause emulsion, which adds extra difficulties in downstream process, such as biodiesel separation, purification and recovery (Demirbas 2009; Balat *et al.* 2010; Sarin 2012). In addition, the lipase-catalysed biodiesel production is also heavily affected by water content. Some essential water is indispensable to activate lipase by unmasking and restructuring the active sites at the oil-water interface (Noureddini *et al.* 2005; Al-Zuhair 2007; Tan *et al.* 2010; Gog *et al.* 2012). The availability of interface assists to maintain lipase activity and the transesterification efficiency depends on the size of

interfacial area which can be aptly increased by the addition of certain amount of water (Al-Zuhair 2007). However, because of the hydrolases nature of lipase, excess water will stimulate the unintended side hydrolysis reactions, thus causing the decrease of biodiesel yield. Therefore, the optimum water content is actually a compromise between maximising lipase activity by increasing the oil-water interface and also the minimisation of hydrolysis reactions. The fixed amount of water for a certain reaction relies on the feedstock, the given lipase type, the immobilised support and the employed co-solvent and needs to be particularly assessed (Tan *et al.* 2010; Gog *et al.* 2012).

2.3.2.3 Kinetic Modelling

There are a number of kinetic studies reported in the literature on the transesterification of oil with alcohol for biodiesel production (H Noureddini 1997; Elena Bikou 1999; D. Darnoko 2000; SK Karmee 2004; Gemma Vicente 2005; Dossin et al. 2006; Dossin et al. 2006; Singh et al. 2007; Xuejun Liu 2008; Pugnet et al. 2010; Vujicic et al. 2010; X Liu 2010; Xiao et al. 2010; Zhang et al. 2010; Chantrasa et al. 2011). However, there is very little information concerning the kinetics of heterogeneous alkali-catalysed transesterification (Dossin et al. 2006; Dossin et al. 2006; Xiao et al. 2010).

The kinetics of heterogeneous methanolysis is influenced by different combinations of chemical and physical processes and states (Karel Komers 2002). Therefore, the studies on the kinetics of heterogeneous alkali-catalysed transesterification need include: the evaluation and suppression of mass diffusion limitations, the determination of reaction rate constants and activation energy (H Noureddini 1997), and the influence of reaction conditions, such as the molar ratio of methanol to oil, catalyst loading and reaction temperature (Gemma Vicente 2005).

2.4 Catalysts for Transesterification

The transesterification reaction requires a catalyst to split the oil molecules and an alcohol to combine with the separated esters (Lin *et al.* 2011). There are three types of catalysts involved in transesterification, i.e. alkali catalyst, acid catalyst, and enzyme catalyst. Each catalyst has its own advantages and disadvantages, detailed comparisons are illustrated in Table 2-4.

Table 2-4 A comparison of acid, alkali and enzyme catalysts

Types	Advantages	Disadvantages
Acid	• Can handle the esterification of FFA and the transesterification of TGs simultaneously	• Requires higher molar ratio of alcohol to oil, higher temperature and longer reaction time
Alkali	• Highest transesterification efficiency	• Sensitive to FFA and water content (the probability of soap formation which consumes catalyst thus reducing the methyl eater yield) • Consumes water for impurities removal
Enzyme	• Favourable reaction rate obtained in moderate conditions and relatively simple downstream processing steps for the purification of biodiesel and by-product	• High cost of lipase; • Lipase inactivation caused by methanol

As stated, the alkali catalysed process has higher efficiency than the acid catalysed process (Lin *et al.* 2011). However, the alkali catalyst is very sensitive to the presence of water and FFA. On the contrary, the acid catalysed process is totally unaffected by FFA and water as it can handle transesterification of triglyceride and esterification of

FFA simultaneously by converting FFA to methyl esters. Despite the merits, the lower reaction rate, higher methanol to oil molar ratio and temperature required for the acid catalysed transesterification seem to be the main deterrents in its further commercialisation. The way of enzymatic catalysts is another case and is increasingly perceived as an important component of solutions to the screening of novel catalysts for biodiesel production due to their mild reaction conditions, unaffected by FFA and simple downstream processing steps for the purification of biodiesel. However, through a more practical lens, the drawbacks such as high cost of lipase, low reaction rate and methanol caused lipase inactivation, result in unsatisfactory economic efficiency and undesirable operability for enzyme catalysts (Al-Zuhair 2007; Zabeti *et al.* 2009; Lam *et al.* 2010).

Moreover, the three types of catalysts can also be classified into either homogeneous or heterogeneous. Enzyme can fall into homogeneous or heterogeneous categories depending on the immobilisation on a solid support or not. A comparison between homogeneous and heterogeneous catalysts is summarised in Table 2-5 (Lin *et al.* 2011).

Table 2-5 A comparison of homogeneously and heterogeneously catalysed transesterification (Lin *et al.* 2011)

Factors	Homogeneous catalysis	Heterogeneous catalysis
Reaction rate	• Fast and high conversion	• Moderate conversion
Post-treatment	•Needs neutralisation, leading to waste chemical production	• Relatively easy separation and purification of products
Catalyst reuse	• Catalyst cannot be recovered and reused	• Catalyst can be recovered and regenerated

2.4.1 Homogenous Catalysts

At present, due to simple usage and relatively high conversion rate, the biodiesel industry is dominated by homogeneous acid and alkaline catalysts. Sulphuric acid and hydrochloric acid are usually used as acid catalysts especially for the oils with high concentrations of FFA and water, while sodium hydroxide and potassium hydroxide are typical examples of homogeneous alkali catalysts (Sharma *et al.* 2011).

2.4.2 Heterogeneous Catalysts

There is an increasing interest in the possibility of replacing the homogeneous catalysts by heterogeneous solid catalysts. Normally, the heterogeneous catalysts consist of a porous support and basic/acidic active sites. Up to now, several types of solid catalysts have been used for biodiesel production, including metal oxides and derivatives, ion exchange resins type acid catalysts, hydrotalcites, silica based catalysts, zeolite based catalysts as well as enzymatic catalysts (Zabeti *et al.* 2009; Lam *et al.* 2010; Chouhan *et al.* 2011; Semwal *et al.* 2011; Sharma *et al.* 2011). Effective factors on the catalytic activity of heterogeneous catalyst are the structural properties of the support (i.e. surface area, pore volume and pore size) and the concentration of active site. The support provides high surface area by virtue of the existence of internal pores where metal particles and enzymes can be anchored. However, until now, investigations of the impact of structural properties of the support on the catalytic performance of catalyst are scarce.

2.4.2.1 Alumina Based Catalysts

Alumina, especially mesoporous alumina has gained great popularity from a heterogeneous catalysis perspective for its wide applications as catalysts and/or catalyst supports utilised in petroleum refining, automobile exhaust emissions control, steam reforming of hydrocarbons, and numerous other chemical processes (Čejka 2003; C

Márquez - Alvarez *et al.* 2008). This is attributed to its mesoporosity features such as uniform channels and large surface area as well as high thermal and mechanical stability (C Márquez - Alvarez *et al.* 2008). However, the catalytic application of alumina in biodiesel synthesis has been largely limited to the use of conventional alumina. As shown in Table 2-6, the heterogeneous catalysts are generally synthesised by introducing sodium (Kim *et al.* 2004; Arzamendi *et al.* 2007), potassium (Xie *et al.* 2006; Xie *et al.* 2006; Alonso *et al.* 2007; Bo *et al.* 2007; Teng *et al.* 2009; Vyas *et al.* 2009) and calcium (Benjapornkulaphong *et al.* 2009; Zabeti *et al.* 2010) species to a commercial alumina by means of direct impregnation (Xie *et al.* 2006; Xie *et al.* 2006; Alonso *et al.* 2007; Arzamendi *et al.* 2007; Bo *et al.* 2007; Benjapornkulaphong *et al.* 2009; Teng *et al.* 2009; Vyas *et al.* 2009; Zabeti *et al.* 2010) or through a sol-gel pathway (Lukic *et al.* 2009; Umdu *et al.* 2009). There has been no investigation of the use of mesoporous alumina as the catalyst support.

2.4.2.2 Other Catalysts

2.4.2.2.1 Other Metal Oxides Based Catalysts

Many kinds of metal oxides include single alkali earth metal oxides (MgO, CaO, SrO and BaO), transition metal oxides (ZnO, TiO_2 and ZrO_2) and mixed metal oxides have been studied for transesterification. Metal oxides contain positive metal ions (cations) with Lewis acid and negative oxygen ions (anions) with Bronsted base, provide adsorptive sites for methanol in transesterification. Then the formedmethoxide groups will attack the carbonyl carbon atom of the triglyceride molecule to produce the corresponding fatty acid methyl esters (FAME) (Zabeti *et al.* 2009). The single alkali earth metal oxides such as MgO, CaO, SrO and BaO are usually directly used as the catalysts while the transition metal oxides like ZnO, TiO_2 and ZrO_2 as well as the mixed metal oxides are normally employed as the catalyst supports.

Table 2-6 A comparison of Al_2O_3 based heterogeneous catalysts

Catalyst	Preparation Method	Feedstock	Reaction Parameters	Yield	Reference
CaO/Al_2O_3	Impregnation	Palm oil	T = 65 ℃, t = 5 h, Methanol/oil = 12:1, Catalyst 6 wt.%	98.6%	(Zabeti *et al.* 2010)
CaO/Al_2O_3	Sol-gel method	Lipid of yellow green microalgae	T = 50 ℃, t = 4 h, Methanol/oil = 30:1, Catalyst 2 wt.%	97.5%	(Umdu *et al.* 2009)
$K_2CO_3+SiO_2/Al_2O_3$	Sol-gel method	Sunflower oil	T =120 ℃, t < 100 min, Methanol/oil = 15:1, Catalyst 2 wt.%	93.0%	(Lukic *et al.* 2009)
$Na+NaOH/\gamma\text{-}Al_2O_3$	-	Soybean oil	T = 60 ℃, t =2 h, Methanol/oil = 9:1, Catalyst 1 wt.%	83.0%	(Kim *et al.* 2004)
$NaOH/Al_2O_3$	Impregnation	Refined sunflower oil	T =50 ℃, Methanol/oil = 12:1	88.0%	(Arzamendi *et al.* 2007)
KNO_3/Al_2O_3	Impregnation	Jatropha oil	T = 70 ℃, t =6 h, Methanol/oil = 12:1,	84.0%	(Vyas *et al.* 2009)

			Catalyst 6 wt.%		
KNO_3/Al_2O_3	Impregnation	Soybean oil	*T* =65 ℃, *t* = 7 h, Methanol/oil = 15:1, Catalyst 6.5 wt.%	87.0%	(Xie *et al.* 2006)
KI/Al_2O_3	Impregnation	Vegetable oils	*T* =65 ℃, *t* = 8 h, Methanol/oil = 15:1, Catalyst 2.5 wt.%	96.0%	(Xie *et al.* 2006)
KF/Al_2O_3	Impregnation	Palm oil	*T* = 65 ℃, *t* = 3 h, Methanol/oil = 12:1, Catalyst 4 wt.%	90.0%	(Bo *et al.* 2007)
KF/Al_2O_3	Impregnation	Soybean oil	*T* = 65 ℃, *t* = 3 h, Methanol/oil = 12:1, Catalyst 2 wt.%	99.0%	(Teng *et al.* 2009)
$Ca(NO_3)_2/Al_2O_3$	Impregnation	Palm kernel oil	*T* = 60 ℃, *t* = 3 h, Methanol/oil = 65:1, Catalyst 10 wt.%	> 90.0%	(Benjapornkulaphong *et al.* 2009)
$Ca(NO_3)_2/Al_2O_3$	Impregnation	Coconut oil	*T* = 60 ℃, *t* = 3 h, Methanol/oil = 65:1, Catalyst 15-20 wt.%	> 90.0%	(Benjapornkulaphong *et al.* 2009)

2.4.2.2.2 Zeolites Based Catalysts

Zeolite is a kind of microporous aluminosilicate crystalline solid which contains silicon, aluminium and oxygen in its framework with characteristics of acidic sites and shape selectivity (Lam *et al.* 2010). Zeolites can be synthesised with extensive variations of acidity, morphology, crystal and structural properties by manipulating the use of template and the silica-aluminium ratio (Helwani *et al.* 2009; Lam *et al.* 2010; Chouhan *et al.* 2011; Endalew *et al.* 2011; Sharma *et al.* 2011).

Until now, a variety of zeolites have undergone wide applications as catalysts for the biodiesel production via esterification and transesterification reactions (Endalew *et al.* 2011; Sharma *et al.* 2011). However, researchers have pointed out the poor catalytic activity in practice (Sasidharan *et al.* 2004; Kiss *et al.* 2006; Peters *et al.* 2006; Brito *et al.* 2007). As a result of its limited pore size, only the molecules with appropriate dimension are allowed to enter the zeolite cavity and diffuse through its pores, which results in unfavourable diffusion limitation of the bulky triglycerides molecules (Kiss *et al.* 2006; Lam *et al.* 2010).

2.4.2.2.3 Silica Materials Based Catalysts

In recent decades, the most frequently investigated silica based materials for biodiesel production are the ordered silica molecular sieves MCM-41 and SBA-15 (Lee *et al.* 2009; Mart ń *et al.* 2010). These mesoporous materials possess high surface areas with uniform mesopores (2 to 50 nm), providing more facile mass diffusion for triglycerides molecules (Mart ń *et al.* 2010). In addition, by incorporating suitable organic or inorganic functional groups into the mesoporous silica matrix, the chemical properties of these mesoporous materials can be manipulated, suggesting potential activity in transesterification (Lam *et al.* 2010).

Up to now, the efforts using silica molecular sieves MCM-41 and SBA-15 in biodiesel production have been largely focused on the acquisition of solid acid catalysts by incorporating organosulfonic groups onto the surface of the molecular sieves. The anchored organosulfonic acid on mesoporous silicas acts as Brønsted acid active site to catalyse esterification and transesterification reactions (Lam *et al.* 2010). Mesostructured silica materials functionalised with sulfonic acid groups have been reported to have good catalytic activity in esterification and transesterification of the refined and unrefined oils (Miao *et al.* 2009; Melero *et al.* 2010).

2.4.2.2.4 Hydrotalcite/Layered Double Hydroxide Derived Catalysts

Hydrotalcite (HT) or Layered Double Hydroxide (LDH) is a class of anionic and basic clay material with a general formula of $M^{z+}{}_{1-x}Mx^{3+}(OH_2)^{x+}(A_{x/n})^{n-}\ yH_2O$, where M^{z+} is a monovalent (alkali metal) or divalent (alkali earth metal) ion and $M_x{}^{3+}$ is a trivalent metal ion (usually Al^{3+}), A^{n-} (usually $CO_3{}^{2-}$, $SO_4{}^{2-}$, Cl^-, $NO_3{}^-$) is a *n*-valent interlayer anion, neutralising the compound electrically (Sharma *et al.* 2011; Borges *et al.* 2012). Owing to the strong surface basicity, HTs and their derivatives have got tremendous attention, as a commendable example alkaline catalysis, including transesterification (Lee *et al.* 2009; Sharma *et al.* 2011).

The main advantages of HT catalysts are their high basicity nature and the tolerance to FFA and water while the low specific surface area is the main drawback (Lee et al. 2009; Sharma et al. 2011). Moreover, HTs have ever been used as the supports for lipase immobilisation. The immobilisation on a Mg-Al hydrotalcite modifies the microenvironment of lipase and also minimises the adverse effect of external factors such as pH, temperature and ionic species, thus leading to a more stable state than free lipase (Sharma *et al.* 2011).

2.4.3 Enzymatic Catalysts

2.4.3.1 Sources of Lipases

Lipase (EC 3.1.1.3) is a kind of carboxylesterase and catalyses the hydrolysis or synthesis of long-chain acylglycerols. Up to now, lipase constitutes the most important group of biocatalysts for biotechnological applications, such as the synthesis of biopolymers and biodiesel, the production of enantiopure pharmaceuticals, agrochemicals, and flavour compounds (Jaeger *et al.* 2002). It can be obtained from organisms in nature such as bacteria and fungi, oil crops and from the livers and pancreases of animal bodies. However, most lipases used as biocatalysts in organic synthesis are of microbial cells origin, obtained by fermentation processes and a few basic purification steps without protein denaturation (Al-Zuhair 2007; Taher *et al.* 2011).

2.4.3.2 Structure

The transesterification reaction catalysed by lipase involves a two-step mechanism. The initial hydrolysis of ester bond followed by the esterification with alcohol, which is usually described as a Ping-Pong Bi-Bi mechanism, the most commonly used nomenclature to describe the lipase catalysed reactions (Fjerbaek *et al.* 2009; Gog *et al.* 2012).

Moreover, there is an interesting structure in the spatial configuration of lipase called ‘lid’, controlling the access to its active sites (Foresti *et al.* 2005; Liu *et al.* 2011; Yan *et al.* 2011). The catalytic activity of lipase is very low in monomeric lipid substrate but can be strongly enhanced once a configuration change (‘‘lid open’’ conformation) of the enzyme occurs at the oil-water interface. The opening can be triggered by an oil-water interface in two-phase systems. So, persistent and stable activity of lipase is possible to achieve if the lid can be kept open (Al-Zuhair 2007). This interfacial activation effect has been employed as effective way in obtaining high performance lipase catalysts by

the addition of non-polar organic solvents, surfactants and divalent cations with water to create oil-water interfaces.

2.4.3.3 Lipase Catalysed Transesterification

To date, studies reporting the direct employment of lipase for the transesterification of TGs have principally focused on the screening of suitable lipases (Kaieda *et al.* 2001; Shah *et al.* 2004) and on exploring the impact of factors on the reaction rate (Zhao *et al.* 2007; Chen *et al.* 2008). The use of free lipase is difficult to separate and handle, which brings extra expenditure to the already cost-intensive lipase heavily (Gog *et al.* 2012).

Table 2-7 A comparison of different lipase immobilisation methods (Tan *et al.* 2010)

Methods	Advantages	Disadvantages
Adsorption	• Moderate preparation conditions with low cost • The support can be regenerated for repeated use	• Weak interaction between lipase and support, making it sensitive to pH, ionic strength and temperature • The adsorption capacity is low and the lipase is easier to be stripped off from the support
Covalent bonding	• High stability because of the strong force between lipase and support	• Rigorous preparation conditions • Some activity loss of the lipase during the immobilisation process
Cross-linking	• The interaction between lipase and support is strong and the immobilised lipase is stable	• Low mechanical strength of the immobilised lipase
Entrapment	• Mild preparation conditions •Applicable to a wide range of supports and lipases	• The immobilised lipase has the mass transfer restriction during reaction

The introduction of immobilisation has given lipase an enhanced level of reusability, operational stability and temperature optimum, leading to higher reaction rate and consequently reduced overall production cost (Gog *et al.* 2012). In the case of

immobilisation, free movement of lipase is restricted to an inert support, making the immobilised lipase a kind of heterogeneous catalyst in nature and opening a new window of opportunity for wider implications (Gog *et al.* 2012).

Until present, several approaches for enzyme immobilisation like adsorption, covalent bonding, entrapment, cross-linkage and micro-encapsulation have been reported (Tan *et al.* 2010; Semwal *et al.* 2011; Taher *et al.* 2011; Gog *et al.* 2012). A comparison of these immobilisation methods is summarised in Table 2-7. These immobilisation methods can be classified into chemical and physical methods and the corresponding catalytic activity in transesterification differs greatly depending on the immobilisation method and the used support. Relevant employments of the immobilised lipase in biodiesel production are summarised in Table 2-8.

2.4.3.4 Lipase Immobilisation Pathways

2.4.3.4.1 Adsorption

Among the immobilisation methods, physical adsorption has been selected by most researchers owing to the absence of expensive and toxic chemicals, the ability to retain the activity, and the feasibility of regeneration (Tan *et al.* 2010; Taher *et al.* 2011). As shown in Figure 2-2, the physical adsorption of lipase is realised by the attachment of lipase on the surface of a support by weak forces, including van der Walls, hydrophobic interactions or dispersion forces under mild conditions. However, the weak adhesion forces between lipase and support are not able to prevent the lipase from stripping off from the support, making the immobilised lipases not stable enough to battle desorption during catalytic process (Tan *et al.* 2010; Zheng *et al.* 2012; Yang *et al.* 2013).

Table 2-8 A comparison of biodiesel production using various immobilised lipases

Immobilisation method	Lipase origin	Support	Feedstock	Reaction Parameters	Yield	Reference
Adsorption	Lipozyme-TL IM	Hydrotalcite	Waste vegetable cooking oil	T = 24 ℃, t = 105 h	92.8%	(Yagiz *et al.* 2007)
Adsorption	Saccharomyces cerevisiae lipase	Hydrotalcite	Refined rape oil	T = 45 ℃, t = 4.5 h, Catalyst 1.5 wt.%	95.0%	(Zeng *et al.* 2009)
Adsorption	Pseudomonas fluorescens lipase	Organosilicate	Sunflower oil	T = 30 ℃,t = 8 h, Ethanol/oil = 8:1	91.0%	(Salis *et al.* 2009)
Covalent bonding	Candida rugosa lipase	SBA-15-NH_2	Lauric acid	T = 37 ℃, t = 24 h	95.0%	(Abdullah *et al.* 2009)
Covalent bonding	Porcine pancreatic lipase	Ordered mesoporous silica	Caprylic acid	T = 50 ℃, t = 24 h, pH = 8.0	67.5%	(Wang *et al.* 2012)

Covalent bonding	Pseudomonas fluorescens lipase	SBA-15-NH_2	Sunflower oil	*T* = 30 ℃, *t* = 10 h, Ethanol/oil = 8:1, Catalyst 4 wt.%	100%	(Salis *et al.* 2010)
Covalent bonding	Pseudomonas cepacia lipase	Fe_3O_4 nanoparticle	Sunflower oil	*T* = 40 ℃, ratio of the volume of soybean oil: water: methanol: n-hexane is 6:3:1:0.2, *t* = 192 h	88.0%	(Wang *et al.* 2011)
Covalent bonding	Pseudomonas cepacia lipase	Fe_3O_4 nanoparticle	Sunflower oil	*T* = 40 ℃, Methanol/oil = 6:1	100%	(Wang *et al.* 2009)
Covalent bonding	Candida rugosa lipase	SBA-15-NH_2	Oleic acid	*T* = 100 ℃, *t* = 24 h, Methanol/oil = 3:1, Catalyst 16.25 wt.%	98.0%	(Liu *et al.* 2011)
Entrapment	Pseudomonas cepacia lipase	Hydrophobic sol–gel support	Sunflower oil	*T* = 35 ℃, *t* = 1 h, Methanol/oil = 7.5:1,	67.0%	(Noureddini *et al.* 2005)
Cross-linking	Candida rugosa lipase	Cellulose and PTFE membranes	Oleic acid	*T* = 25 ℃, *t* = 3.5 h	Over 35.0%	(Hilal *et al.* 2004)

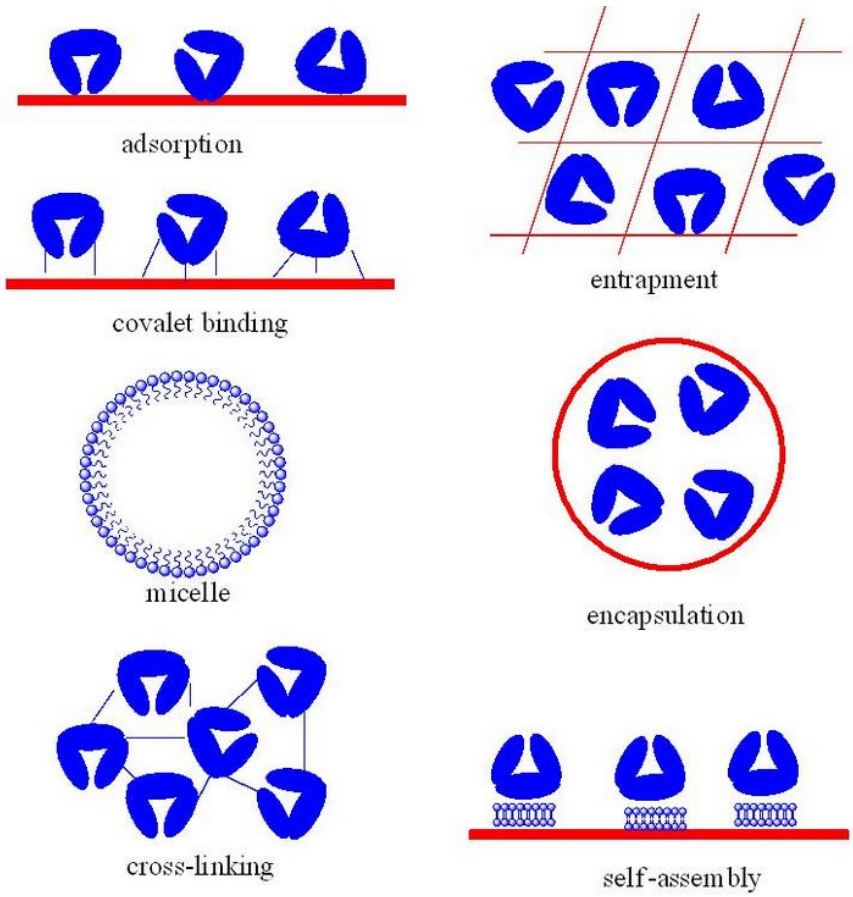

Figure 2-2 A comparison of different lipase immobilisation methods (Tan *et al.* 2010)

2.4.3.4.2 Covalent Bonding

As an alternative, chemisorption aims to covalently bind lipase to a solid support. This irreversible binding normally gives the biocatalyst high stability and performance (Tan *et al.* 2010). After covalent bonding, the resultant strong interaction between lipase and support makes enzyme leaching uncommon during catalysis. Such chemical immobilisation depends on the occurrence of suitable groups such as carboxyl (Yang *et al.* 2013), amino (Wang *et al.* 2009; Salis *et al.* 2010; Wang *et al.* 2011) and aldehyde (Bai *et al.* 2006) groups introduced to the surface of a support. These groups can covalently bind to amino acid residues on lipase external surface. In this chemisorption process, due to high strength of the covalent bond, partial deactivation, structure distortions and unfavourable enzyme orientations of a fraction of lipase have been reported (Salis *et al.* 2010).

2.4.3.4.3 Entrapment, Encapsulation and Cross-linking

In addition to physical adsorption and covalent bonding, there are several other techniques for lipase immobilisation such as entrapment, encapsulation and cross-linking. Entrapment of an enzyme indicates the capture of enzyme within an existing inorganic/organic hybrid polymer matrix (Tomin *et al.* 2011). While the sol–gel encapsulation process is usually carried out with an initial acid- or alkali-catalysed hydrolysis followed by the polycondensation of silicon alkoxide precursors to form a matrix in which the enzyme is trapped. Lipase is ultimately immobilised in the resultant hydrogel (Kawakami *et al.* 2009; Tomin *et al.* 2011). Sol–gel encapsulation has proved to be a particularly simple and effective pathway to immobilise lipase and at the same time maintains high thermostability, long-term operational stability and storage life (Noureddini *et al.* 2005; Tomin *et al.* 2011).

Besides, a new area of promising immobilisation method is the cross-linked enzyme aggregates (CLEAs) (López-Serrano *et al.* 2002; Fjerbaek *et al.* 2009). Immobilisation of Candida rugosa lipase as CLEAs in cellulose and PTFE membranes for the esterification of oleic acid and n-butanol has been tested with promising result (over 35% conversion of oleic acid in 3.5 h) (Hilal *et al.* 2004). However, some further studies in terms of CLEAs and their usage for biodiesel production are required.

2.4.3.5 Immobilisation Supports

2.4.3.5.1 Alumina

Immobilisation is able to endow lipase with an enhanced level of reusability, operational stability and temperature optimum, leading to higher reaction rate and shorter reaction time (Gog *et al.* 2012). Owing to the high surface area and large pore volume, alumina has been employed as the support for lipase immobilisation (Kahveci *et al.* 2011; Scherer *et al.* 2011; Izrael-Zivkovic *et al.* 2015). Aluminas with varied

surface areas have been reported to adsorb about double as much lipase as the silica and zirconia supports (Kahveci *et al.* 2011). The esterification activity of the alumina adsorbed lipase also differs substantially, varies about 10-fold, increased with the increasing surface area of alumina.

2.4.3.5.2 Other Supports

Except for alumina, until present, various materials have been frequently investigated as the lipase immobilisation supports, such as alginate (Mondal *et al.* 2006), celite (Fishman *et al.* 2003), resin (Liu *et al.* 2011; Scherer *et al.* 2011), kaolinite (Scherer *et al.* 2011), zeolite (MacArio *et al.* 2007; Yagiz *et al.* 2007; Scherer *et al.* 2011), hydrotalcite (Yagiz *et al.* 2007; Zeng *et al.* 2009), SBA-15 (Lü *et al.* 2008; Serra *et al.* 2008; Li *et al.* 2009; Li *et al.* 2009; Salis *et al.* 2009; Salis *et al.* 2010; Zou *et al.* 2010; Guncheva *et al.* 2011; Gustafsson *et al.* 2012; Wang *et al.* 2012; Wilson *et al.* 2012), polypropylene (Foresti *et al.* 2005; Salis *et al.* 2009), textile membrane (Nie *et al.* 2006; Chen *et al.* 2009), vesicular silica (Wu *et al.* 2012), nano-sized magnetite (S-NSM) particles (Lee *et al.* 2009), and zirconia nanoparticles (Chen *et al.* 2008), etc. These studies normally focus on the immobilisation method, the enhancement of lipase activity and the reusability of catalyst.

2.5 Mesoporous Alumina

2.5.1 Synthesis of MA

Considerable efforts have been dedicated to extending the synthesis of mesoporous silica materials to alumina (Kim *et al.* 2004; Maekawa 2004; Xu *et al.* 2006; C Márquez‐Alvarez 2008; Paul *et al.* 2012). Unfortunately, typical recipes for the preparation of ordered mesoporous silica do not work effectively for the synthesis of alumina analogues, due to the fast hydrolysis and condensation rates of aluminium alkoxides, which often result in the formation of disordered alumina. As such, in most

reported cases, disordered mesostructures with amorphous walls are obtained (Maekawa 2004). At present, mesoporous alumina materials are commonly synthesised by the following pathways: (1) by solvent-deficient synthesis without the structure-directing agent (SDA) (Huang *et al.* 2013; Huang *et al.* 2013), (2) by adopting the nanocasting method with polymers and carbon molds as the hard templates (Wu *et al.* 2010), and (3) a pathway based on a modified sol-gel self-assembly process in the presence of a soft template such as a cationic, anionic, or nonionic surfactant as the SDA (Čejka 2003; Kim *et al.* 2004; Maekawa 2004; Xu *et al.* 2006; C Márquez‐Alvarez 2008; Kondo *et al.* 2008; Paul *et al.* 2012; Ghosh *et al.* 2014).

2.5.1.1 Surfactant Free Pathway

Solvent-deficient synthesis without the use of a template involves mixing an aluminium salt (e.g., aluminium nitrate, chloride, alkoxide, etc.) with a base (e.g., ammonium bicarbonate) to initiate the reaction before calcining the intermediate at high temperatures (Huang *et al.* 2013). Though the procedure for this pathway is simple, the synthesised MAs are usually restricted to discrete surface areas and pore sizes, as opposed to template assisted methods which accommodate a continuum of micelle structures and therefore meso-structures. This allows template assisted synthesis methods to produce MAs with a high involvement in size-selective catalysis, in contrast to the template free, solvent deficient method (Huang *et al.* 2013).

2.5.1.2 Hard Template Pathway

MAs synthesised through a hard template pathway can mitigate the tendency for pores to collapse during calcination (Li *et al.* 2005). The hard template pathway involves the impregnation of a pre-made exoskeleton with carbon based materials. Then the exoskeleton is etched away with HF or NaOH before surrounding the carbon endoskeleton with aluminium source. Through calcination, the carbon endoskeleton is

combusted away and the aluminium is calcined to achieve the desired MA phase (Wu *et al.* 2010). However, it must be noted that the structural properties of the resulting MAs rely heavily on the loading of carbon mold and the thermal treatment used (Li *et al.* 2005). It is clear that while the hard template approach can achieve thermally stable MA with uniform PSD in the range of 3-6 nm, the synthesis procedure requires numerous complex steps and the synthesised MAs are still restricted to small surface areas and pore sizes.

2.5.1.3 Soft Template Pathway

Compared to the former two pathways, soft template pathway has attracted great attention as its easily accessible and reproducible manner in fabricating MA through a facile sol-gel process (Q *et al.* 2008). It can bypass the complex and time-consuming process of the hard template pathway and also realise the modulation of pore size continuously, better than the surfactant free pathway. In this process, the hydrolysis behaviour of aluminium precursors is very complicated and is easily affected by the synthetic conditions such as acid, water and crystallization temperature, leading to the need of rather strict control of the conditions and consequently differed structural properties of the obtained MAs (Bleta *et al.* 2012). Understanding the effect of synthetic conditions on MA synthesis would enable the control of the mesoporosity features of MA.

In detail, the soft template synthesis pathway fundamentally relies on the use of amphiphilic surfactant that acts as the SDA. The surfactant forms micelles in solution whereby the hydrophilic ends exist in contact with the solvent molecules, and the hydrophobic ends meet at the micelle centre (Bleta *et al.* 2012). The aluminium source (e.g. aluminium iso-propoxide), when introduced into solution, surrounds the outer surface of the micelle structure. After evaporation, the micelle groups condense together

and the aluminium packs tighter against the micelle groups (Ghosh *et al.* 2014). Through calcination, the template is removed and the alumina undergoes phase transitions according to the temperature of calcination.

There are three types of soft templates used for the synthesis of MA, classified as anionic, cationic and nonionic, depending on the charge of amphiphilic component of the surfactant. Anionic template hydrolyses into an amphiphilic anion, and a cation (generally an alkaline metal or a quaternary ammonium ion). Some common examples include sodium dodecylbenzene sulphonate (SDS) and long chain carboxylic acids (often with sodium) (Valange *et al.* 2000; Pal *et al.* 2013). Anionic template assisted method is restricted to obtain MA with ordered pore size smaller than 3.5 nm, which limits its applicability in catalysis. In contrast, cationic template hydrolyses into a hydrophilic cation and an anion (often halide type). The majority of templates in this class belongs to nitrogenous compounds such as amine salts and quaternary ammoniums, with one or more long chain alkyl groups. Some common examples include quaternary alkylammonium salt C16TMABr (CTAB) and N-Dodecyl pyridium chloride (Pal *et al.* 2013). Nonionic templates are amphiphilic surfactants, which do not dissociate in solution in the same way as anionic and cationic templates. The most commonly used nonionic surfactants are composed of hydrophilic ethylene oxide (EO) chains and hydrophobic propylene oxide (PO) chains. A range of di-block copolymers (Tergitol, Igepal and Triton) and tri-block copolymers (pluronic P-123, F-127, L-64 and F-108) have been adopted as the SDAs (Ghosh *et al.* 2014).

Recently, a major improvement has been made by using water as the synthesis medium to achieve crystalline mesoporous γ-Al_2O_3 with high surface areas (Liu *et al.* 2008; Bleta *et al.* 2012; Alphonse *et al.* 2013). Upon the hydrolysis of aluminium precursor in the presence of a surfactant, the formation of an intermediate boehmite/surfactant nano-composite is identified to occur. However, to the best of the authors' knowledge,

systematic work on the modulation of structural properties of MA is scarce, which has limited its further penetration in heterogeneous catalysis and adsorption. Though Alphonse and his co-workers have tried to modify the structural properties of MA by the choice of the boehmite precursor, surfactant, the ratio of surfactant/AlOOH and the addition of hydrocarbons (Bleta *et al.* 2012), it is still a significant challenge to interpret the complex synthesis process and also to synthesise γ-Al_2O_3 with larger pores and higher surface areas.

2.5.2 Applications of MA as Catalyst Supports in Biodiesel Production

Up to now, as mentioned above, there has been no report regarding the use of MA as the catalytic support for biodiesel production. The catalysis application of alumina in biodiesel synthesis has been largely limited to conventional alumina. Heterogeneous catalysts based on alumina are normally prepared by either direct impregnation of sodium, potassium and calcium species. The use of MAs with controllable structural properties is insufficient.

2.6 Conclusions from Literature Review and Specific Objectives

On the basis of the above literature review, the following conclusions may be drawn:

- Compared to traditional homogeneous catalysts, the use of heterogeneous catalysts for transesterification reactions would be preferred, owing to the relatively fast separation of products and the easy recovery and regeneration of catalyst;
- There is a broad consensus on the high effectiveness of the alkaline catalysts in catalysing the transesterification reactions. However, very little work has been reported regarding the synthesis of new heterogeneous alkaline catalysts using

MAs as the supports. And the reaction mechanisms and reaction pathways need further investigation;

- Lipase catalysed transesterification is increasingly perceived as an alternative for biodiesel production owing to the mild reaction conditions, unaffected by FFA and simple downstream processing steps. Nevertheless, the high cost, easy denaturation and low operability of the free lipase need a proper support to get it immobilised and in this means to turn it into a type of heterogeneous catalyst;
- MA is considered a good catalyst support to prepare heterogeneous catalysts in virtue of its high porosity and large surface area. However, the catalytic applications of alumina have been largely confined to conventional alumina and the synthesis of MA itself requires a systematic investigation to realise its full potential in future applications;
- MA synthesized by the soft template pathway with the aid of a template is competent to improve the structural properties of the resulting MAs, but it needs a rather strict manipulation of the synthetic conditions.

The specific objectives of the present study are:

- To establish the synthesis methods and strategies of MA by following the modified sol-gel pathway using water as the synthesis medium;
- To facilely control the structural properties of the synthesised MAs by systematically manipulating the synthesis conditions, including: (1) the amount of nitric acid addition, (2) the amount of template addition, (3) template type, (4) calcination temperature and (5) the doping of inorganic aluminium precursors;
- To synthesise the heterogeneous alkaline MAK catalyst by incorporating potassium to MA and to investigate its catalytic performance in the transesterification of canola oil with methanol for biodiesel production;

- To reveal the reaction mechanism of the MAK catalysed transesterification;
- To synthesise the heterogeneous enzymatic catalyst by immobilising lipase on MA and to investigate its catalytic performance in transesterification.

The outcomes to be derived from this research will not only enhance the understanding of the complex organic-inorganic sol-gel process for MA synthesis and the effect of different synthesis conditions on the structural properties of the resultant MAs and also provide valuable insights of the developed heterogeneous MAK and enzymatic catalysts in the transesterification of canola oil with methanol for biodiesel production.

Chapter 3 Methodology, Approach and Techniques

This chapter details the research methodology and approach employed to achieve the research aims and objectives as outlined in Chapter 1 and 2, along with the descriptions and explanations of experimental and modelling techniques. This mainly includes an overview of the overall research methodology, experimental setup and the analytical techniques.

3.1 Overall Research Strategies

Two categories of heterogeneous catalysts would be investigated in this thesis, including the alkaline catalysts (potassium supported by MA, MAK) and enzymatic catalysts (lipase immobilised by MA). MAs with tunable surface areas, pore volumes and pore sizes were synthesised and employed as the catalyst supports. The MAs were synthesised following an aqueous phase sol-gel self-assembly pathway and characterised using a group of techniques such as N_2 physisorption techniques, TEM, XRD and TG–DTA.

The MAK catalysts were prepared following the one-pot self-assembly of potassium precursor KNO_3 and aluminium isopropoxide simultaneously while the enzymatic catalysts were synthesised by immobilising the pseudomonas fluorescens lipase on MAs by physical adsorption.

The transesterification of canola oil with methanol for biodiesel production was performed in a batch reactor, consisted of a round-bottom flask equipped with a condenser and a magnetic stirrer. The resulting crude biodiesel phase containing methyl esters (ME) was recovered and analysed for the biodiesel composition using an Agilent 7890 GC. Reaction kinetics of the MAK catalysed transesterification were studied following a model built on the Eley-Rideal mechanism. The effect of reaction

temperature, catalyst loading and the molar ratio of methanol to oil on biodiesel yield and kinetics were investigated.

In addition, for the case of enzymatic catalyst, a central composite experimental design strategy was applied to determine the significant parameters and the optimal conditions for biodiesel production. Figure 3-1 shows a schematic of the overview of the research methodology.

3.2 Material Synthesis and Experimental Designs

3.2.1 MA Synthesis Following the Aqueous Phase Synthesis Pathway

In this thesis, MAs were synthesised following an aqueous phase sol-gel self-assembly pathway with the aid of a template. In brief, 2 mol of hot water (85 ℃) was added to 20 mmol of aluminium (in the form of aluminium isopropoxide with or without the inorganic aluminium precursors) under vigorous stirring in a 100 mL flask (Schott Pty Ltd) for 15 min.

Then, HNO_3 (68%, Fluka) was added and the mixture was stirred and maintained at 85 ℃ for 12 h, during which the flask was kept uncovered in the first 2 h to allow the evaporation of isopropanol formed during the hydrolysis. A template was added to the sol and the mixture was kept under gentle stirring for another 12 h period at room temperature. Finally, a MA product was obtained by drying the sol in air in an electric oven operating at 70 ℃ for 12 h, followed by calcination in air for 4 h.

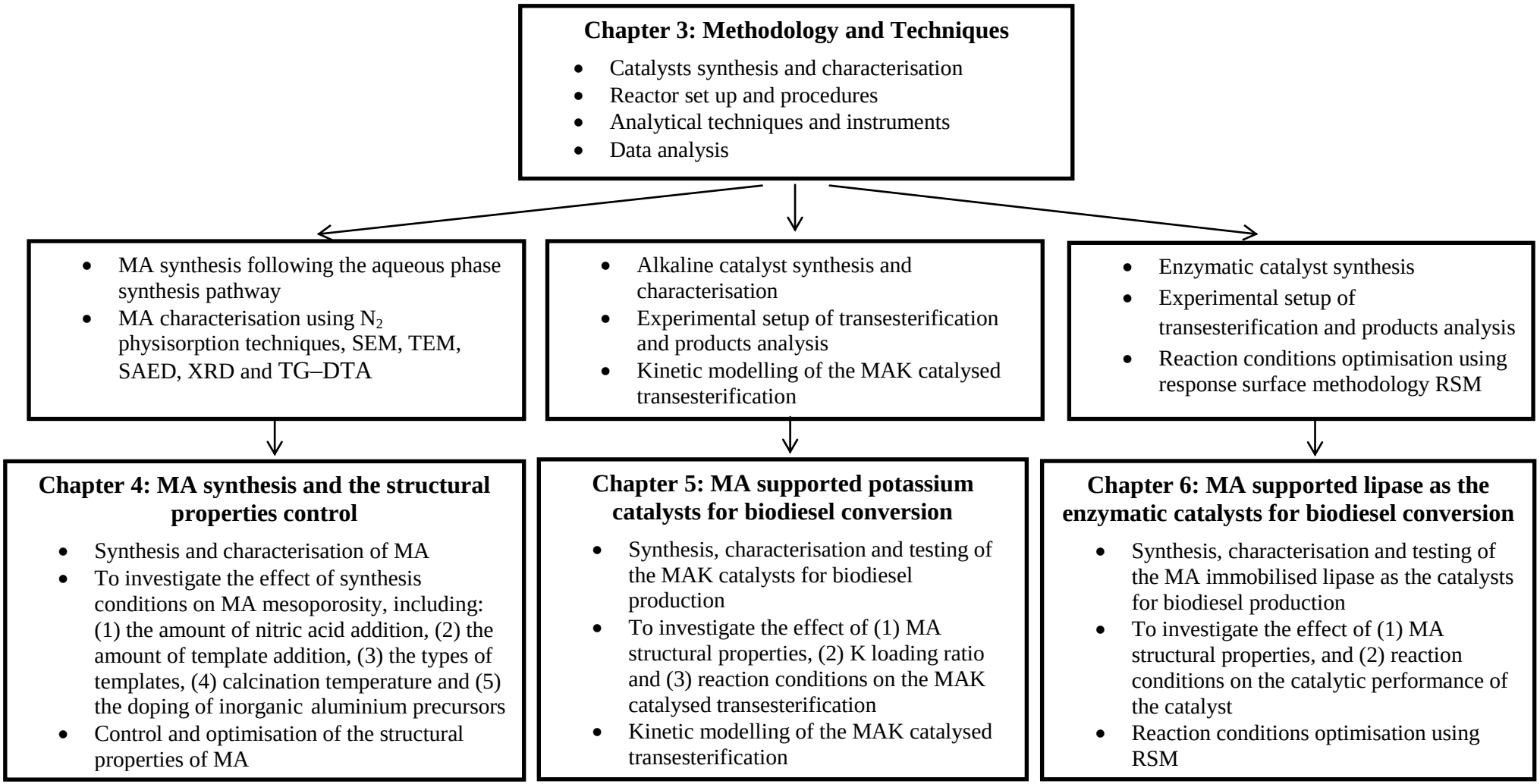

Figure 3-1 A schematic of the overview of the research methodology

3.2.2 Synthesis of Alkaline MAK Catalysts

MAK catalysts were synthesised following the one-pot self-assembly of potassium precursor KNO_3 (Sigma Aldrich) and aluminium isopropoxide simultaneously. P123 was selected as the template. Accordingly, MAK catalysts were synthesised as per the depicted recipe in Section 3.2.1. The only difference was that a desired amount of KNO_3 was added in the sol together with template P123 to trigger the simultaneous self-assembly of potassium and aluminium species. In order to modulate the structural properties of the resulting samples and investigate the effect of potassium loading on the catalytic activity of the catalysts, different amount of P123 and KNO_3 were added in, respectively. The total quantity of the metal species (20 mmol) was kept constant, and the molar ratio of K was adjusted accordingly (5%, 10%, 15%, 20%, 25%).

3.2.3 Synthesis of Enzymatic Catalysts

A series of enzymatic catalysts were synthesised by the immobilisation of pseudomonas fluorescens lipase (Sigma Aldrich) on MAs by physical adsorption. Lipase adsorption capabilities on the MAs synthesised were tested. For the purpose of comparison, the lipase adsorption capability on a commercial alumina (Sigma Aldrich, analytical grade) was also measured. In a typical adsorption experiment, an appropriate amount of pseudomonas fluorescens lipase was dissolved in sodium phosphate buffer (20 mM) at pH 8.0, the optimal pH for pseudomonas fluorescens lipase, to make a 1 $mgmL^{-1}$ stock solution. Then, 30 mg of a support material was added to 30 mL lipase solution with gentle stirring at room temperature. The solid samples were collected after 2 h by filtration and then thoroughly washed with deionised water and vacuum dried at 40 ℃ overnight. The resulting solid was used as the catalyst for transesterification.

Experiments to determine the amount of lipase adsorption as a function of time were conducted. A sample of 2 mL of the emulsion solution was withdrawn periodically, at

10 min, 30 min, 60 min and 120 min, for immediate analysis using a UV-vis spectrophotometer at wavelength 280 nm and then returned to the mixture. The solution sample taken was separated by centrifugation at 10000 rpm for 5 min to obtain supernatant for analysis. The amount of lipase adsorbed was determined by the difference on the lipase concentrations before and after the UV adsorption according to:

$$A = V_0(C_0 - C_t)/M \quad (3\text{-}1)$$

where A (mgg^{-1}) is the adsorption amount of lipase, C_0 (mgL^{-1}) is the initial lipase concentration, C_t (mgL^{-1}) is the residual concentration of lipase in the supernatant, V_0 (mL) is the volume of lipase solution and M (g) is the weight of the support material sample.

3.2.4 Experimental Setup of Transesterification and Products Analysis

Transesterification experimentation was performed with canola oil (Goodman Fielder Ltd., > 99.0%) and methanol (Sigma Aldrich, > 99.9%) to investigate the performance of various catalysts in biodiesel synthesis. In case of the MAK catalysed transesterifications, reactions were carried out in a 50 ml round-bottom flask equipped with a condenser and a magnetic stirrer. All transesterification reaction runs were conducted under identical conditions of 5.0 g canola oil, 0.1 g catalyst (2.0 wt%, relative to oil weight), M/O 12:1 at 70 ℃ with 5 h of reaction time under stirring. The reusability of the MAK catalysts after five successive runs was also tested using MA1P20K as the catalyst. After reaction, the catalyst was recovered from the centrifuge tube and properly washed with methanol to remove glycerol and afterwards with n-hexane to remove any undesired materials attached on the surface. The catalyst was then calcined at 700 ℃ for 3 h and then reused. After each reaction, the liquid was subjected to centrifuging at 5,000 rpm for 20 min to two phases, with glycerol at the bottom and crude biodiesel containing methyl esters (ME) at the top.

Table 3-1 Fatty acid composition of canola oil

Fatty Acid	Composition (wt.%)
C 14:0 Myristic acid	0.04
C 16:0 Palmitic acid	4.00
C 16:1 Palmitoleic acid	0.21
C 18:0 Stearic acid	1.82
C 18:1 Oleic acid	62.89
C 18:2 Linoleic acid	19.62
C 18:3 Linolenic acid	8.47
C 20:0 Arachidic acid	0.62
C 20:1 Eicosenoic acid	1.29
Others	1.04

For the enzymatic catalysts, the reaction was carried out in a 10 ml round-bottom flask equipped with a condenser and a magnetic stirrer using 5.0 g of canola oil with 0.15 g of catalyst and 0.2 g of water, at a constant reaction temperature of 40 ℃ for 24 h. 0.54 g of methanol was added stepwise to prevent the potential denaturing effect on lipase (Yuji Shimada 1999). Specifically, 0.18 g of methanol was added into the flask when the experiment commenced to ensure that the initial molar ratio of methanol to oil equalled 1. Then a further amount of 0.18 g of methanol was added into the flask after 6 h and 14 h, respectively, to maintain the same methanol to oil molar ratio during the whole period of the experiment (Yuji Shimada 1999). After 24 h of operation, the liquid was subjected to separation by centrifuging at 5,000 rpm for 20 min into two phases, with glycerol at the bottom and crude biodiesel containing methyl esters (ME) at the top.

Standard fatty methyl esters, methyl myristate (C14:0), methyl palmitate (C16:0), methyl palmitoleate (C16:1), methyl stearate (C18:0), methyl oleate (C18:1), methyl linoleate (C18:2), methyl linolenate (C18:3), methyl arachidate (C20:0), methyl cis-11-

eicosenonate (C20:1) and methyl behenate (C22:0) were also purchased from Sigma-Aldrich, and utilised as the reference standards for gas chromatograph (GC) analysis, while methyl nonadecanoate (C19:0) was used as the internal standard. All chemicals were used as received without further purification. The fatty acid compositions of the used canola oil are summarised in Table 3-1. It was composed of 6.5% saturated fatty acids and 93.5% unsaturated fatty acids, dominated by the one double bond oleic acid C18:1 (63.9%).

The methyl esters phase was easily recovered and analysed for the biodiesel composition using an Agilent 7890 GC equipped with a J&W (Folsom, CA, USA) DB-Wax capillary column (30 m×0.25mm I.D, a fused-silica column coated with 0.25 μm polyethylene glycol film) and a flame ionization detector (FID). The GC column was heated from 60 ℃ to 210 ℃ at a heating rate of 20 ℃/ min and then held for 9 minutes at 210 ℃. MEs were identified by matching the retention times with those of a mixture of standard MEs while the content was determined using the internal standard method using methyl nonadecanoate as the reference. The injector and detector temperatures were set at 250 ℃. The yield of biodiesel was calculated according to:

$$Y(\%) = \frac{M_1 \times f}{M_2} \times 100\% \qquad (3\text{-}2)$$

Where Y is the biodiesel yield, M_1 is the mass of top phase obtained after separation, M_2 is the initial mass of canola oil used in the experiment, f is the percentage of ME content obtained from the GC analysis.

In addition, in case of enzymatic catalysts, the lipase activity ($\mu molh^{-1}g^{-1}$) was defined as the amount of methyl esters converted from triglycerides per hour per unit mass (g) of lipase in the system. In addition, a sole MA support, MA4P15AlN, without lipase adsorption, was also tested, but there were no methyl esters produced. This indicated

that the transesterification activity was entirely due to the lipase and MA only acted as a support for lipase immobilisation.

3.2.5 Kinetic Modelling of the MAK Catalysed Transesterification

Reaction kinetics of the MAK catalysed transesterification of canola oil with methanol were studied. A MAK catalyst MA1P20K was selected as the catalyst. The transesterification experimentation was similarly performed in a 50 ml round-bottom flask equipped with a condenser and a magnetic stirrer using 5.0 g of canola oil. A sample of 0.5 mL of liquid was withdrawn periodically, at 10 min, 20 min, 30 min, 40 min, 50 min, 60 min, 90 min, 120 min, 150 min and 180 min, followed by centrifugation at 5,000 rpm for 20 min and then went through GC analysis.

The effect of the mass transport resistance including the external and internal diffusion limitations of the catalyst was assessed by varying the stirring rate and catalyst particle size, respectively (Pugnet *et al.* 2010; Xiao *et al.* 2010; Chantrasa *et al.* 2011). Experiments were performed under four stir rates (200 rpm, 400 rpm, 500 rpm and 600 rpm) and five catalyst particle size fractions (<160 μm, 160-250 μm, 250-380 μm, 380-600 μm, 600-830 μm). Other reaction conditions were kept identical: reaction temperature 70 ℃, M/O 12:1, 2 wt% catalyst loading within 1 h of reaction time.

The Eley-Rideal mechanism, assuming a pseudo first-order for the forward reaction and a second-order for the reverse reaction of transesterification, was used. The effect of reaction temperature (from 50 ℃ to 70 ℃), methanol to canola oil molar ratio (6:1 to 15:1) and catalyst loading (1.0 wt% to 2.5 wt%, relative to the weight of oil) on biodiesel yield and kinetics was investigated. Kinetic parameters were determined by fitting the model to the experimental data. The reaction below shows the generalized transesterification reaction, where A stands for triglyceride, B methanol, C methyl ester

and D glycerol. The stoichiometric relationship (Lapis *et al.* 2008; Sivasamy *et al.* 2009) between reactants and products is shown:

$$A + 3B \xrightarrow{Catalyst} 3C + D \tag{3-3}$$

Herein, the general rate equation of transesterification can be written as:

$$-dC_A/mdt = k_1 C_A - k_{-1} C_C C_D \tag{3-4}$$

where k_1 and k_{-1} are the rate constants of the forward and reverse reaction, respectively. In addition:

$$C_A = C_{A0}(1-Y) \tag{3-5}$$

C_{A0} is the initial concentration of triglyceride, Y is the biodiesel yield, which can be measured by GC following Eq. (3-2). Therefore, the Eq. (3-4) can be derived as:

$$dY/dt = m[k_1(1-Y) - k_{-1} C_{A0} Y^2] \tag{3-6}$$

Integration of Eq. (3-6) leads:

$$\frac{1}{(X_e - q)C_{A0}m} \ln \left| \frac{(Y - X_e)q}{X_e(Y - q)} \right| \equiv f(Y) = k_{-1}t \tag{3-7}$$

Where

$$q = \frac{-K_e - \sqrt{K_e^2 + 4K_e C_{A0}}}{2C_{A0}} \tag{3-8}$$

And

$$K_e = \frac{k_1}{k_{-1}} = \frac{X_e^2 C_{A0}}{(1 - X_e)} \tag{3-9}$$

Xe is the equilibrium conversion, which is defined as the biodiesel yield after 24 h of reaction, where the reaction has already reached the equilibrium and the conversion is stable (Sanjib Kumar Karmee 2004). The slope of the plot of f(*Y*) against time is the reverse reaction rate k_{-1}, while the forward rate constant k_1 can be obtained using Eq. (3-9). When the reaction rate constants at different temperatures are determined, the activation energy E_a for the transesterification will be calculated using Arrhenius formula Eq. (3-10):

$$k_1 = k_0 e^{-\frac{E_a}{RT}} \tag{3-10}$$

By integrating, it gives Eq. (3-11).

$$\ln k_1 = -\frac{E_a}{R} \times \frac{1}{T} + \ln k_0 \tag{3-11}$$

where R is the gas constant, T is temperature in Kelvin, and k_0 is the pre-exponential factor.

3.2.6 Optimisation of Reaction Conditions using RSM

An experimental design using RSM based on the three-variable central composite design (CCD) method was applied to the MA4P15AlN immobilised lipase as the catalyst to determine the significant parameters and the optimal conditions for biodiesel production. (Kafuku *et al.* 2010; SathyaSelvabala *et al.* 2011; Bussemaker *et al.* 2013; Zhao *et al.* 2013; Zhao *et al.* 2013; Zhao *et al.* 2014).

The key variables investigated included water addition, reaction temperature and catalyst loading. Water is indispensable to activate lipase by unmasking and restructuring the active sites through a conformational change of the lipase molecule (Petkar *et al.* 2006). The reaction parameters such as water addition (nil to 8 wt%), reaction temperature (30 ℃ to 50 ℃) and catalyst loading (2 wt% to 6 wt%) were

varied with an aim to obtain the optimal reaction conditions. The CCD was used to investigate the linear, quadratic and cross-product effect of these three independent process variables on biodiesel yield (Kafuku *et al.* 2010). The ranges and levels of the three variables studied are shown in Table 3-2. A total of 14 factorial points and 5 centre points were used for fitting a second-order response surface.

Table 3-2 Experimental ranges and levels of independent variables

Variable	Coding	Ranges and levels				
		-2	-1	0	+1	+2
Reaction temperature (℃)	X_1	30	35	40	45	50
Water addition (wt%)	X_2	0	2	4	6	8
Catalyst loading (wt%)	X_3	2	3	4	5	6

The response of the experimental data was applied to develop a mathematical expression correlating biodiesel yield against the reaction variables studied through the first order, second order and interaction terms, according to the following quadratic polynomial equation (Kafuku *et al.* 2010; Ghosh *et al.* 2012; Zhao *et al.* 2013):

$$Y = \mathrm{b}_0 + \sum_{j=1}^{3} b_j X_j + \sum_{ij=1}^{3} b_{ij} X_i X_j + \sum_{j=1}^{3} b_{jj} X_j^2 \qquad (3\text{-}11)$$

where Y is the predicted biodiesel yield, X_i and X_j represent the parameters, including X_1 reaction temperature, X_2 water addition and X_3 catalyst loading, b_o is an offset term, b_j is the linear effect, b_{ij} is the first order interaction effect and b_{jj} is the squared effect. A Design Expert software (Version 8.0.6, State Ease Inc., Minneapolis, MN, USA) was used to perform the analysis of variance (ANOVA) and generate response surfaces.

3.3 Analytical Methods and Instrumentation

In order to characterise the prepared materials, a combination of several advanced analytical techniques and instruments was employed in the present work. The synthesised samples were characterised using N_2 physisorption technique for porous structural properties, X-ray diffraction (XRD) for bulk crystallinity, transmission electron microscopy (TEM) for nano-scale morphology, thermogravimetry–differential thermal analysis (TG–DTA) for decomposition and mass loss characteristics upon calcination.

3.3.1 N_2 Physisorption Techniques

Structural parameters of samples including the BET surface area, pore volume V_p, average pore size D_a and pore size distribution PSD were determined from the nitrogen physisorption isotherms obtained using a Tristar 3020 volumetric analyser (Micromeritics Co. Ltd). Prior to a measurement, the sample was degassed under vacuum at 200℃ overnight to remove moisture and other absorbed species. The specific surface area was calculated from the adsorption branch using the BET method in the relative pressure (p/p_o) range of 0.05–0.3 (Sing 1985). V_p showed the total pore volume calculated from the adsorbed nitrogen amount at a relative pressure p/p_o of 0.997 (Tian *et al.* 2014; Tian *et al.* 2014). D_a indicated the average pore diameter while D_p was defined as the peak value of the PSD curve derived from adsorption branch of the isotherm using the BJH calculation method (Sing 1985; Tian *et al.* 2014). Before the test, the instrument was calibrated using standard Al_2O_3 and SiO_2 samples to ascertain the instrument in a good condition.

3.3.2 Transmission Electron Microscopy (TEM)

TEM and its associated advanced techniques including the selected area electron diffraction (SAED) and high resolution transmission electron microscopy (HRTEM)

can provide sufficient information on the morphological properties of the sample at near-atomic resolutions. In this study, TEM imaging was acquired using a JEM-2100 JEOL electron microscope equipped with LaB6 filament at 120 kV for further analysis and interpretation. The magnification of 50,000x was used during the observation to reveal the morphological features. The acquired TEM images were processed using the DigitalMicrograph software (Gatan Inc) to directly yield the projected data.

3.3.3 X-ray Diffraction (XRD)

Powder X-ray diffraction (XRD, Empyrean, PANalytical, Cu-Kα radiation at 40 kV, 40 mA) was used to perform wide angle X-ray scattering (WAXS) from 10 ° to 80 °. The diffraction patterns generated allow to determine the chemical composition and phase composition of the MA samples and MAK catalysts. Samples were scanned in a wide-angle X-ray goniometer, and the scattering intensity is plotted as a function of the 2θ angle. X-ray diffraction is a non-destructive method of characterisation of solid materials. When X-rays are directed in solids they will scatter in predictable patterns based upon the internal structure of the solid. A crystalline solid consists of regularly spaced atoms (electrons) that can be described by imaginary planes.

3.3.4 Thermogravimetry–differential Thermal Analysis (TG–DTA)

The MA samples were subjected to non-isothermal analysis using a thermogravimetric analyser (SDT Q600, TA Instrument) to obtain the mass loss characteristics during calcination. This allows simultaneous measurements of weight loss and heat flow as a function of time and temperature. The TGA tests were conducted in an atmosphere of high purity air at the flow rate of 50 $mLmin^{-1}$ with a heating rate of 5 $℃min^{-1}$ from 70 ℃ to 700 ℃. Each sample was analysed three times to assure the method reproducibility. Thermogravimetry–differential thermal analysis (TG–DTA) curves

were obtained to reveal the differences in the key thermal behaviours of different MA samples.

Chapter 4 MA Synthesis and Control of Structural Properties

MA synthesis and its structural properties control are discussed in this chapter. The synthesis of MA followed a sol-gel process via hydrolysis of aluminium isopropoxide associated with a SDA as template in an acidic aqueous system. For the control of structural properties, the effect of nitric acid addition amount, template type, template addition amount, inorganic aluminium precursor doping and calcination temperature were systematically investigated.

4.1 MA Synthesis

MAs were successfully synthesised in this study via an aqueous phase sol-gel self-assembly process under acidic conditions with the aid of a template. The aluminium sources were hydrolysed with the addition of water and the hydrolysis was promoted by the acidic environment induced by the addition of nitric acid. The released isopropanol was evaporated. This process involved complicated organic–inorganic assemblies using a template as the SDA to form a hybrid organic–inorganic mesophase by the simultaneous condensation of Al ions and the self-assembly of SDA molecules. Self-assembly of Al^{3+} was assisted by different amounts of template, leading to the formation of diverse mesoporosity of the resulting MAs. The template was finally removed by calcination. The structural properties of MA were modulated through the manipulation of different soft templates (nonionic triblock copolymers P123 and F127, cationic cetyltrimethylammonium bromide CTAB and anionic sodium dodecyl sulfate SDS), HNO_3 addition, inorganic aluminium precursors ($Al(NO_3)_3$, $AlCl_3$ and $Al_2(SO_4)_3$) doping ratios and calcination temperature. The detailed synthesis recipes and the resulting MA products are summarised in Table 4-1.

For convenience in discussion, the MA samples synthesised in this work were nominally denoted in a general form of MA*x*A*y*AlB*z*N-T, where A (P, F, C, S) refers to the template types (P123, F127, CTAB, SDS) and B (N, S, Cl) refers to the doped inorganic aluminium precursors ($Al(NO_3)_3$, $Al_2(SO_4)_3$, $AlCl_3$), respectively. For P123, *x* refers to "*x*" g of P123 while for F127, CTAB and SDS, *x* denotes the equivalent moles of F127, CTAB and SDS per "*x*" g of P123. In addition, *y* signifies "*y*" mol% of inorganic aluminium precursor (if applicable) relative to the total 20 mmol of Al, *z* means "z" times of 0.097 mL HNO_3 added in synthesis. T indicates the calcination temperature. Unless otherwise specified, the HNO_3 addition and temperature were 1N (0.097 mL HNO_3 per 20 mmol of Al) and 700 ℃, respectively. For instance, MA0A indicates a MA0A sample synthesised without template. MA1P15AlN presents a MA sample prepared using 1 g of P123, 0.097 mL of HNO_3, 15% molar fraction (3 mmol) of $Al(NO_3)_3$ and then calcined at 700 ℃. MA6P-500 presents a MA prepared using 6 g of P123 calcined at 500 ℃ without the doping of inorganic aluminium precursors.

Table 4-1 MA labelling and corresponding synthesis conditions

Samples	Template (g)	Aluminium source (mmol)	HNO_3 (mL)	Calcination temperature (℃)
MA0A	-	$Al(O\text{-}i\text{-}Pr)_3$ 20	0.097	700
MA1P0N	P123 1.00	$Al(O\text{-}i\text{-}Pr)_3$ 20	-	700
MA1P	P123 1.00	$Al(O\text{-}i\text{-}Pr)_3$ 20	0.097	700
MA1P3N	P123 1.00	$Al(O\text{-}i\text{-}Pr)_3$ 20	0.291	700
MA1P10N	P123 1.00	$Al(O\text{-}i\text{-}Pr)_3$ 20	0.970	700
MA2P	P123 2.00	$Al(O\text{-}i\text{-}Pr)_3$ 20	0.097	700
MA4P	P123 4.00	$Al(O\text{-}i\text{-}Pr)_3$ 20	0.097	700
MA6P	P123 6.00	$Al(O\text{-}i\text{-}Pr)_3$ 20	0.097	700
MA1F	F127 2.17	$Al(O\text{-}i\text{-}Pr)_3$ 20	0.097	700

MA2F	F127 4.34	$Al(O\text{-}i\text{-}Pr)_3$ 20	0.097	700
MA4F	F127 8.68	$Al(O\text{-}i\text{-}Pr)_3$ 20	0.097	700
MA1C	CTAB 0.06	$Al(O\text{-}i\text{-}Pr)_3$ 20	0.097	700
MA2C	CTAB 0.12	$Al(O\text{-}i\text{-}Pr)_3$ 20	0.097	700
MA4C	CTAB 0.25	$Al(O\text{-}i\text{-}Pr)_3$ 20	0.097	700
MA10C	CTAB 0.62	$Al(O\text{-}i\text{-}Pr)_3$ 20	0.097	700
MA20C	CTAB 1.24	$Al(O\text{-}i\text{-}Pr)_3$ 20	0.097	700
MA1S	SDS 0.05	$Al(O\text{-}i\text{-}Pr)_3$ 20	0.097	700
MA2S	SDS 0.10	$Al(O\text{-}i\text{-}Pr)_3$ 20	0.097	700
MA4S	SDS 0.20	$Al(O\text{-}i\text{-}Pr)_3$ 20	0.097	700
MA10S	SDS 0.50	$Al(O\text{-}i\text{-}Pr)_3$ 20	0.097	700
MA20S	SDS 1.00	$Al(O\text{-}i\text{-}Pr)_3$ 20	0.097	700
MA1P10AlN	P123 1.00	$Al(O\text{-}i\text{-}Pr)_3$ 18 $Al(NO_3)_3 \cdot 9H_2O$ 2	0.097	700
MA1P15AlN	P123 1.00	$Al(O\text{-}i\text{-}Pr)_3$ 17 $Al(NO_3)_3 \cdot 9H_2O$ 3	0.097	700
MA1P20AlN	P123 1.00	$Al(O\text{-}i\text{-}Pr)_3$ 16 $Al(NO_3)_3 \cdot 9H_2O$ 4	0.097	700
MA1P1AlS	P123 1.00	$Al(O\text{-}i\text{-}Pr)_3$ 19.8 $Al_2(SO_4)_3 \cdot 14H_2O$ 0.1	0.097	700
MA1P2AlS	P123 1.00	$Al(O\text{-}i\text{-}Pr)_3$ 19.6 $Al_2(SO_4)_3 \cdot 14H_2O$ 0.2	0.097	700
MA1P3AlS	P123 1.00	$Al(O\text{-}i\text{-}Pr)_3$ 19.4 $Al_2(SO_4)_3 \cdot 14H_2O$ 0.3	0.097	700
MA1P10AlCl	P123 1.00	$Al(O\text{-}i\text{-}Pr)_3$ 18 $AlCl_3$ 2	0.097	700
MA1P20AlCl	P123 1.00	$Al(O\text{-}i\text{-}Pr)_3$ 16 $AlCl_3$ 4	0.097	700
MA1P30AlCl	P123 1.00	$Al(O\text{-}i\text{-}Pr)_3$ 14 $AlCl_3$ 6	0.097	700
MA1P35AlCl	P123 1.00	$Al(O\text{-}i\text{-}Pr)_3$ 13 $AlCl_3$ 7	0.097	700

MA6P-500	P123 6.00	$Al(O\text{-}i\text{-}Pr)_3$ 20	0.097	500
MA6P-900	P123 6.00	$Al(O\text{-}i\text{-}Pr)_3$ 20	0.097	900
MA6P-1100	P123 6.00	$Al(O\text{-}i\text{-}Pr)_3$ 20	0.097	1100
MA4P15AlN	P123 4.00	$Al(O\text{-}i\text{-}Pr)_3$ 17 $Al(NO_3)_3 \cdot 9H_2O$ 3	0.097	700
MA4P30AlCl	P123 4.00	$Al(O\text{-}i\text{-}Pr)_3$ 14 $AlCl_3$ 6	0.097	700
MA4P2AlS	P123 4.00	$Al(O\text{-}i\text{-}Pr)_3$ 19.6 $Al_2(SO_4)_3 \cdot 14H_2O$ 0.2	0.097	700

4.2 Effect of Synthesis Conditions on MA Mesoporosity

4.2.1 Amount of Nitric Acid Addition

The structural properties, depicted by BET surface area, pore volume V_p, pore size D_a and D_p derived from the nitrogen isotherms of all the samples, are summarised in Table 4-2. Figure 4-1a presents the nitrogen sorption isotherms while Figure 4-1b shows the corresponding BJH PSD curves of MA1PzN. All the isotherms except for MA1P0N are of Type IV with the characteristic H1 hysteresis loops, indicating their uniform mesopores. According to the IUPAC classification, the well-developed H1 hysteresis loop is believed to be associated with the capillary condensation in large pore channels with possible channel modulation (Sing 1985; Cai *et al.* 2011). Without HNO_3 addition, sample MA1P0N showed a disordered PSD, indicating the deficiency of uniformity in the pore arrangement. However, in comparison, for the samples MA1P, MA1P3N, and MA1P10N, with increasing HNO_3 addition, the condensation steps occurring in the hysteresis loops clearly shifted to greater relative pressures, suggestive of larger mesopores. This trend was directly evidenced by the PSD curves in Figure 4-1b, where it is seen that D_p gradually increased from 13.9 nm to 28.7 nm. However, when the addition of HNO_3 reached 10N, the PSD became very broad, and the surface area also

noticeably reduced (to 227 m^2g^{-1}). Sample MA1P showed the largest surface area (287 m^2g^{-1}) with a narrow PSD.

Table 4-2 Adsorption parameters of MAs

Samples	BET Surface Area (m^2g^{-1})	Pore Volume V_p (cm^3g^{-1})	D_a (nm)	D_p (nm)
MA0A	236	0.4	5.2	7.0
MA1P0N	261	0.8	9.2	10.0
MA1P	287	0.9	9.5	13.9
MA1P3N	250	0.9	12.2	19.4
MA1P10N	227	0.8	13.1	28.7
MA2P	295	1.2	13.7	11.0
MA4P	325	1.8	19.3	28.2
MA6P	323	1.9	20.4	30.7
MA1F	309	1.4	14.9	17.3
MA2F	348	1.6	17.7	23.2
MA4F	358	1.9	20.8	30.1
MA1C	241	0.4	5.9	8.2
MA2C	253	0.5	6.2	8.3
MA4C	258	0.6	6.7	9.2
MA10C	294	0.8	7.7	10.0
MA20C	319	1.1	10.2	13.4
MA1S	236	0.4	4.4	5.5
MA2S	249	0.4	4.6	5.6
MA4S	254	0.4	4.9	5.5
MA10S	258	0.4	5.7	7.3
MA20S	260	0.5	6.7	8.6

MA1P10AlN	258	1.0	12.5	19.7
MA1P15AlN	263	1.1	13.8	22.4
MA1P20AlN	178	0.7	14.7	28.1
MA1P1AlS	290	0.9	9.7	13.3
MA1P2AlS	309	0.9	9.3	14.0
MA1P3AlS	293	0.8	9.4	-
MA1P10AlCl	298	1.0	10.7	15.9
MA1P20AlCl	282	1.0	12.1	15.5
MA1P30AlCl	254	1.1	14.6	26.6
MA1P35AlCl	197	0.8	15.1	-
MA6P-500	409	2.5	21.2	31.5
MA6P-900	219	1.5	24.3	36.5
MA6P-1100	104	0.7	27.1	34.0

It is reported that the self-assembly is essentially a condensation process, during which the cross-linked aluminium species can arrange around the triblock copolymer to form the ordered mesophases (Pérez *et al.* 2013). Nitric acid acts as a coordination agent and a pH adjuster in the synthesis system to maintain the medium acidic (Cai *et al.* 2011). A recent study has pointed out that in the polymer-templated synthesis of mesoporous alumina, the role of acidic condition was to provide protons to allow the interaction between the poly ethylene oxide (PEO) blocks and aluminium precursors to form the corona structure and the concentration of acid would also affect the micelle size (Grant *et al.* 2012). The increased addition of HNO_3 resulted in an increase in the Pluronic micelle size due to the affinity of protons to the PEO blocks and also increased the NO_3^- concentration at the corona/water interface. There was an elevated capacity for the corona to coordinate with NO_3^- at higher acid concentrations.

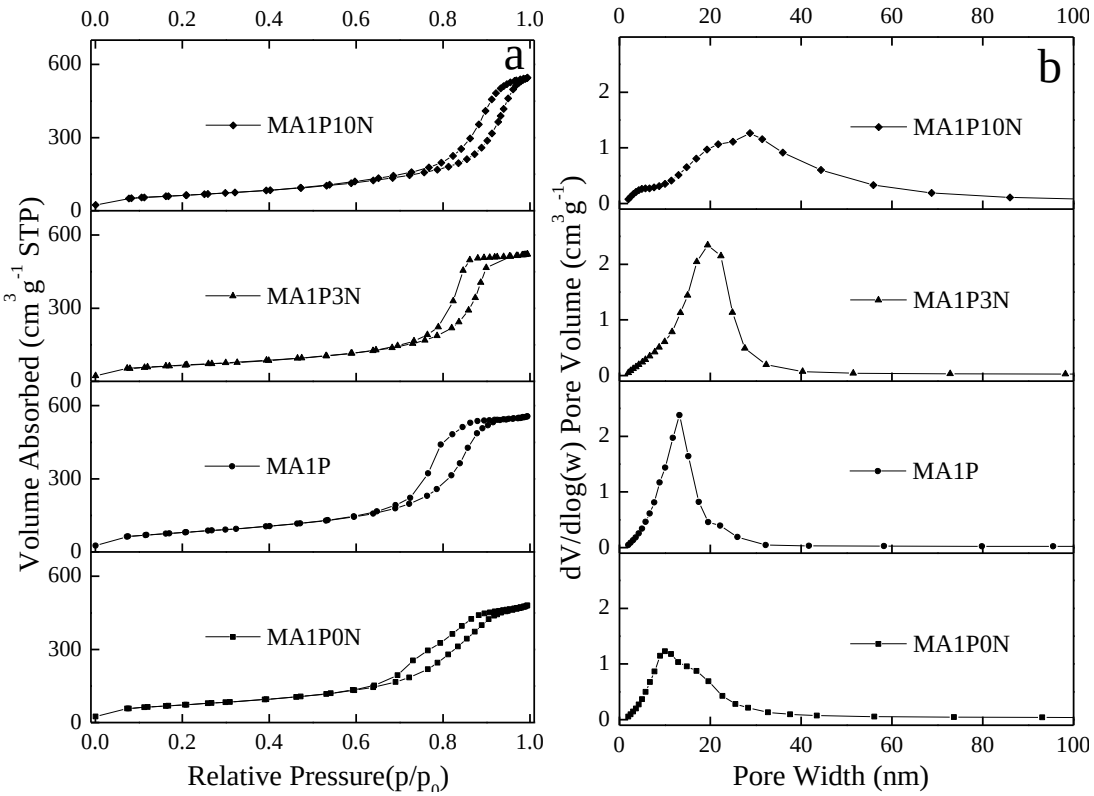

Figure 4-1 Nitrogen physisorption isotherms (a) and corresponding pore size distributions (b) of MA1PzN

Moreover, it has been also reported that the extreme low pHs of the synthesis medium would decrease the rate of condensation reactions (Pérez *et al.* 2013). This indicates that the synthesis system with very low pH may hinder condensation of the framework, which hampers the self-assembly process to provide an organised meso-porous structure. Therefore, the effect of HNO_3 addition on the structural properties of MA, especially on the pore size is most likely a consequence of the increased concentrations of H^+ and NO_3^- ions in the solution. An increase in the HNO_3 concentration can promote the interaction between the PEO blocks and aluminium precursors and also increase the micelle size, leading to larger pores of the resulting MAs. However, excessive HNO_3 addition would obstruct the condensation of the porous framework, thus causing detrimental effect on the mesoporosity and leading to a broad PSD. Herein, HNO_3 addition between 1N and 3N was benign for the formation of organised MAs and 1N was used for synthesising the remaining samples.

4.2.2 Type of Template

The structural properties of all MA samples are summarised in Table 4-2. The nitrogen physisorption isotherms of MA1A, MA2A and MA4A are plotted in Figure 4-2 (a, c, e) while the corresponding BJH PSD curves are shown in Figure 4-2 (b, d, f). As can be seen, all the isotherms are of Type IV, which refers to mesoporous materials (Sing 1985; Cai *et al.* 2011). The isotherms measured on MA*x*P and MA*x*F present the H1 hysteresis loops while in the cases of MA*x*C and MA*x*S, the desorption branches decline steeply at the relative pressure of 0.5~0.6, exhibiting the characteristics of the H2 hysteresis loops. The H1 hysteresis loop relates to the capillary condensation taking place in large pore channels with channel modulation (Sing 1985; Cai *et al.* 2011). This shape is often associated with porous materials consisting of agglomerated uniform particles with narrow PSD (Marszewski *et al.* 2013). In comparison, MA*x*C and MA*x*S samples showed Type H2 loops, indicative of the 'ink bottle' pores with narrow necks and wide bodies (Bai *et al.* 2009). This suggests that MA*x*C and MA*x*S were less uniform and their agglomeration resulted in irregular porous structures (Marszewski *et al.* 2013).

Obviously, the addition of nonionic templates F127 and P123 induced greater changes in the structural properties of the resulting MAs than the cationic template CTAB and anionic SDS did. Isotherms of MA*x*F and MA*x*P showed relatively steeper condensation steps, indicating uniform mesopore sizes. This is consistent with the results presented in Table 4-2, from which it is notable that the pore size D_a and D_p, pore volume V_p and surface area of MA samples presented in a descending order of MA*x*F > MA*x*P > MA*x*C > MA*x*S (*x*=1, 2, 4).

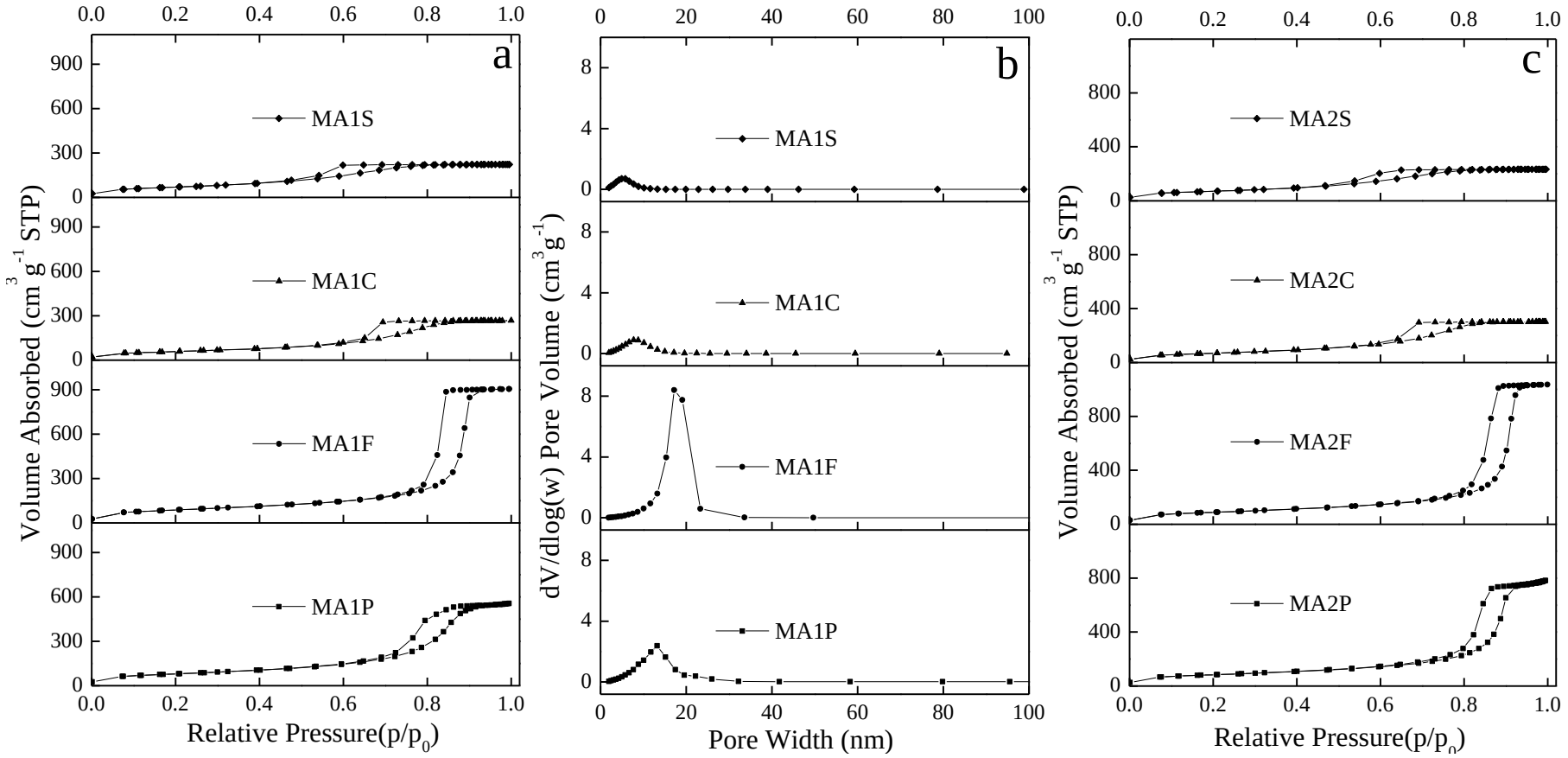

Figure 4-2 Nitrogen physisorption isotherms (a, c, e) and corresponding pore size distributions (b, d, f) of MA*x*A

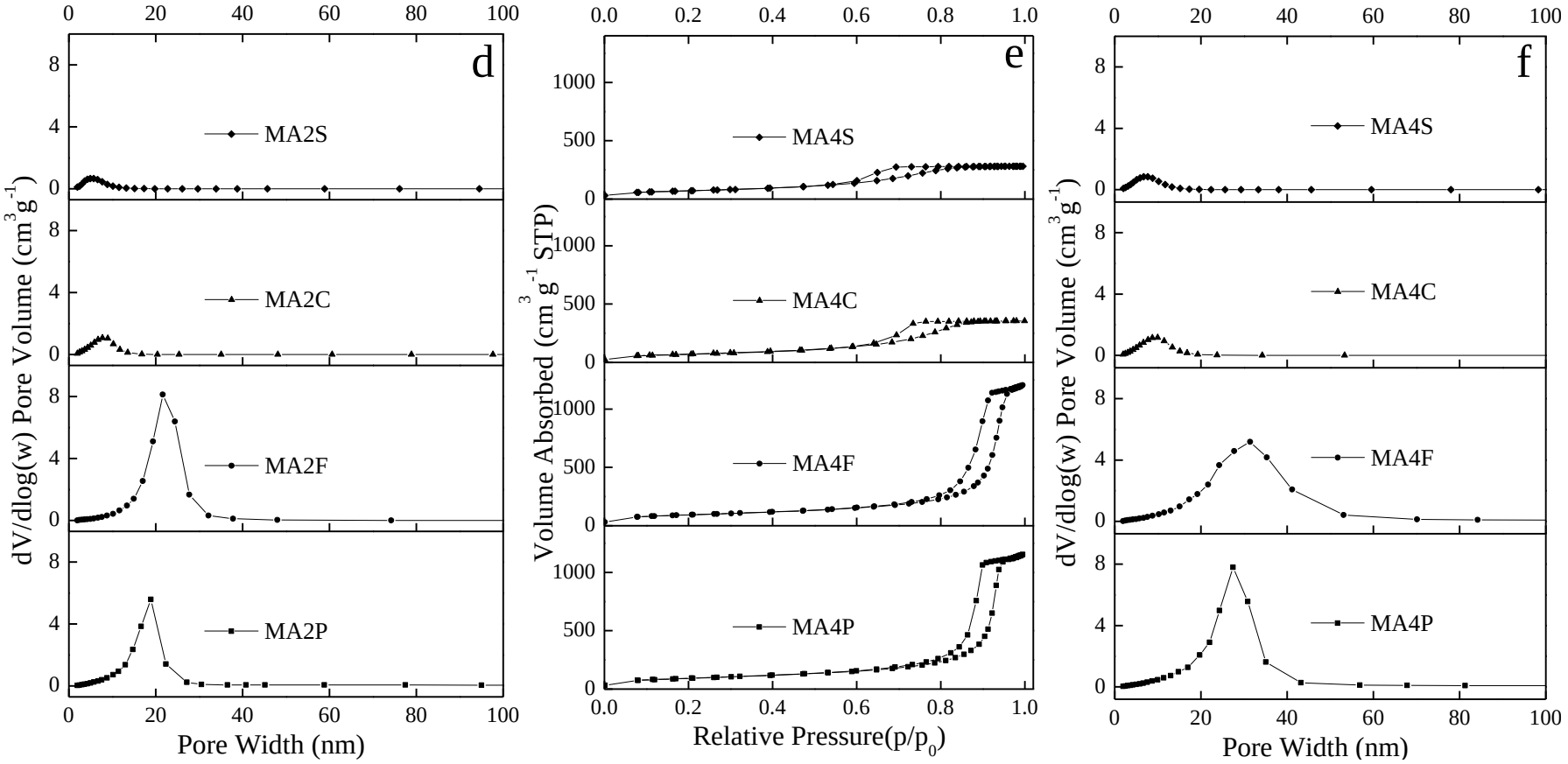

Figure 4-2 Nitrogen physisorption isotherms (a, c, e) and corresponding pore size distributions (b, d, f) of MA*x*A (to be continued)

Specifically, for MA1A, the BET surface area increased from 236 m^2g^{-1} of MA1S, 241 m^2g^{-1} of MA1C and 287 m^2g^{-1} of MA1P to 309 m^2g^{-1} of MA1F. The same trend can be also observed over MA2A and MA4A and the highest BET surface area reached 358 m^2g^{-1} of MA4F. Similarly, the largest pore volume 1.9 cm^3g^{-1} was obtained over MA4F, followed by MA4P (1.8 cm^3g^{-1}), MA4C (0.6 cm^3g^{-1}) and MA4S (0.4 cm^3g^{-1}). A clear shift of the condensation steps occurring in the hysteresis loops to greater relative pressures is evident in Figure 4-2 (a, c, e), suggestive of larger mesopores in the identical sequence of MA*x*F > MA*x*P > MA*x*C > MA*x*S. This pattern is consistent with the corresponding PSD curves in Figure 4-2 (b, d, f).

Figure 4-3 shows the TG-DTA curves of MA0A, MA1A and MA1P*y*AlB. A 4-step reaction mechanism has been proposed to explain the thermal transformation of nanocrystalline boehmite into alumina (Bleta *et al.* 2012), involving: (1) removal of physically adsorbed water at around 90 ℃ ~ 100 ℃; (2) removal of chemisorbed water up to 200 ℃; (3) conversion of boehmite into transition alumina at around 380 ℃; and (4) dehydration of transition alumina (due to the removal of residual hydroxyl groups ending with crystallization in α-alumina).

Evidently, the addition of SDAs had a marked effect on the thermal decomposition process. For MA1P and MA1F, they showed similar TG-DTA curves. A sharp exothermic peak was observed with the maxima at ca. 200 ℃ on the DTA curves of both MA1P and MA1F, also accounting for a weight loss of about 25% and 50% in the corresponding TG curves, respectively. This exothermic peak was believed to be associated with the decomposition and removal of the embedded P123 and F127 (Liu *et al.* 2008; Cai *et al.* 2011). The remaining weight loss before the levelling off in the 250 ℃ – 400 ℃ range was attributed to the dehydroxylation of the OH- groups and the conversion of hydrated alumina into transitional alumina (Cai *et al.* 2011; Bleta *et al.* 2012).

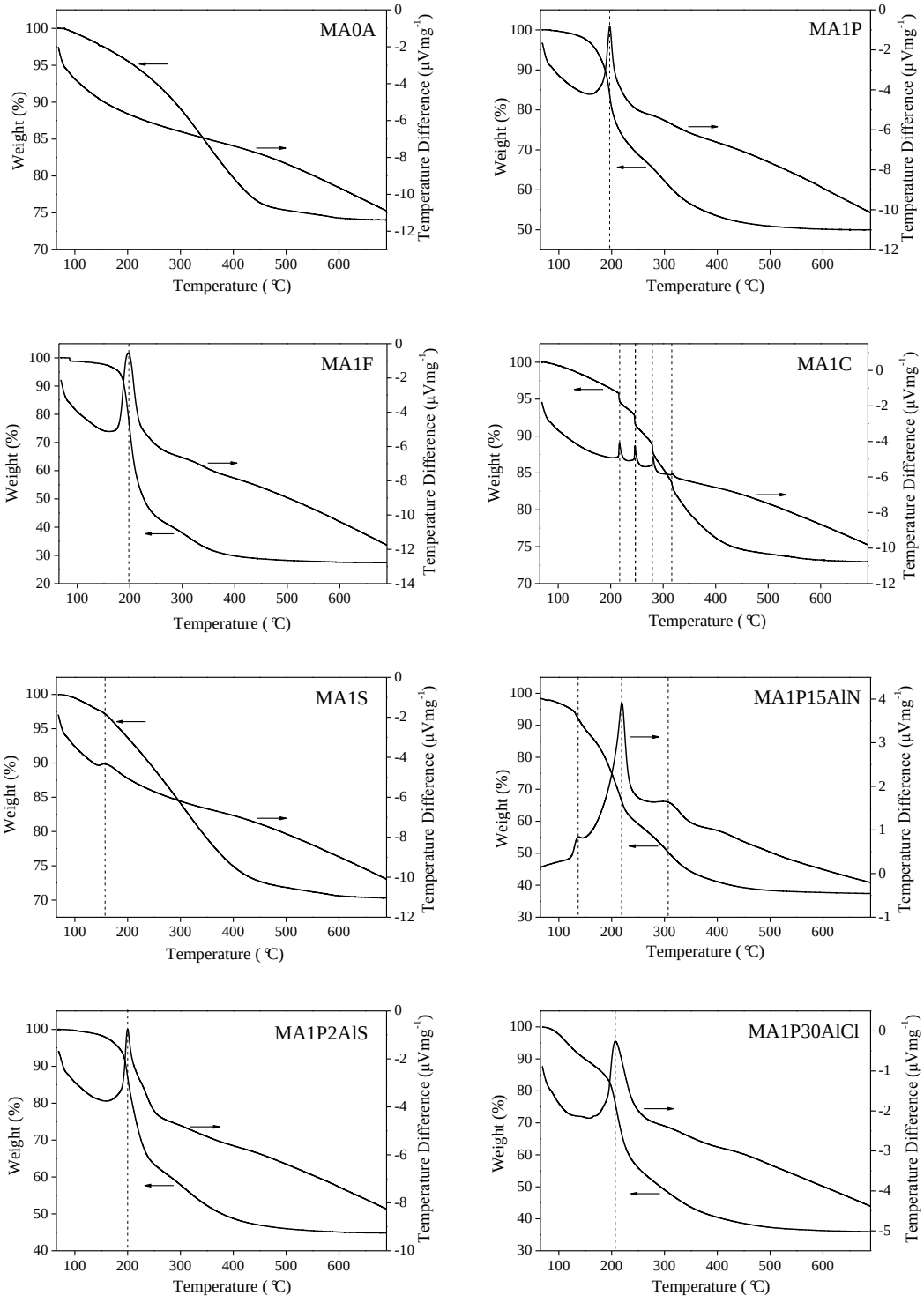

Figure 4-3 TG-DTA curves for MA0A, MA1P, MA1F, MA1C, MA1S, MA1P15AlN, MA1P2AlS and MA1P30AlCl

In comparison, there were no similar peaks observed for MA0A, and instead, a gradual trend with a total weight loss of 25% was presented. An analogous TG-DTA curve was found for MA1S, with only a small exothermic peak occurring at around 170 ℃.

However, it should be noted that MA1C showed a distinct TG-DTA curve. Four exothermic peaks in the 200 ℃–320 ℃ range were clearly evident, believed to be caused by the decomposition and oxidation of CTAB, which was consistent with the literature report elsewhere (Ramimoghadam *et al.* 2012). A further analysis of the TG-DTA curves of MA1P*y*AlB will be discussed in Section 4.2.4 below.

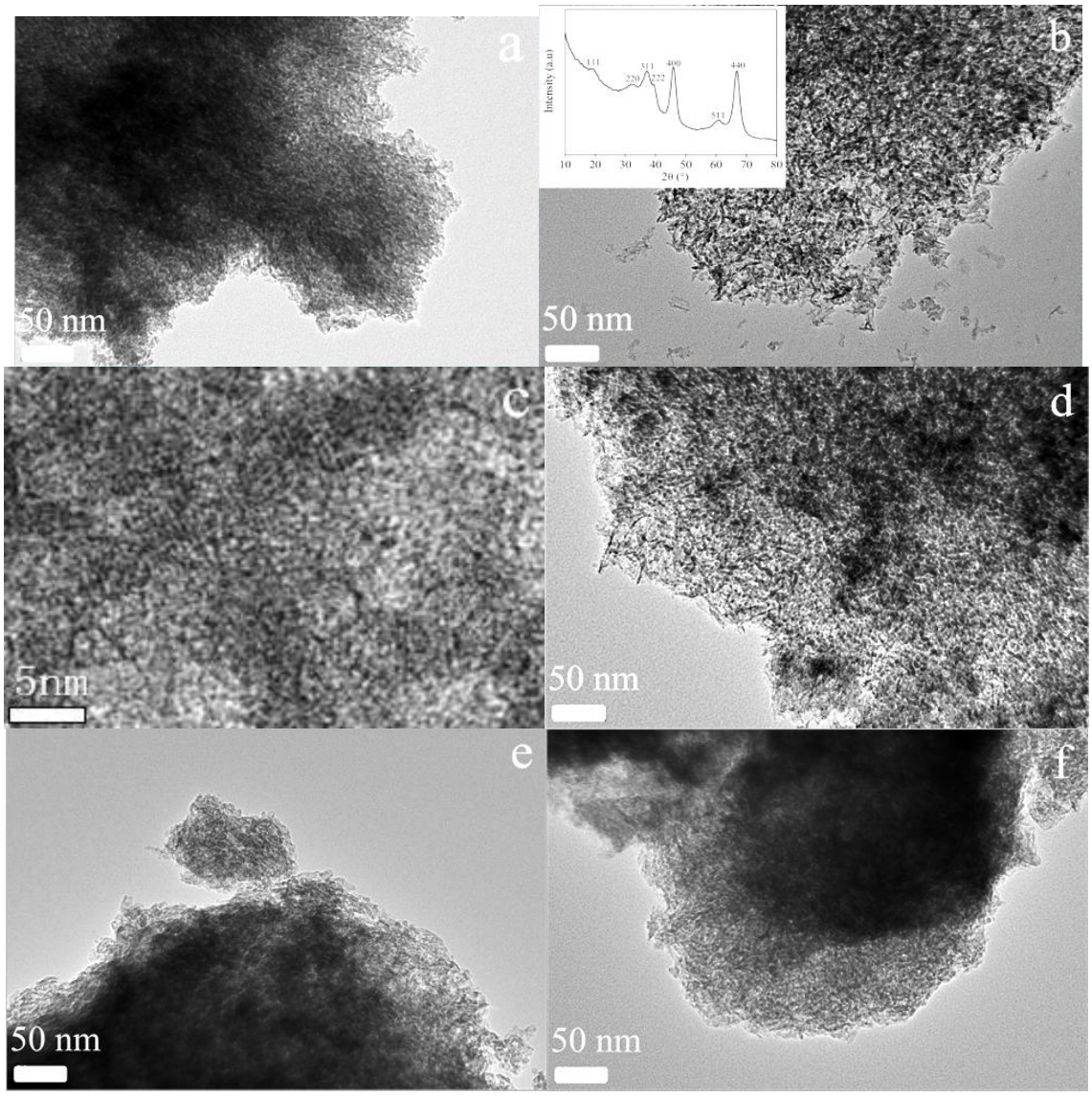

Figure 4-4 TEM images of (a) MA0A, (b) MA1P, (d) MA1F, (e) MA1C and (f) MA1S, (c) HRTEM image of MA1P, the insert in (b) is the wide-angle XRD pattern of MA1P

Figure 4-4 shows TEM images of the synthesised MA samples. MA0A (Figure 4-4a), prepared in the absence of template, presented a dense structure with irregular shape. Similar nano-scale morphology was observed for MA1C (Figure 4-4e) and MA1S

(Figure 4-4f). These MAs were mainly composed of closely packed adjacent nanoparticles. This observation was in line with their structural properties shown in Table 4-2, where MA0A, MA1C and MA1S presented similar BET surface areas, pore volumes and pore sizes. In contrast, MA1P (Figure 4-4b) and MA1F (Figure 4-4d) displayed a lath-like or a scaffold-like configuration, though no significant ordering in the pore arrangement could be observed. Such porous structure arose from the entanglement of nanolaths (Bleta *et al.* 2012).

Though remarkable differences in the structural properties and nano-scale morphology have been observed over the MAs prepared with different templates, their XRD patterns were almost identical (Figure 4-4b inset). Therefore, it is considered that the addition of different SDAs in the boehmite colloidal sols did not affect the crystalline microstructure of the resulting MAs. Rather, they only acted on the organisation of the crystallites. This is consistent with the report by Bleta and co-workers (Bleta *et al.* 2012), where MAs prepared using P123 and F127 showed virtually the same XRD pattern. Herein, all the MAs showed a highly crystalline diffraction pattern, indicating the crystallization of the amorphous framework to either γ-alumina or η-alumina. Considering the calcination temperature of 700 ℃ other than 1000 ℃, the pattern refers to γ-alumina (JCPDS Card No. 10-0425). Additional proof for the high crystallinity was found from the HRTEM image of MA1P (Figure 4-4c), where the presence of crystalline nanoparticles with well-defined lattice planes can be clearly observed.

The self-assembly of boehmite particulates is actually a condensation process, during which the cross-linked aluminium species can arrange around the SDAs to form the ordered mesophases (Pérez *et al.* 2013). The addition of surfactants can induce crystal growth following a layer-by-layer self-assembly mechanism or a surfactant-induced fibre formation (SIFF) mechanism (H. Y. Zhu 2002). Initially, before thermal treatment, the colloidal sol was composed of crystallized boehmite (Bleta *et al.* 2012). In the

absence of a template, boehmite can only form anhedral laths which assemble into a compact structure upon calcination, as evidenced by the TEM image in Figure 4-4a. In contrast, with the aid of a template, boehmite nanocrystallites can act as "building blocks" to form a meso-structure consisting of loosely stacked boehmite particles, leading to large pore volumes and pore sizes of the resulting MAs. This mechanism is thought to be analogous to the formation of the boehmite-surfactant "sandwich" structure, in which the template might intercalate into the boehmite layers to generate a randomly packed boehmite-surfactant sandwich-like structure (Liu *et al.* 2008). For the nonionic templates P123 and F127, the formation of boehmite nanorods can be ascribed to the *in-situ* micelle templating mechanism, whereby the surfactant molecules self-aggregated into bundle-like micelles and then act as the templates during the assembly process (Cai *et al.* 2012). The hydrophilic PEO head groups of P123 and F127 can weakly interact with the surface hydroxyl groups of boehmite layers through hydrogen bonding (Liu *et al.* 2008; Bleta *et al.* 2012). In addition, driven by the weak coordination bonding, the alkylene oxide segments of P123 and F127 can form a crown-ether-type complex with the boehmite particles (H. Y. Zhu 2002). Such hydrogen bonding and coordination bonding can effectively induce the stacking of boehmite colloids (Liu *et al.* 2008).

An important note for the different impact of P123 and F127 on the structural properties of the resultant MAs is closely correlated to the length of their hydrophilic and hydrophobic chains (González-Peña *et al.* 2005; Cai *et al.* 2011). F127 ($EO_{106}PO_{67}EO_{106}$) is predominantly composed of ethylene oxide chain, especially in comparison to P123 ($EO_{20}PO_{70}EO_{20}$). For F127, more hydrophilic EO chain relative to hydrophobic propylene oxide chain means a larger hydrophile-lipophile balance (HLB) value. It has been proven that an increase in the HLB value of surfactant molecules would facilitate and favour the hydrogen bonding between the EO chains and the

hydroxyl group bonded to Al nanoparticles. This could then promote the degree of surfactant aggregation, and thus affect the textural development (González-Peña *et al.* 2005). The surface area, pore volume and pore size of the MAs synthesised using a number of surfactants with different HLB values substantially increased with increasing HLB value (González-Peña *et al.* 2005). This is consistent with the variations observed over the MA*x*F and MA*x*P samples in this study.

However, compared with the nonionic counterparts (P123 and F127), neither the cationic template CTAB nor the anionic template SDS showed an equivalent capability in modulating the structural properties of the resulting MAs. As evidenced by the nitrogen physisorption isotherms and TEM imaging, upon the introduction of CTAB and SDS into the synthesis medium, the obtained MAs presented limited improvement in the structural properties. For instance, for MA20S with the largest addition amount of the template, only a relatively low surface area of 260 m^2g^{-1}, pore volume of 0.5 cm^3g^{-1} and pore size of 8.6 nm were attained.

Obviously, the structural properties of MAs prepared from the boehmite/surfactant aqueous system depend largely on the surfactant type. An evident and clear trend can be summarised in that the pore size, pore volume and BET surface area of MA samples using F127, P123, CTAB and SDS as the templates exhibited in the descending order of MA*x*F > MA*x*P > MA*x*C > MA*x*S (*x*=1, 2, 4). The employment of the nonionic surfactants P123 and F127 led to much improved structural properties compared with the cationic CTAB and anionic SDS.

4.2.3 Amount of Template Addition

The effect of template addition on the structural properties of MAs using the four templates, respectively, was also investigated. A series of MA*x*A samples were prepared accordingly. The nitrogen physisorption isotherms and the PSD curves are shown in

Figure 4-5 (a, c, e, g) and Figure 4-5 (b, d, f, h), respectively. Table 4-2 summarises the structural properties. As mentioned above, MA0A prepared without template showed very low nitrogen adsorption volume and mainly consisted of the interpenetrated particles with low regularity, which densely cohered to each other.

However, with an increase in the surfactant concentration, irrespective of surfactant type, the nitrogen adsorption volume was generally enhanced, indicating a marked improvement in the porosity. The isotherms of MA*x*P and MA*x*F presented the H1 hysteresis loops, while MA*x*C and MA*x*S showed the H2 hysteresis loops. As interpreted in Section 4.2.2, this signifies that the agglomeration of boehmite particulates in MA*x*P and MA*x*F was more uniform and regular in porous structures. Furthermore, F127 and P123 were more competent to induce greater changes in terms of the control of structural properties of MA.

It is evident from Table 4-2 that the structural properties of MAs were strongly affected by the addition of P123 and F127. From MA0A to MA4P and MA4F, increasing trends in the BET surface area (from 236 m^2g^{-1} to 325 m^2g^{-1} and 358 m^2g^{-1}), V_p (from 0.4 cm^3g^{-1} to 1.8 cm^3g^{-1} and 1.9 cm^3g^{-1}), D_a (from 5.2 nm to 19.3 nm and 20.8 nm) and D_p (from 7.0 to 28.2 nm and 30.1 nm) were observed, respectively. Further addition of P123 and F127 resulted in MAs with larger surface areas, pore volumes and pore sizes. Moreover, the adsorption and desorption branches of the hysteresis loops for MA*x*P and MA*x*F were nearly parallel and almost perpendicular to the relative pressure axis, suggestive of the uniformly agglomerated boehmite particulates (Sing 1985; Grant *et al.* 2012).

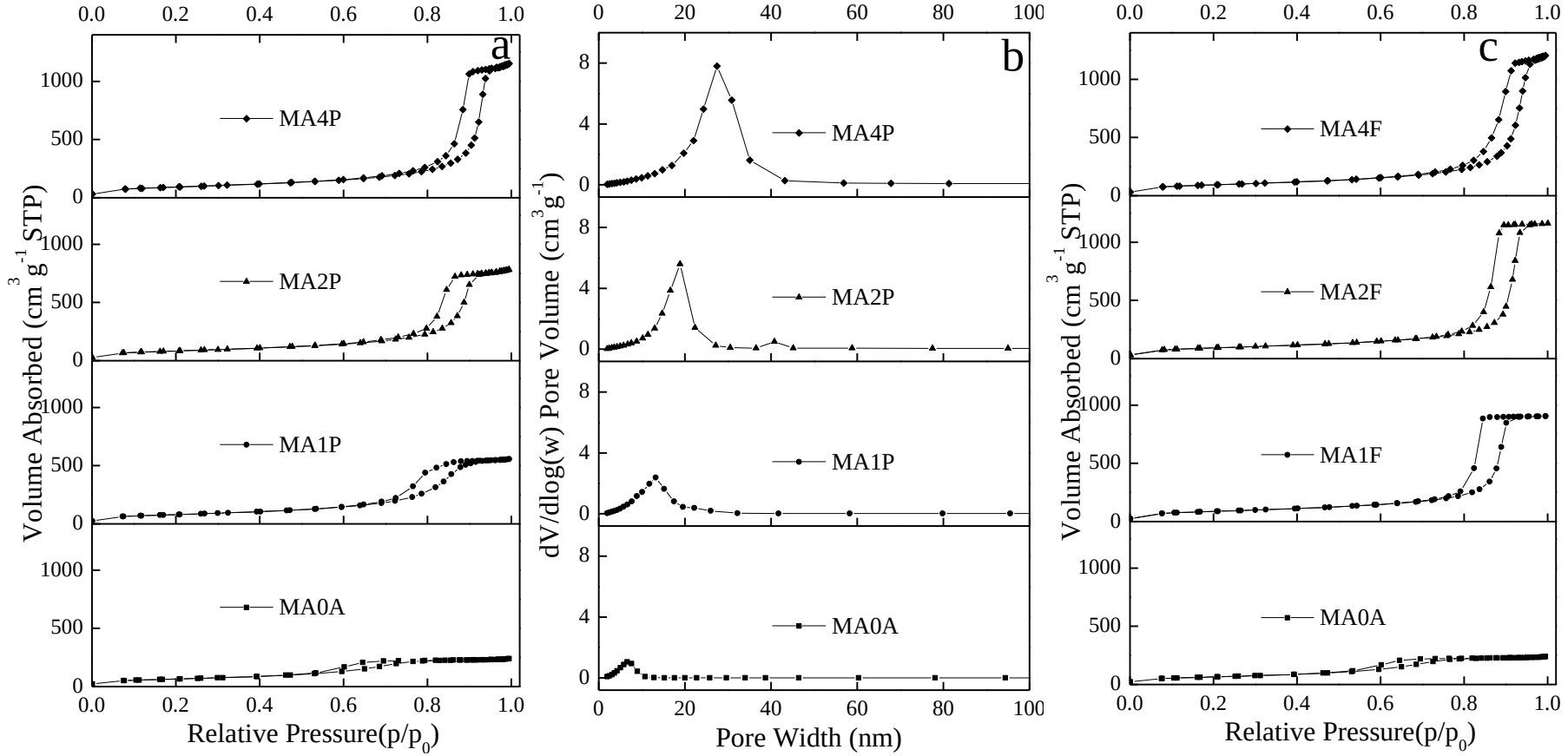

Figure 4-5 Nitrogen physisorption isotherms (a, c, e, g) and corresponding pore size distributions (b, d, f, h) of MA*x*A

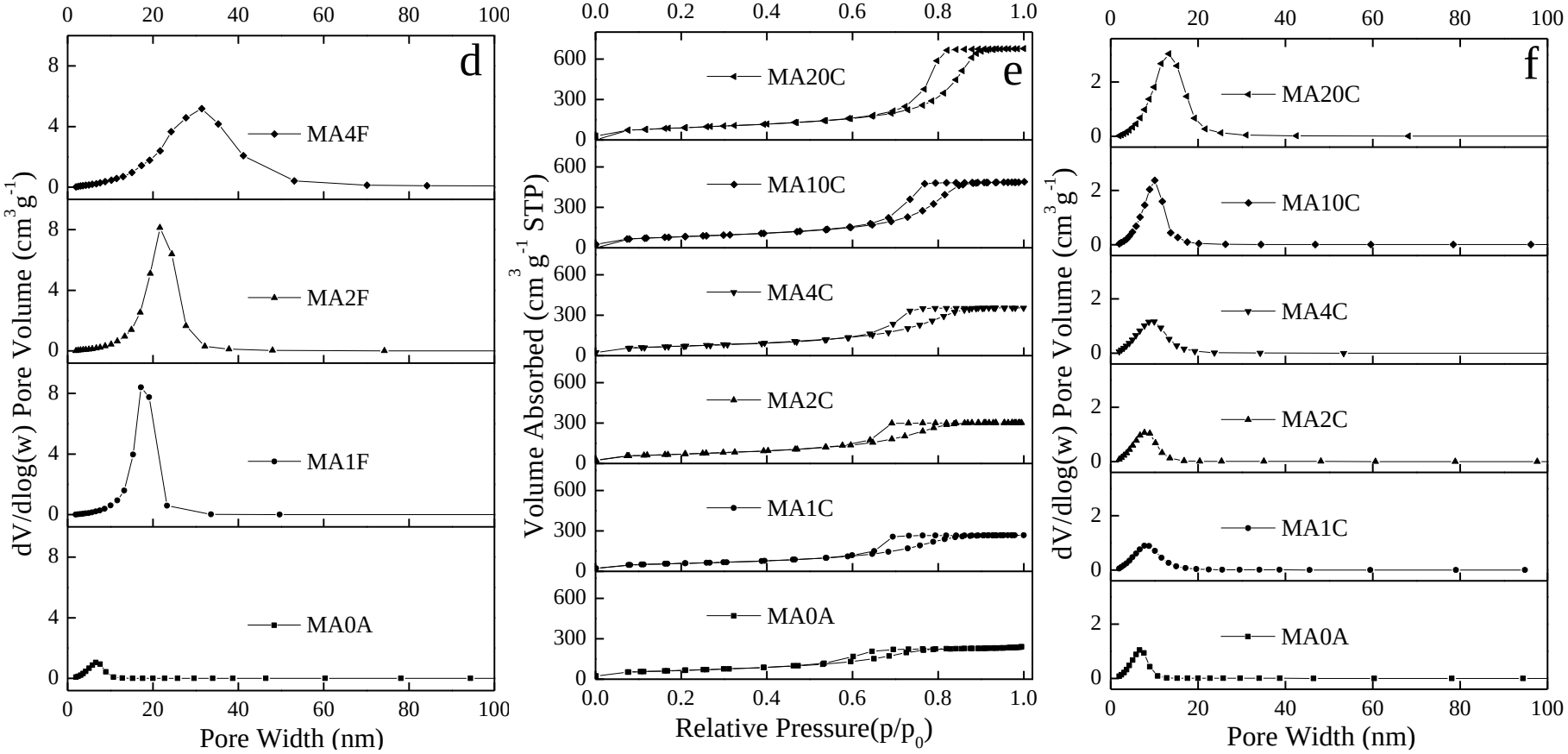

Figure 4-5 Nitrogen physisorption isotherms (a, c, e, g) and corresponding pore size distributions (b, d, f, h) of MA*x*A (to be continued)

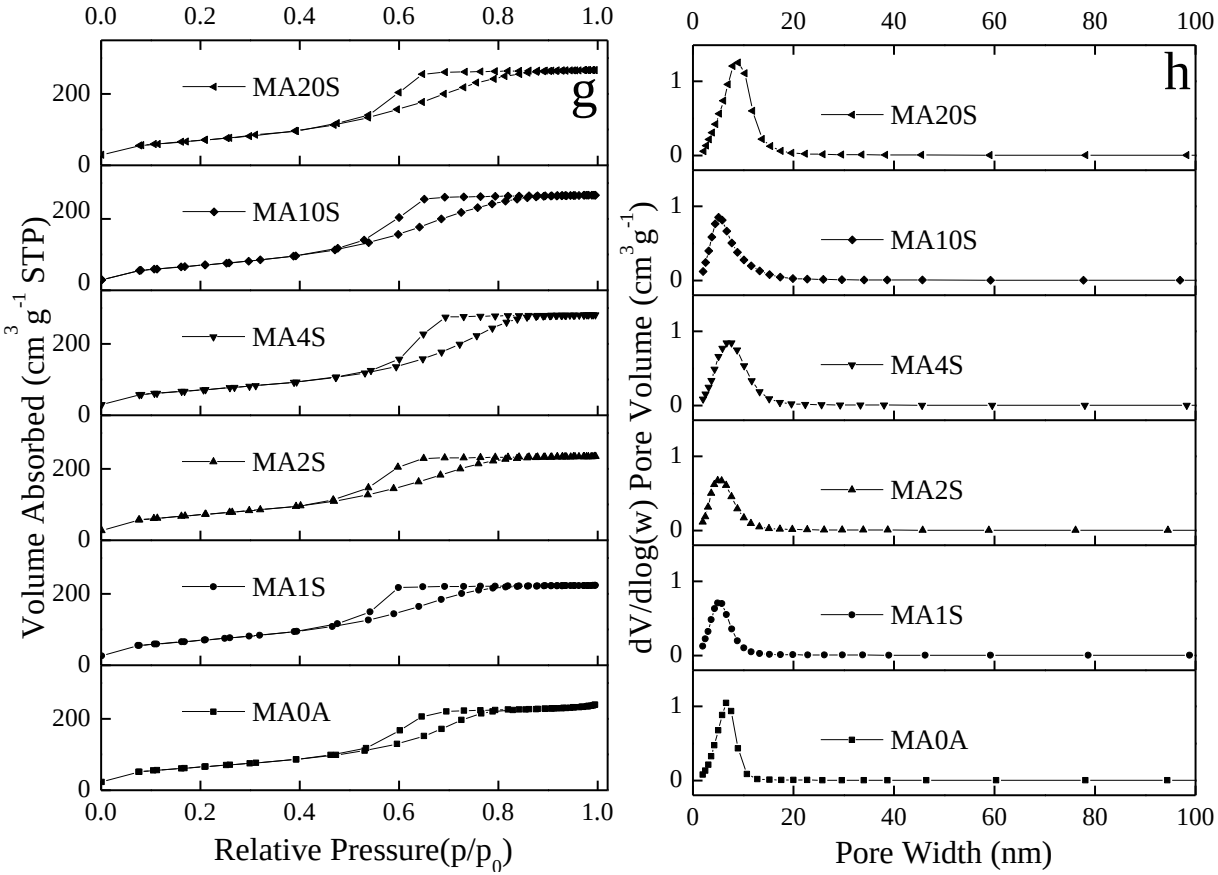

Figure 4-5 Nitrogen physisorption isotherms (a, c, e, g) and corresponding pore size distributions (b, d, f, h) of MA*x*A (to be continued)

However, it is worth noting that the PSD curves broadened with increasing template addition. A relatively narrow PSD could be attained when the pore size was increased from 7.0 nm for MA0A up to 28.2 nm for MA4P. But in the case of MA4F, though D_p reached 30.1 nm, the broadening was particularly evident, indicating a gradual deficiency of uniformity in the pore arrangement. This may be attributed to the micellization of the triblock copolymer surfactant, which could bring about significantly increased solution viscosity, and thus reduce the mobility of the nanoparticles and hinder the subsequent self-assembly process (Peng Bai 2007). As a result, with increasing addition of P123 and F127, especially for MA4F, the PSD became progressively broader.

In contrast, upon the introduction of the template, MA*x*C showed a similar but much gentler trend while MA*x*S was quite stable. Specifically, from MA0A to MA4C, the BET surface area, pore volume and pore size gradually increased from 236 m^2g^{-1} to 258 m^2g^{-1}, 0.4 cm^3g^{-1} to 0.6 cm^3g^{-1} and 7.0 nm to 9.2 nm, respectively. More significant changes were observed when the CTAB content was further increased. For MA20C, the BET surface area, pore volume and pore size finally reached 319 m^2g^{-1}, 1.1 cm^3g^{-1} and 13.4 nm. However, within the identical range of the SDS addition amounts, the structural properties of MA*x*S seemed to be hovered, stuck at around 250 m^2g^{-1}, 0.5 cm^3g^{-1} and 6.0 nm, respectively. For MA*x*S, there was no comparable strong impact of template addition on the structural properties of MA.

Figure 4-6 suggests that, with an increase in the template addition from MA1A to MA4A, almost the same nano-scale morphology of MA was retained. MA1P, MA4P, MA1F and MA4F displayed a lath-like or scaffold-like configuration without noticeable ordering in the pore arrangement. MA4C and MA4S still showed a similar compact structure to that of MA1C and MA1S. However, for MA20C and MA20S, owing to the further increase in the template addition, three-dimensional interconnected scaffold-like

mesostructured MAs were obtained. Hence, the abundant nanospace between the interpenetrated particles created by increased template addition could be conducive to the improvement in porosity.

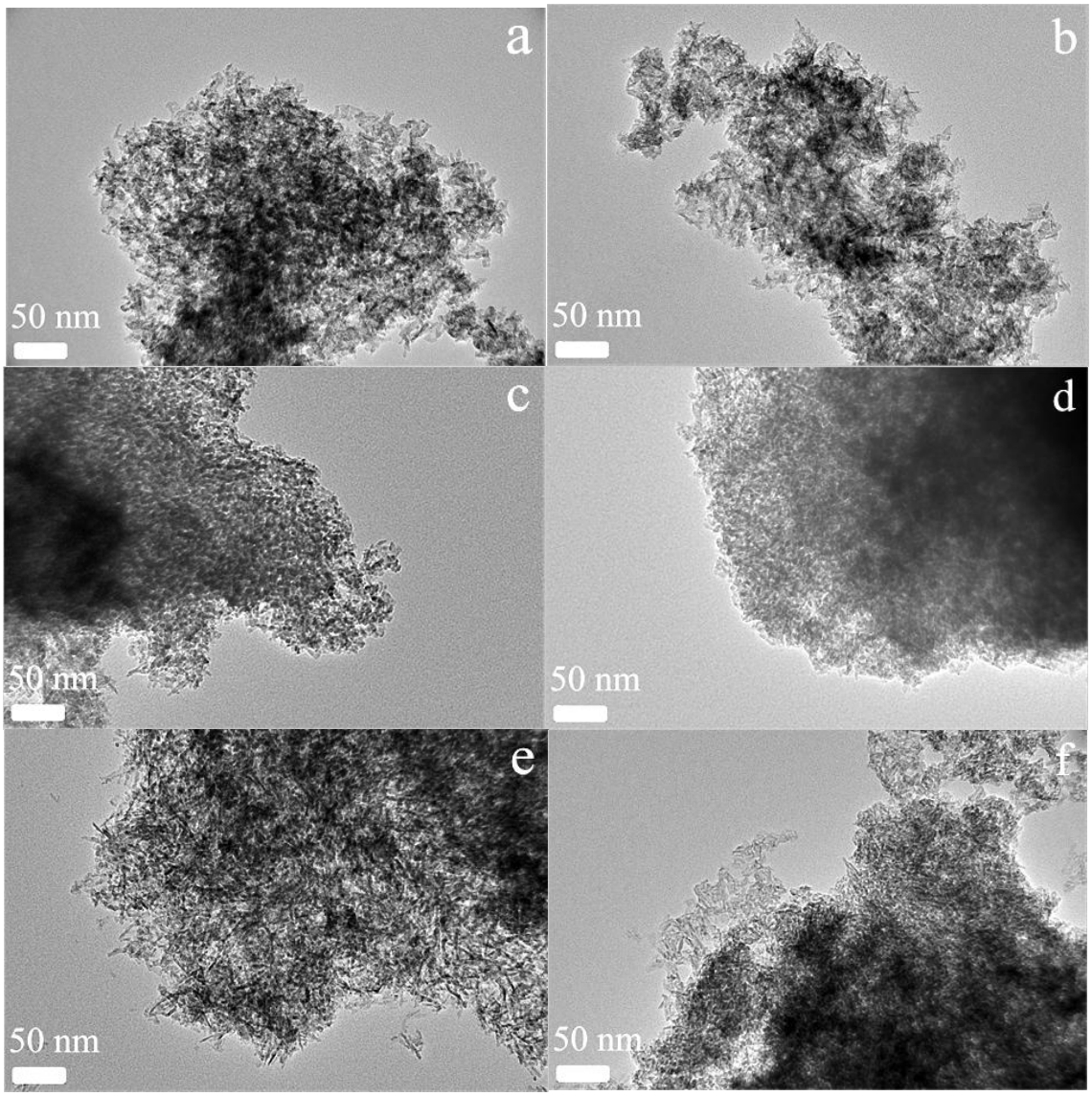

Figure 4-6 TEM images of (a) MA4P, (b) MA4F, (c) MA4C, (d) MA4S, (e) MA20C and (f) MA20S

4.2.4 Doping of Inorganic Aluminium Precursor

$Al(NO_3)_3$, $AlCl_3$ and $Al_2(SO_4)_3$ were employed in this study to investigate the effect of the doping ratio of inorganic aluminium precursors on the structural properties of MAs. The nitrogen physisorption isotherms and corresponding PSD curves for a series of MAs with varying doping ratios are shown in Figure 4-7. Increasing the fractions of

$Al(NO_3)_3$ and $AlCl_3$ substitution in the total Al up to 15% and 30% led to a substantial increase in the pore volume and pore diameter, from 0.9 cm^3g^{-1} and 13.9 nm for MA1P to 1.1 cm^3g^{-1} and 22.4 nm for MA1P15AlN and then to 1.1 cm^3g^{-1} and 26.6 nm for MA1P30AlCl, with relatively narrow PSDs. A higher adsorption uptake of N_2 seen in Figure 4-7a and Figure 4-7e confirms the larger pore volumes of MA1P15AlN and MA1P30AlCl, while the clear shift of the capillary condensation steps to greater relative pressures signifies the increased pore sizes. However, a further rise in the doping ratios of $Al(NO_3)_3$ and $AlCl_3$ to 20% and 35% resulted in further expansion of pore size. This change also caused a significant fall in the surface area (from 287 m^2g^{-1} for MA1P to 178 m^2g^{-1} and 197 m^2g^{-1} for MA1P20AlN and MA1P35AlCl, respectively) and pore volume (from 0.9 cm^3g^{-1} to 0.7 cm^3g^{-1} and 0.8 cm^3g^{-1}) accompanied by much broader PSD curves, indicating the collapse of mesoporosity.

Therefore, 15% and 30% are probably the optimal substitution ratios of $Al(NO_3)_3$ and $AlCl_3$ in terms of the controlling of the structural properties of MAs to achieve high surface area, large pore volume and expanded pore size with a narrow PSD. However, for MA1P*y*AlS, only 2% doping of $Al_2(SO_4)_3$ could be withstood by evaluating the changes in structural properties. The substitution of $Al_2(SO_4)_3$ in the total Al to 3% gave rise to a broad and disordered PSD, suggestive of the noticeably reduced uniformity in pore arrangement.

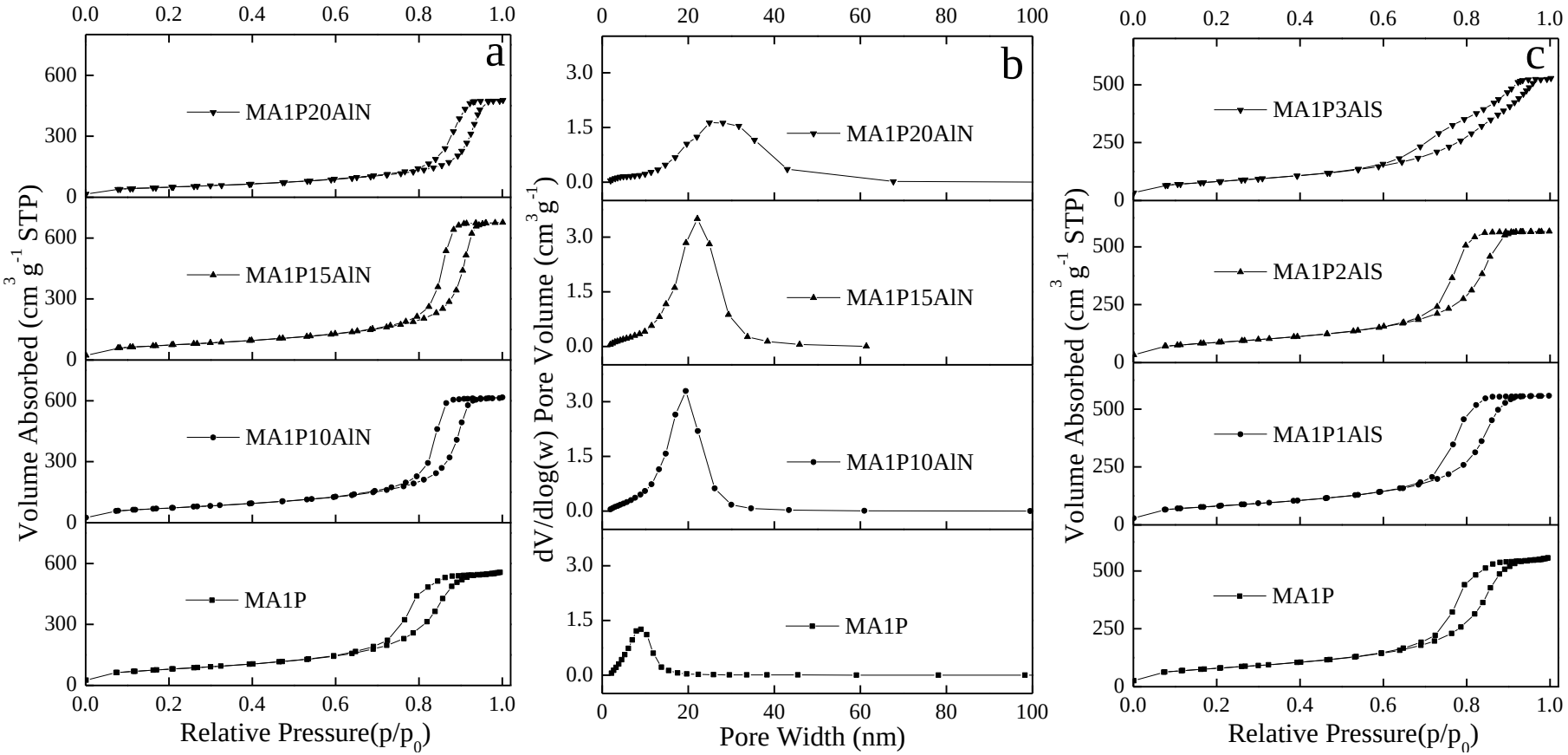

Figure 4-7 Nitrogen physisorption isotherms (a, c, e) and corresponding pore size distributions (b, d, f) of MA1P*y*AlB

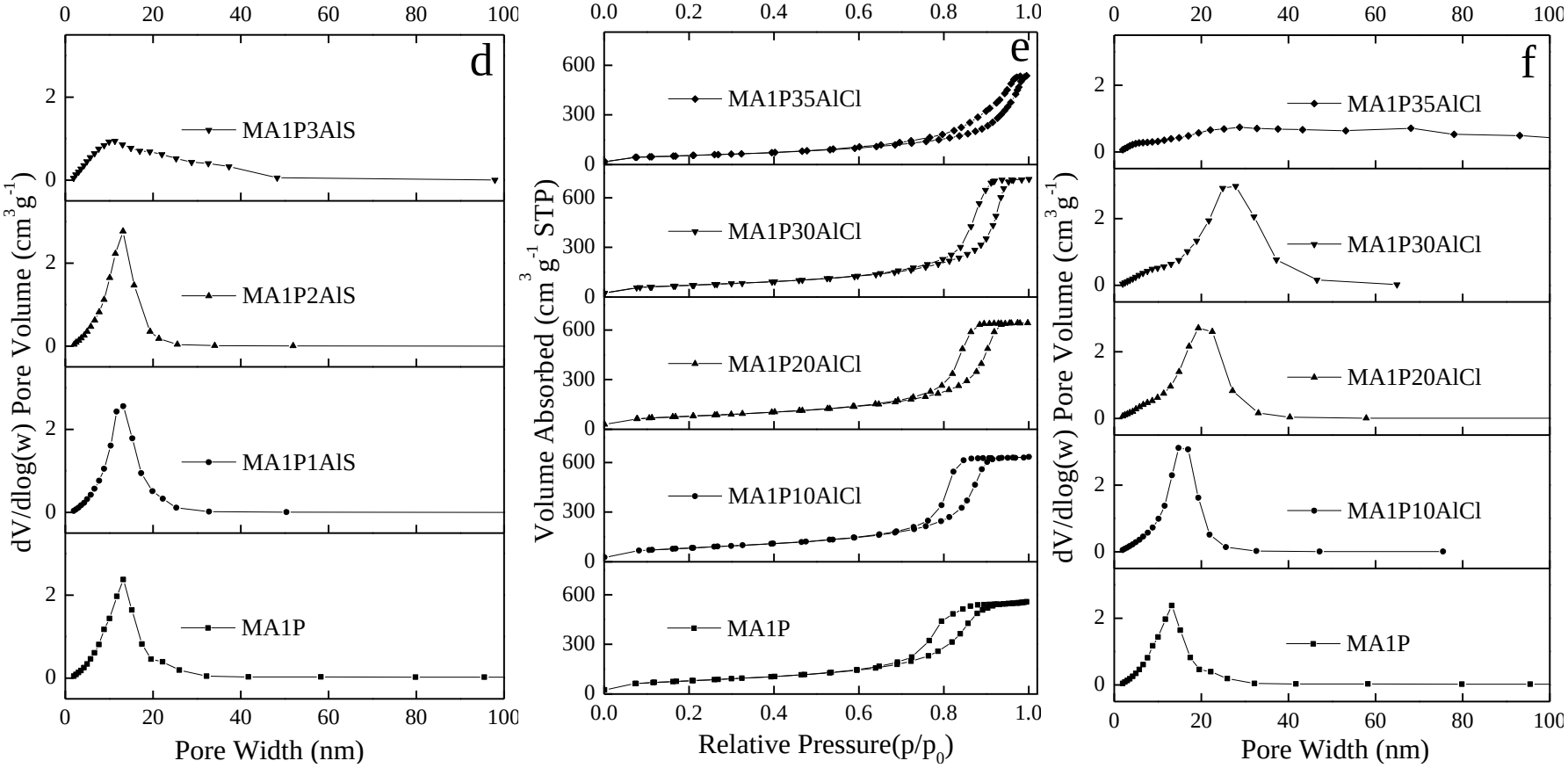

Figure 4-7 Nitrogen physisorption isotherms (a, c, e) and corresponding pore size distributions (b, d, f) of MA1P*y*AlB (to be continued)

The corresponding TG-DTA curves seen in Figure 4-3 are quite similar to those of MA1P, especially for MA1P30AlCl and MA1P2AlS. The sharp exothermic peaks at around 200 ℃ can be explained by the removal of template P123. The remaining weight loss starting from 250 ℃ was attributed to the transformation of Al_2O_3 from boehmite to γ phase. The characteristic feature of MA1P15AlN was an unique exothermic step centered around 135 ℃, ascribed to the decomposition of $Al(NO_3)_3$. The TEM images of MA1P15AlN, MA1P30AlCl and MA1P2AlS in Figure 4-8 showed the same morphology as that of MA1P with a lath-like or a scaffold-like configuration.

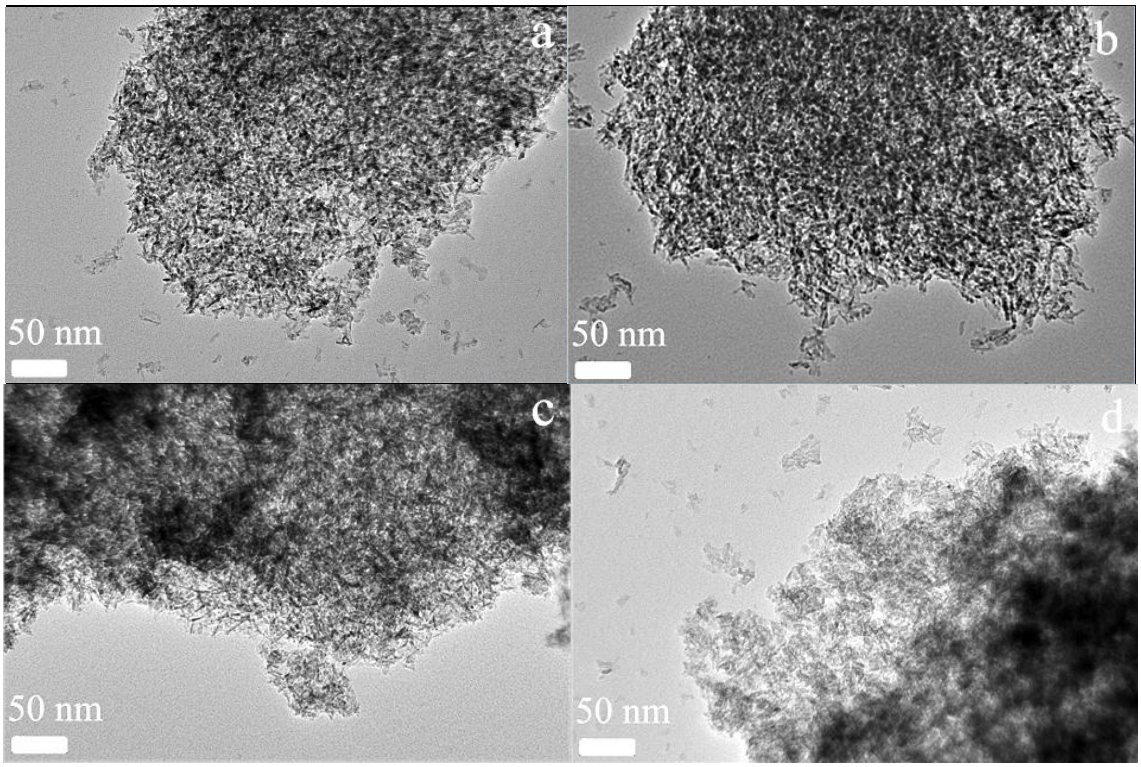

Figure 4-8 TEM images of (a) MA1P, (b) MA1P15AlN, (c) MA1P2AlS and (d) MA1P30AlCl

Clearly, the impact of different inorganic aluminium precursors on the structural properties of MA varied greatly, depending on the precursor type and doping ratio. The role of NO_3^- in the synthesis system was reported to improve the overall acidity as a consequence of the hydrolysis of Al^{3+}, which generates H^+. Then the decreased pH facilitated the interaction between the PEO blocks and aluminium precursors and also

increased the micelle size, resulting in larger pore size and pore volume. However, a further increase in acidity as a result of the doping of $Al(NO_3)_3$ over 15% may hinder the structure condensation, leading to disordered MAs.

It was reported that the radius and charge of the anions can profoundly influence the assembly process (Cai *et al.* 2011; Cai *et al.* 2011; Alphonse *et al.* 2013). Herein, NO_3^- has a weaker complexation ability than that of Cl^- as the ionic radius of NO_3^- (206 pm) is larger than Cl^- (183 pm). Therefore, Cl^- can more strongly coordinate with Al^{3+} and consequently suppress the participation of Al^{3+} in the assembly process, thus leading to larger pore size and pore volume and possibly partial collapse of the mesostructure. On the other hand, the volatility of HCl in the synthesis system is higher than that of HNO_3, so the acidity of the $AlCl_3$ added system reduces more quickly than that of $Al(NO_3)_3$. As mentioned before, the reduction in acidity can result in smaller pore size and pore volume. Therefore, the high volatility of HCl compared to HNO_3 not only reduces the system acidity, thus leading to smaller pore size and pore volume of the resulting MAs, but also decreases the concentration of Cl^- in the synthesis system, which alleviates the coordination of Cl^- with Al^{3+}. This explains why MA1P10AlCl and MA1P20AlCl showed smaller pore sizes and pore volumes than those of MA1P10AlN and MA1P20AlN. Therefore, in the case of MA1P*y*AlCl, the effect of the doped $AlCl_3$ on the structural properties of MAs was determined by the balance between the coordination of Cl^- with Al^{3+} and the evaporation of the generated HCl.

With regard to MA1P*y*AlS, it was reported that the greater the precipitating capacity of the anion, the more compact the alumina structure is obtained, owing to the compression of the double electric layer of the primary colloidal particles (Bai *et al.* 2009; Cai *et al.* 2012). Therefore, MAs prepared with $Al_2(SO_4)_3$ usually have denser structures (normally depicted as lower pore volume and smaller pore size) than those

synthesised from nitrate or chloride salts, which is consistent with the structural properties of MA1P*y*AlS shown in Table 4-2.

4.2.5 Calcination Temperature

The nitrogen physisorption isotherms and PSD curves of MA6P calcined at different temperatures of 500 ℃, 700 ℃, 900 ℃ and 1100 ℃ are shown in Figure 4-9 (a and b). Similarly, all the four curves are of Type IV with H1-shaped hysteresis loops, indicative of their uniform pores. It can be seen that the structural properties of MAs heavily depend on the calcination temperature. Specifically, an increase in the calcination temperature from 500 ℃ to 1100 ℃ caused a continuous increase in the pore size, but significant decreased the BET surface area and pore volume. Among them, MA treated at 500 ℃ has the largest BET surface area (409 m^2g^{-1}) and pore volume (2.5 cm^3g^{-1}). The decreasing N_2 uptake in Figure 4-9a clearly suggested the reduction in pore volume. The initial increase in the pore size of the samples calcined from 500 ℃ to 700 ℃ should be attributed to sample densification associated with local crystallization (Stacy M. Morris *et al.* 2008). As the calcination temperature continued to increase up to 1100 ℃, the variation in the pore size observed should be due to the shrinkage of the structure relating to the formation of larger irregular mesopores as a result of further densification and sintering (Q. Yuan 2008; Bleta *et al.* 2012). This change caused a significant broadening of the pore size distribution accompanied by a marked decrease in the surface area and pore volume. However, MA6P-1100 still showed a high surface area of 104 m^2g^{-1} and a large pore volume of 0.7 cm^3g^{-1}, confirming the good thermal stability of the resulting MAs. Generally, uniform and relatively narrow PSD (over 30.0 nm) can be maintained despite that the pore sizes of MA6P-T slightly increased with increasing calcination temperature except for sample MA6P-1100.

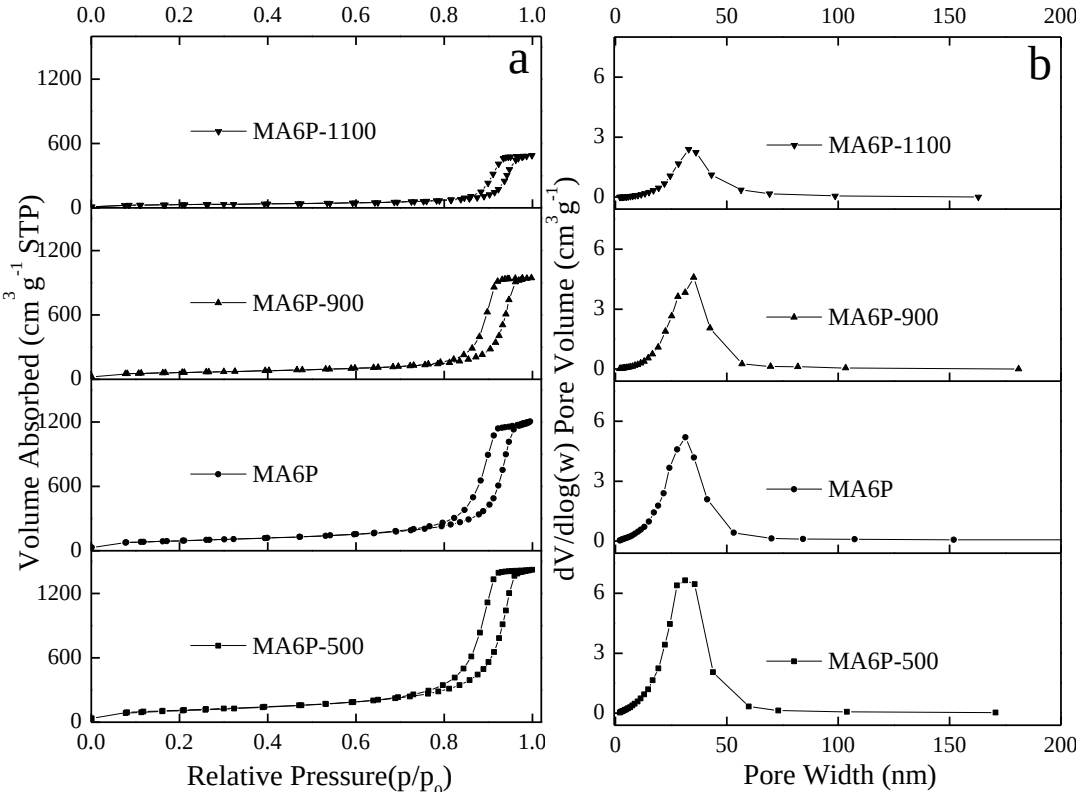

Figure 4-9 Nitrogen physisorption isotherms (a) and corresponding pore size distributions (b) of MA6P-T

Figure 4-10 shows the wide-angle XRD patterns of the MA6P-T samples. Calcination at 500 ℃ only gave rise to very mild peaks. But after the treatment at 700 ℃ or 900 ℃, sharper diffraction peaks were clearly observed, which indicated the crystallization of the amorphous framework to γ-alumina (JCPDS Card No. 10-0425). These changes observed on the samples calcined at 500 ℃ to 700 ℃ and 900 ℃ suggested that the crystallinity of MA was improved upon high-temperature treatment.

The selected area electron diffraction pattern of MA6P-900 in Figure 4-11c (the insert) exhibited a polycrystalline reflection ring pattern, corresponding to the characteristic diffuse electron diffraction rings (400), (440) and (311) of γ-alumina, verifying the high crystallinity of MA sample calcined at 900 ℃ (Bai *et al.* 2008; Q. Yuan 2008; Bai *et al.* 2009; Cai *et al.* 2011). Additional proof for the crystallinity of the framework is also evidenced by the HRTEM image of MA1P (Figure 4-4c). After calcination at 700 ℃,

the existence of crystalline nanoparticles with well-defined lattice planes (the measured lattice distance was ~0.38 nm) can be identified.

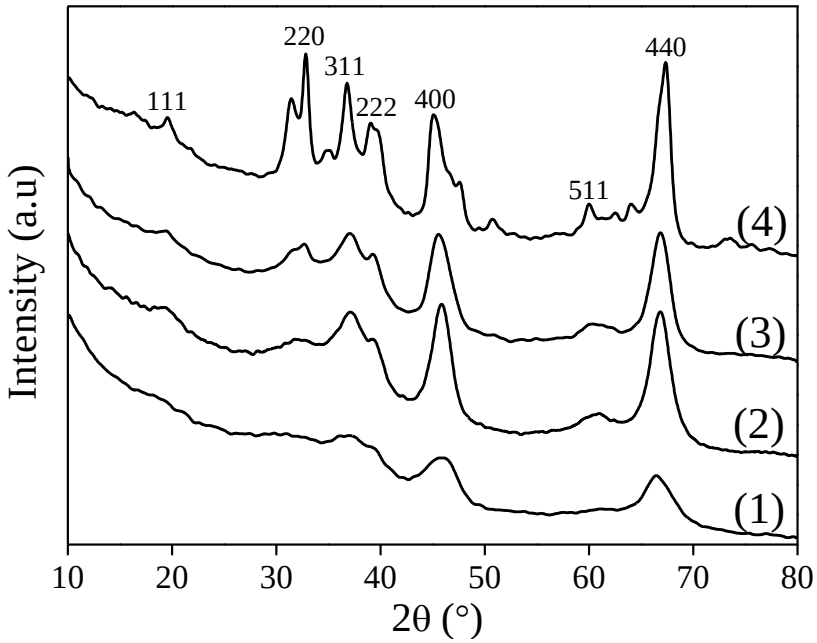

Figure 4-10 Wide-angle XRD patterns of (1) MA6P-500, (2) MA6P, (3) MA6P-900 and (4) MA6P-1100

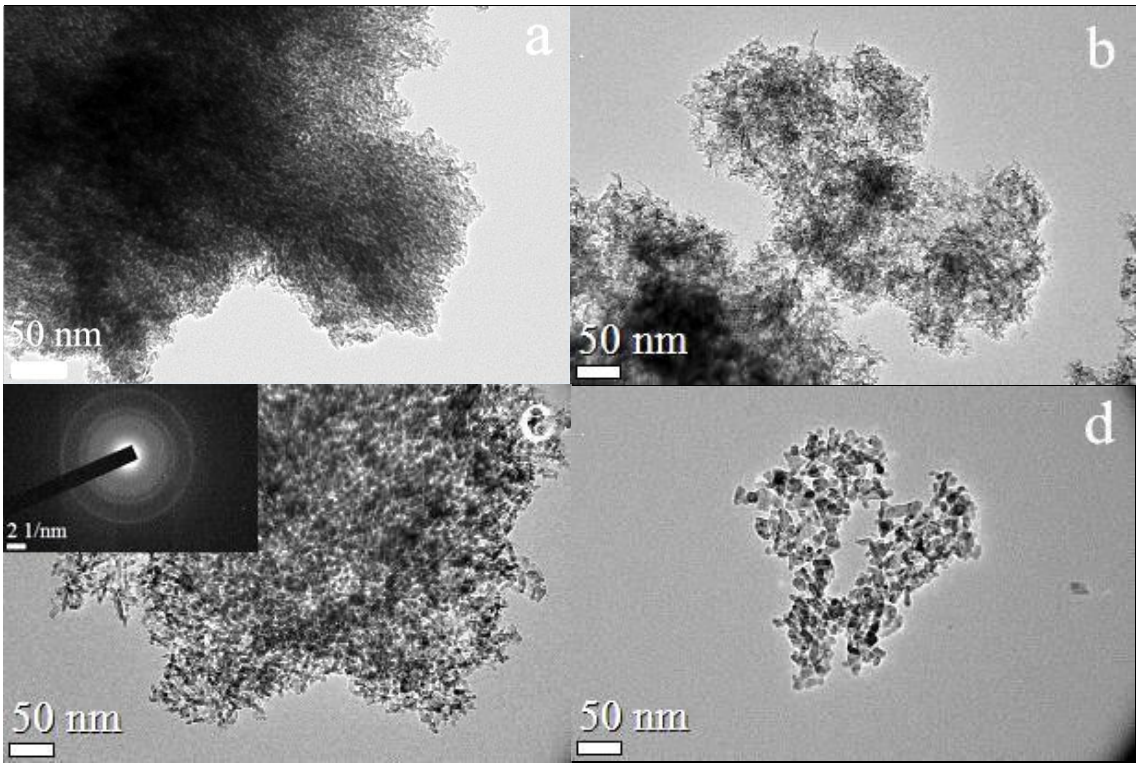

Figure 4-11 TEM images of (a) MA0P, (b) MA6P, (c) MA6P-900 and (d) MA6P-1100, respectively. The insert in (c) shows the selected area electron diffraction pattern of MA6P-900

However, calcination at 1100 ℃ resulted in the apparent additional diffraction lines associated with the formation of a new phase, most probably θ-Al_2O_3 (JCPDS Card 35-0121) coexisting with γ-Al_2O_3 (Bleta *et al.* 2012). This could be further confirmed by the morphological changes imaged by TEM. MA6P-1100 (Figure 4-11d) showed rough spherical shape due to sintering. It was markedly different from the images of MA6P (Figure 4-11b) and MA6P-900 (Figure 4-11c). The high thermal stability of MA should be closely related to the peculiar lath-like or scaffold-like morphology as the low contact areas between the platelet-like "building blocks" could effectively hinder the sintering (Liu *et al.* 2008).

4.3 Optimisation of the Structural Properties of MA

Carefully considering the effect of P123 addition and inorganic aluminium precursors doping on the structural properties of the resulting MA, MA4P*y*AlB was further synthesised. Nitrogen physisorption isotherms and the PSD curves of MA4P*y*AlB (MA4P15AlN, MA4P30AlCl, MA4P2AlS) are shown in Figure 4-12a and Figure 4-12b, respectively. The structural properties are summarised in Table 4-3. Compared to MA4P, though the BET surface area decreased, MA4P15AlN and MA4P30AlCl showed substantial increases in pore volume and pore diameter, from 1.8 cm^3g^{-1} and 28.2 nm of MA4P to 2.8 cm^3g^{-1} and 60.2 nm of MA4P15AlN and 1.7 cm^3g^{-1} and 64.1 nm of MA4P30AlCl. However, for MA4P2AlS, the variations in the structural properties were only marginal, with the BET surface area increasing from 325 m^2g^{-1} of MA4P to 335 m^2g^{-1} of MA4P2AlS while pore size slightly decreasing from 28.2 nm to 28.1 nm. This was consistent with the aforementioned observations over MA1P*y*AlB.

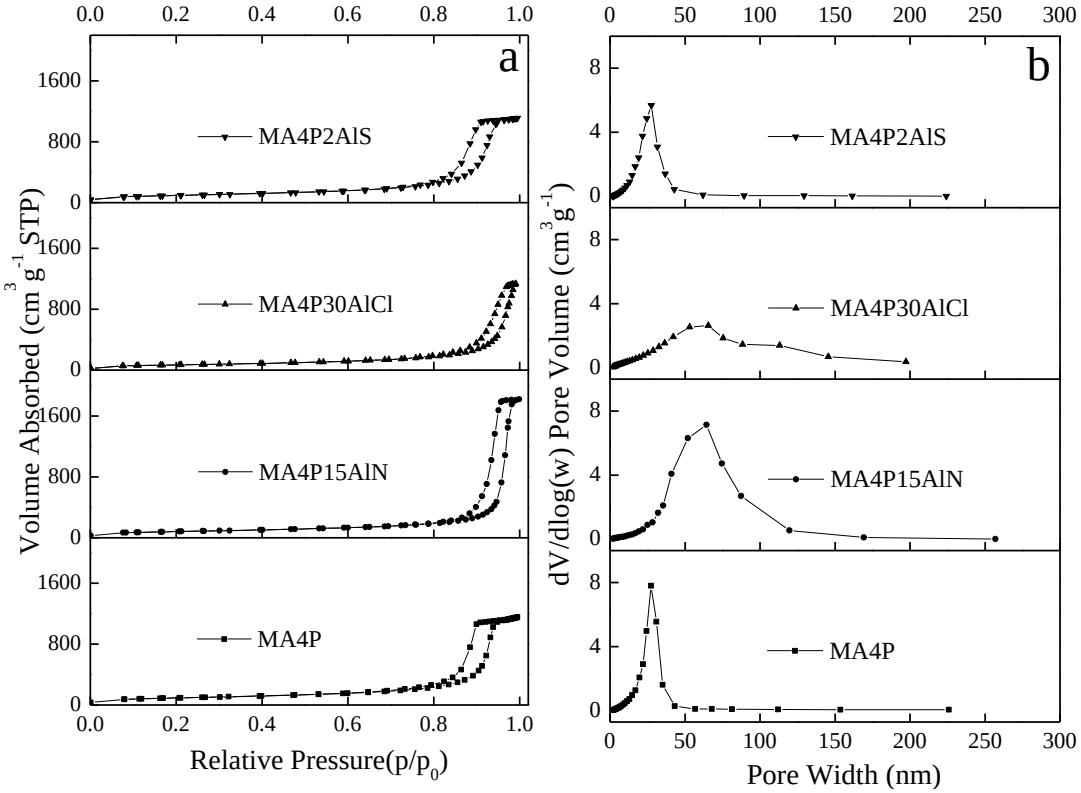

Figure 4-12 Nitrogen physisorption isotherms (a) and corresponding pore size distributions (b) of MA4P and MA4P*y*AlB

Table 4-3 Adsorption parameters of MA4P and MA4P*y*AlB

Samples	BET Surface Area (m^2g^{-1})	Pore Volume V_p (cm^3g^{-1})	D_a (nm)	D_p (nm)
MA4P	325	1.8	19.3	28.2
MA4P15AlN	287	2.8	38.6	60.2
MA4P2AlS	335	1.7	18.3	28.1
MA4P30AlCl	244	1.7	27.5	64.1

Figure 4-13 shows the TEM images of MA4P*y*AlB. A lath-like or a scaffold-like configuration with no significant structural ordering in the pore arrangement was observed, similar to that of MA4P. This indicates that the doping of inorganic

aluminium precursors over MA4P did not change its nano-scale morphology, arose from the similar entanglement of nanoliths (Bleta *et al.* 2012).

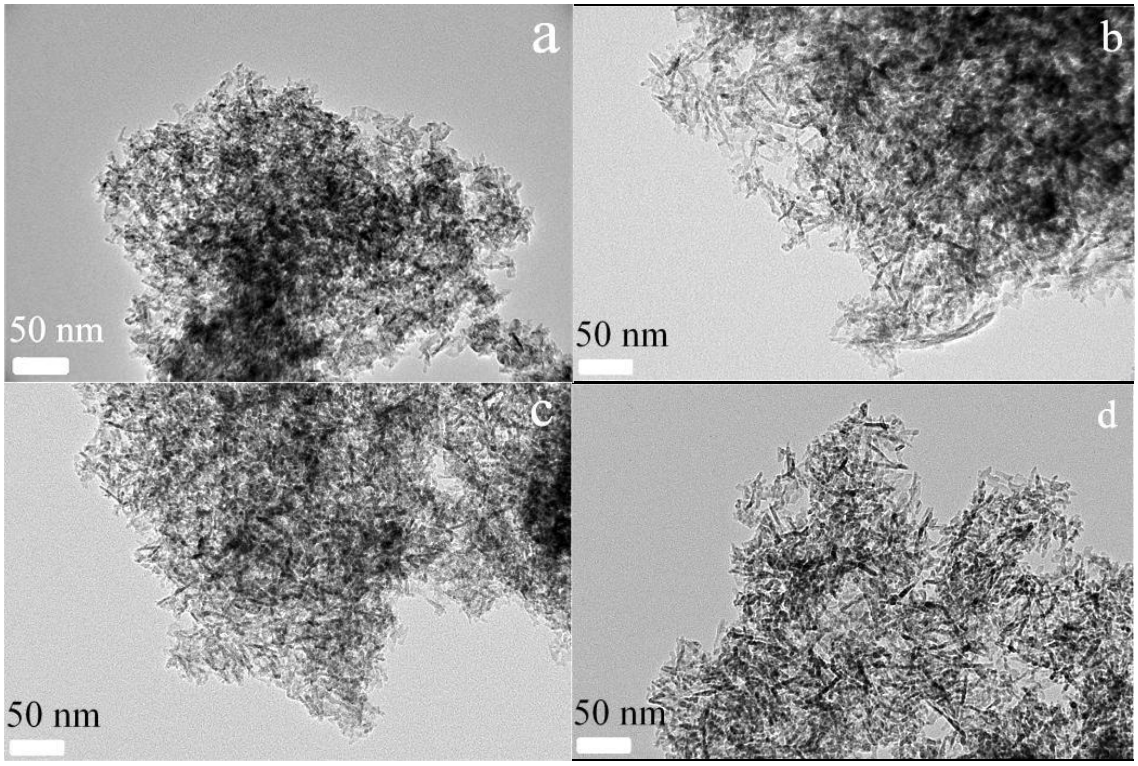

Figure 4-13 TEM images of (a) MA4P, (b) MA4P15AlN, (c) MA4P2AlS and (d) MA4P30AlCl

4.4 Summary

A facile route for the aqueous phase synthesis of mesoporous alumina with tunable structural properties was demonstrated in this study by adjusting nitric acid addition amount, template type, template addition amount, inorganic aluminium precursor doping ratio and calcination temperature. Results showed that the increased HNO_3 addition in the range of 1N~3N (0.097~ 0.291 mL HNO_3 per 20 mmol of Al) led to larger pores of the formed MAs while further increasing HNO_3 addition beyond 3N resulted in disordered pores with broad PSD. The nonionic surfactants P123 and F127 were shown to strongly influence the structural properties compared to CTAB and SDS with a given surfactant concentration, exhibiting in a descending order of F127 > P123 > CTAB > SDS. The optimal doping ratios of $Al(NO_3)_3$ and $AlCl_3$ were 15% and 30%,

respectively, at which much larger pore volumes and pore sizes with narrow PSDs were obtained. In the case of $Al_2(SO_4)_3$, the high precipitating capacity of SO_4^{2-} resulted in a low doping ratio of 2% and a compact structure. In addition, increasing the calcination temperature upon MA6P from 500 ℃ to 1100 ℃ caused an increase in pore size, but significantly decreased surface area and pore volume. By modulating the five aforementioned factors, an effective means to control the structural properties of MA over a wide range could be realised. The surface area up to 409 m^2g^{-1}, pore volume from 0.4 cm^3g^{-1} to 2.5 cm^3g^{-1} and pore size from 5.5 nm to ~36.5 nm were achieved. The as-synthesised MAs with diverse structural properties were adopted as the supports for MAK catalyst and enzymatic catalyst synthesis in the following Chapter 5 and Chapter 6.

Chapter 5: MA Supported Potassium Catalysts for Biodiesel Production

Many metal oxides include alkali earth metal oxides and transition metal oxides have been studied for transesterification process of oils. Among them, potassium based catalysts are widely used owing to its high basicity (Zabeti *et al.* 2009). In the present chapter, potassium supported by MA samples (KNO_3 as the K precursor) were synthesised following the one-pot self-assembly pathway. The prepared materials were adopted as the solid alkali catalysts for biodiesel production by transesterification of canola oil with methanol. The effect of potassium loading and P123 addition on the structural properties of the catalysts and thus on the catalytic activity was investigated. An experimental and kinetic study of the MAK catalysed transesterification for biodiesel synthesis was also performed.

5.1 Testing of MAK Catalysts for Biodiesel Production

5.1.1 MAK catalysts synthesis

MAK catalysts were synthesised via the simultaneous one-pot self-assembly of potassium precursor KNO_3 and aluminium isopropoxide in an acidic aqueous solution. P123 was used as the template to direct the self-assembly of K^+ and Al^{3+} and then removed by calcination in 700 ℃. The detailed synthesis recipes and the resulting samples are summarised in Table 5-1. For convenience in discussion, the final samples were nominally denoted as MA*x*P*m*K, where *x* refers to "*x*" g of P123 per 20 mmol of Al during the material preparation, and *m* signifies "*m*" mol% of K-species in a sample.

5.1.2 Effect of K Loading Ratio

The effect of K loading on both the structural properties and catalytic activity of MA was investigated. Nitrogen sorption isotherms and corresponding pore size distributions

of MA1P*m*K samples are shown in Figure 5-1. As clearly shown, the introduction of K species leads to a continuous reduction of the BET surface area, but a progressive increase in the pore size, especially when the K loading is higher than 10%. For the pore volume, further increase of the K ratio over 10% will result in substantial decrease of pore volume. The excessive K loading results in the formation of disordered mesopores and broader PSD. Up to 10% K species loading, the samples display uniformity and uniform mesopores. Similar trends have been reported by other researchers by incorporating metals like Ni, Mg, Fe, Cr, Cu, Ce, La, Y, Ca, and Sn into the framework of MA. The EISA synthesis pathway ensured a homogeneous distribution of metal species within MA framework and generally induced a pore size enlargement due to the lattice expansion (Cai *et al.* 2011).

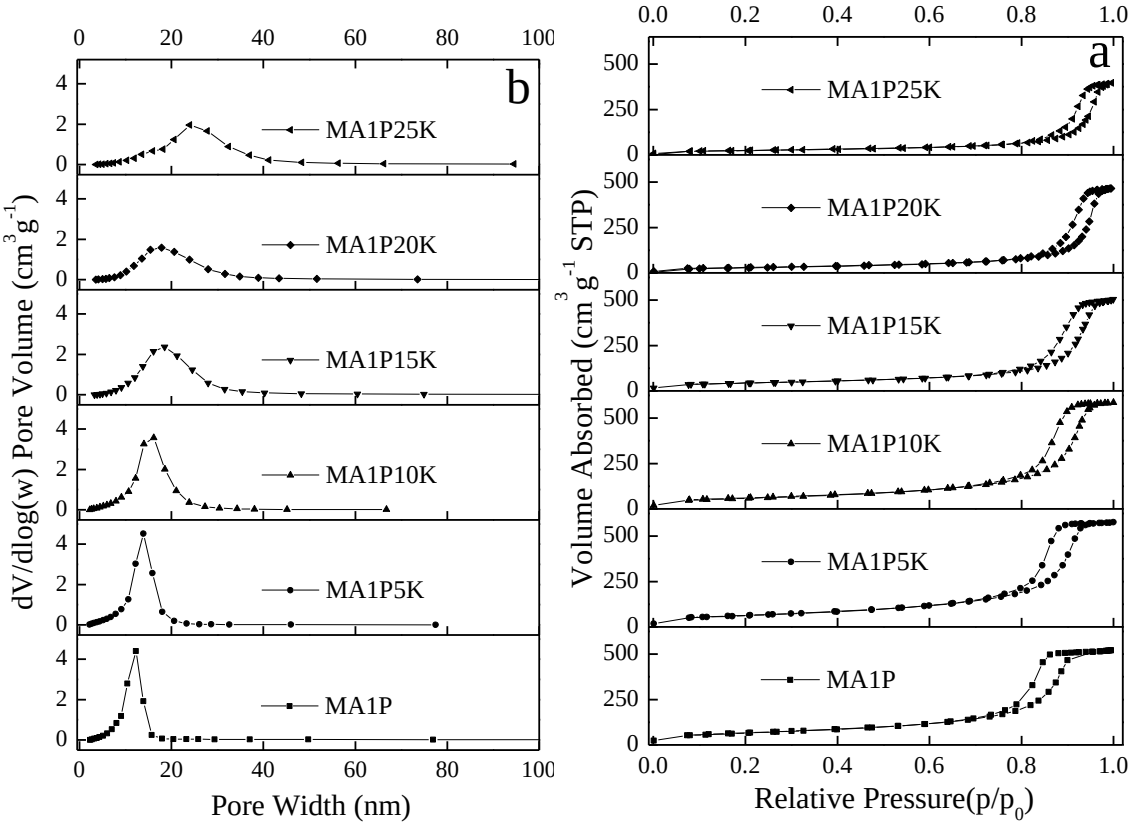

Figure 5-1 Nitrogen physisorption isotherms (a) and corresponding pore size distributions (b) of MA1P*m*K

Table 5-1 Samples labelling and corresponding synthesis conditions of the MAK catalysts

Samples	Template (g)	Aluminium source (mmol)	HNO_3 (mL)	Calcination temperature (℃)
MA0P	-	$Al(O\text{-}i\text{-}Pr)_3$ 20	0.097	700
MA1P	P123 1.00	$Al(O\text{-}i\text{-}Pr)_3$ 20	0.097	700
MA1P5K	P123 1.00	$Al(O\text{-}i\text{-}Pr)_3$ 19 KNO_3 1	0.097	700
MA1P10K	P123 1.00	$Al(O\text{-}i\text{-}Pr)_3$ 18 KNO_3 2	0.097	700
MA1P15K	P123 1.00	$Al(O\text{-}i\text{-}Pr)_3$ 17 KNO_3 3	0.097	700
MA1P20K	P123 1.00	$Al(O\text{-}i\text{-}Pr)_3$ 16 KNO_3 4	0.097	700
MA1P25K	P123 1.00	$Al(O\text{-}i\text{-}Pr)_3$ 15 KNO_3 5	0.097	700
MA0P20K	-	$Al(O\text{-}i\text{-}Pr)_3$ 16 KNO_3 4	0.097	700
MA0.25P20K	P123 0.25	$Al(O\text{-}i\text{-}Pr)_3$ 16 KNO_3 4	0.097	700
MA0.5P20K	P123 0.50	$Al(O\text{-}i\text{-}Pr)_3$ 16 KNO_3 4	0.097	700
MA1P20K	P123 1.00	$Al(O\text{-}i\text{-}Pr)_3$ 16 KNO_3 4	0.097	700

Figure 5-2 shows the wide-angle XRD patterns for the K-containing alumina samples MA1P*m*K calcined at 700°C. The alumina is in γ phase (JCPDS Card No. 10-0425). The patterns show two main sharp peaks at 2θ = 45.8 and 66.6°. As the molar fraction of K increases from 5K to 20K, the gradually reduced peak intensity and peak broadening were observed, suggesting the reduction in crystallinity. Besides, no K compounds in any form can be found. But for MA1P25K, except for γ-Al_2O_3,

$KAl(CO_3)_2(OH)_2$ was identified, most likely owing to the reactions of K_2O generated from KNO_3 decomposition with Al_2O_3, CO_2, O_2 and H_2O exposed in the open air.

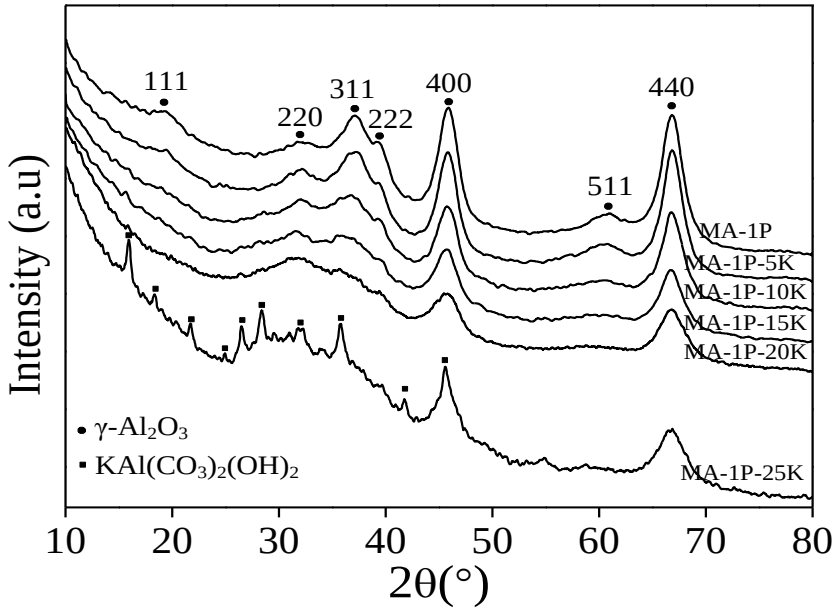

Figure 5-2 Wide-angle XRD patterns from 10 °to 80 °of the MA1P*m*K samples

Table 5-2 Adsorption parameters of MA1P*m*K and the catalytic activity in biodiesel synthesis

Samples	BET Surface Area (m^2g^{-1})	Pore Volume V_p (cm^3g^{-1})	D_a (nm)	D_p (nm)	Biodiesel yield [a]
MA1P	287	0.9	9.5	13.9	-
MA1P5K	230	0.9	11.0	14.1	4.8%
MA1P10K	212	0.9	12.7	15.0	44.3%
MA1P15K	151	0.8	16.1	17.5	72.4%
MA1P20K	106	0.7	19.7	17.3	92.2%
MA1P25K	87	0.6	20.4	24.5	91.4%

Note: [a] Reactions were carried out with M/O of 12:1, temperature of 70 ℃ and catalyst loading of 2.0 wt% within 5 h of reaction time. The same reaction conditions were used for the biodiesel yields shown in Table 5-3 and Table 5-4.

The catalytic activity of MAK catalyst in tranesterification of canola oil with methanol is highly dependent on the K loading. The yield of biodiesel reached 92.2% by using the catalyst MA1P20K and then reduced to 91.4% by MA1P25K (Table 5-2). The methyl ester composition in the resulting biodiesel from GC analysis is shown in Table 5-3. It is interesting to note that the concentrations of methyl esters in the biodiesel obtained corresponded to the fatty acid compositions of the canola oil (in Table 3-1), indicating that the catalysts did not favour any particular fatty acids in this catalytic transesterification process. The structural properties of catalysts only affected the yield, not the composition, of the biodiesel.

Table 5-3 Methyl ester compositions in percentage (%) in the obtained biodiesel

Samples	Yield	Methyl Ester Compositions (%)				
		C16:0	C18:1	C18:2	C18:3	Others
MA1P5K	4.8%	0	77.82	22.18	0	0
MA1P10K	44.3%	3.86	64.90	21.48	9.76	0
MA1P15K	72.4%	4.27	64.28	20.22	9.43	1.8
MA1P20K	92.2%	4.19	63.82	19.88	9.32	2.79
MA1P25K	91.4%	4.18	63.88	19.84	9.32	2.78
MA0P20K	41.7%	4.26	63.56	20.76	9.20	2.22
MA0.25P20K	83.4%	4.11	64.79	20.01	9.24	1.85
MA0.5P20K	91.8%	3.99	63.68	20.07	9.25	3.01

5.1.3 Effect of Catalyst Structural Properties

A series of MA*x*P20K catalysts were prepared to investigate the effect of the structural properties of catalyst on the catalytic activity in biodiesel synthesis. Based on the analysis discussed above, different amounts of P123 were used in the synthesis to

control the structural properties of the resulting catalyst. The measured isotherms and the corresponding structural parameters are summarised in Figure 5-3 and Table 5-4, respectively. In the nitrogen sorption isotherms shown in Figure 5-3a and BJH pore size distribution shown in Figure 5-3b, with increased addition of P123 from 0 to 1 g, the higher adsorption volume indicates a greater pore volume and the shift of the hysteresis loops to greater relative pressures illustrates the expansion of the pore width.

Table 5-4 Adsorption parameters of MA*x*P20K and the catalytic activity in biodiesel synthesis

Samples	BET Surface Area (m^2g^{-1})	Pore Volume V_p (cm^3g^{-1})	D_a (nm)	D_p (nm)	Biodiesel yield
MA0P20K	16.7	0.1	4.0	3.7	41.7%
MA0.25P20K	68.8	0.2	9.9	12.1	83.4%
MA0.5P20K	85.8	0.4	14.0	15.0	91.8%
MA1P20K	105.7	0.7	16.2	17.3	92.2%

A strong correlation between the structural properties of MA*x*P20K samples and their catalytic activities in biodiesel synthesis were observed. In this case, under the same reaction conditions, the yield of biodiesel increased from only 41.7% over the catalyst MA0P20K to 83.4% of MA0.25P20K and further achieved 92.2% by using MA1P20K (Table 5-4). The methyl ester compositions of the biodiesel obtained are also shown in Table 5-3. These results show that a higher surface area, greater pore volume and pore size can greatly reduce the mass transfer in the catalyst, allowing the freer mass transfer of the reactants and reaction products and providing bigger surface area for adsorption

and desorption in catalysis, thus achieving much higher yields.

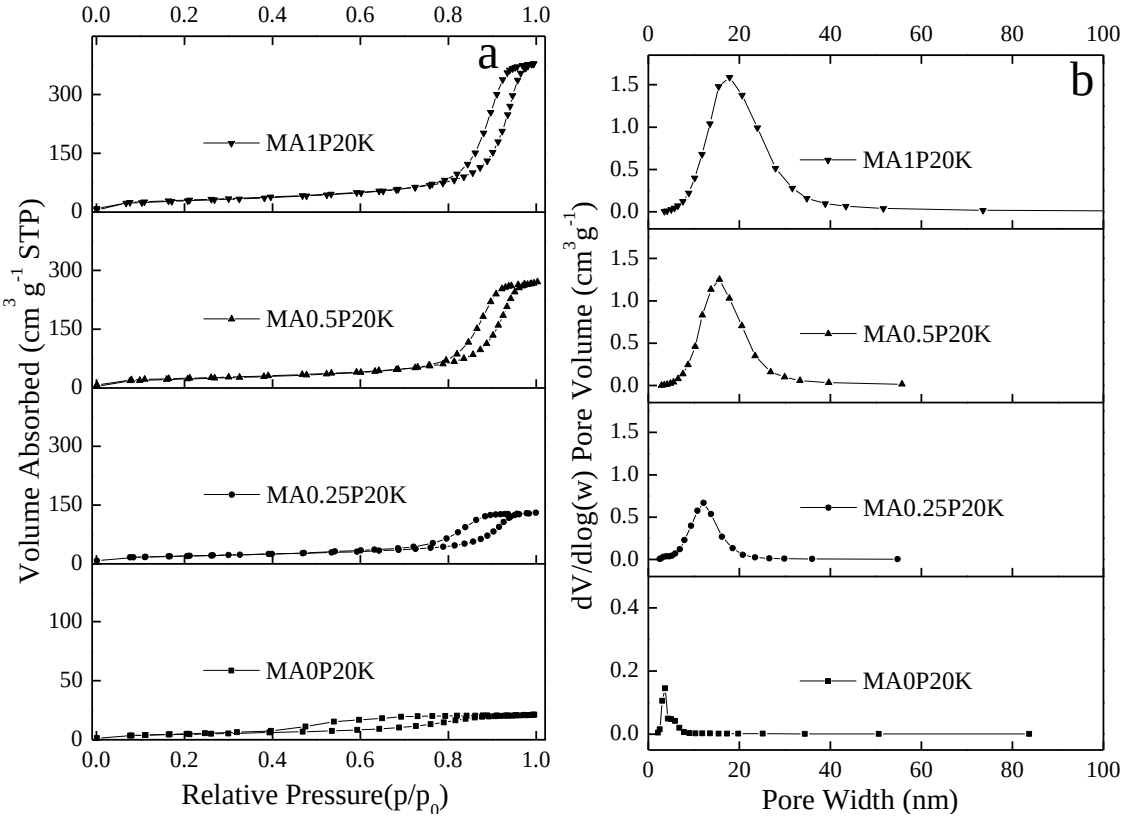

Figure 5-3 Nitrogen physisorption isotherms (a) and corresponding pore size distributions (b) of MA*x*P20K

Figure 5-4 shows the TEM images of the synthesised MA samples. As stated in Section 4.2.2, MA0P (Figure 5-4a) prepared in the absence of template, presented a dense structure mainly composed of closely packed adjacent nanoparticles, while MA1P exhibits a lath-like or a scaffold-like configuration, arose from the entanglement of nanolaths (Bleta *et al.* 2012). Compared with MA0P and MA1P, with 20% K loading, MA0P20K and MA1P20K show significant changes to the microstructure of MA, no randomly arranged pores and small particles could be observed. Combined with the subsequent nitrogen sorption analysis, such microstructural change resulted in a decrease of surface area and pore volume, but an increase in average pore diameter.

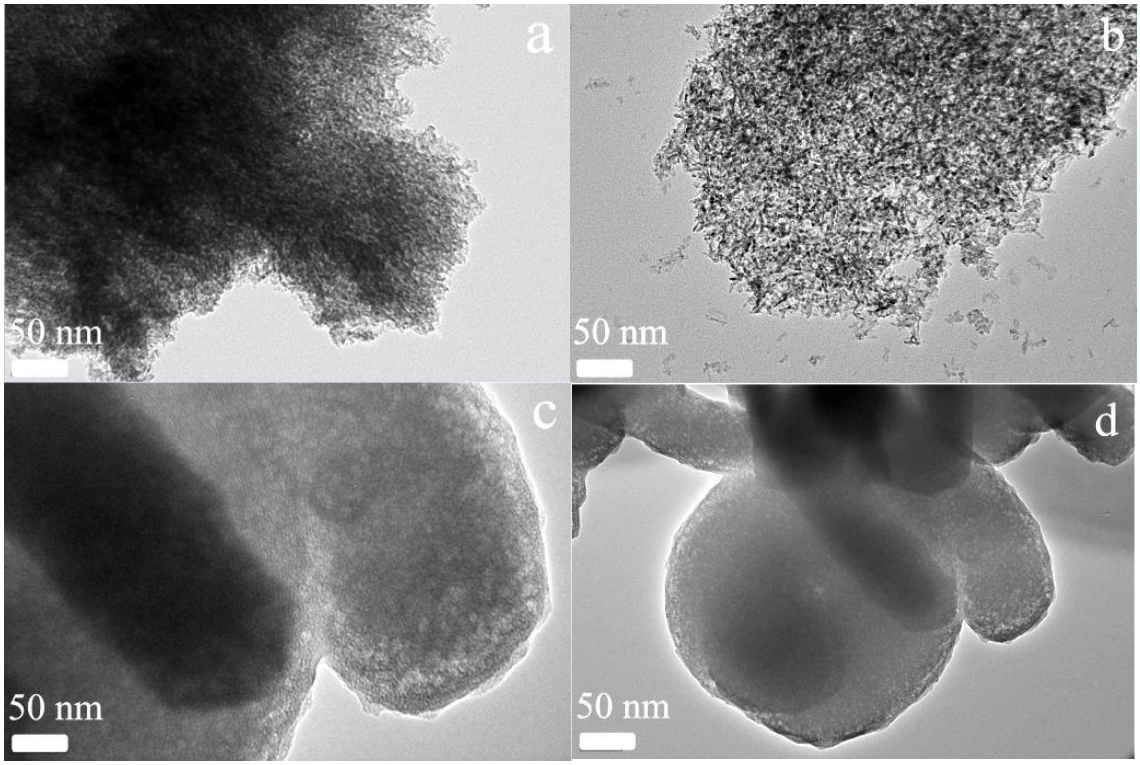

Figure 5-4 TEM images of (a) MA0P, (b) MA1P, (c) MA0P20K and (d) MA1P20K

5.1.4 Catalyst reusability

The effect of repeated use of the MAK catalyst on biodiesel yield is illustrated in Figure 5-5. Transesterification reactions were carried out using the MA1P20K catalyst. As can be seen, only a slight decrease in the biodiesel yield was observed after five successive cycles, gradually dropped from 92.2 % in the 1st use to 86.8% in the 5th use. This indicated a good reusability of the MAK catalyst as a sustained activity could be maintained after repeated uses.

When the catalyst is applied in an industrial process, a good reusability of the catalyst is one of the most important advantages since it enables an easy separation of catalyst from the reaction medium and then added to a fresh substrate solution. The slight drop in the biodiesel yield after recycled uses could be attributed to two main causes: (1) the leaching of the K species from the catalyst to the alcoholic phase and (2) the

deactivation of active sites due to their poisoning by some molecules present in the reaction mixture (Mootabadi *et al.* 2010).

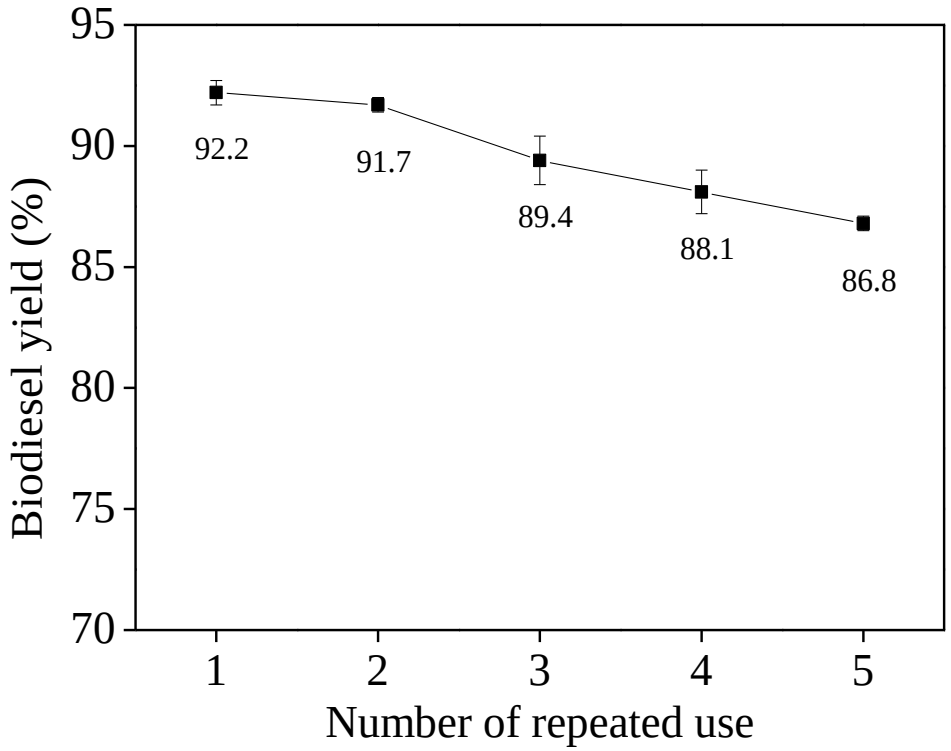

Figure 5-5 Effect of repeated use of the MA1P20K catalyst on biodiesel yield

5.2 Experimental and Kinetic study of the MAK Catalysed Transesterification

5.2.1 Mass transfer limitations

In the present study, the effect of mass transport, both external and internal of the catalyst, on the biodiesel yield was evaluated by varying the stirring rate and catalyst particle size, respectively. The results are plotted in Figure 5-6. As can be seen, biodiesel yield was largely affected by the stir rate when it was less than 500 rpm. Biodiesel yield substantially increased from 40.3% at 200 rpm to 47.7% at 500 rpm. However, as the stir rate further increased from 500 rpm to 600 rpm, the biodiesel yield became practically invariant, only slightly raised from 47.7% to 47.9%. This trend

indicates that the effect of external diffusion limitation on catalysis could be significantly eliminated if the experiments were performed at 600 rpm, consistent with the results presented elsewhere (Gemma Vicente 2005). The trend of the effect of the mechanical agitation of the mixture on the biodiesel yield suggests that the reaction was diffusion controlled.

For the assessment of the internal mass transfer effect, the MAK catalyst was sieved into five particle size fractions, namely, <160 μm, 160-250 μm, 250-380 μm, 380-600 μm, 600-830 μm, and then used to catalyse the transesterification at a stir rate of 600 rpm. As internal surface area was the overwhelming majority of the total BET surface area, the sieving of catalyst into different particle size ranges did not affect the surface area. The highest biodiesel yield 47.9% was achieved over the catalyst with the smallest particle size (<160 μm), and then lightly decreased to 47.6% for the catalyst with particle size of 160-250 μm. Further increase in the particle size led to a descending trend in biodiesel yield, finally arrived at 39.3 % for the catalyst with particle size of 600-830 μm. This suggests that the effect of internal mass transport limitation on catalysis was negligible if the catalyst particle size smaller than 160 μm. Therefore, results from the investigation showed that the stir rate of 600 rpm and catalyst particle size <160 μm could largely suppress the mass transfer limitations.

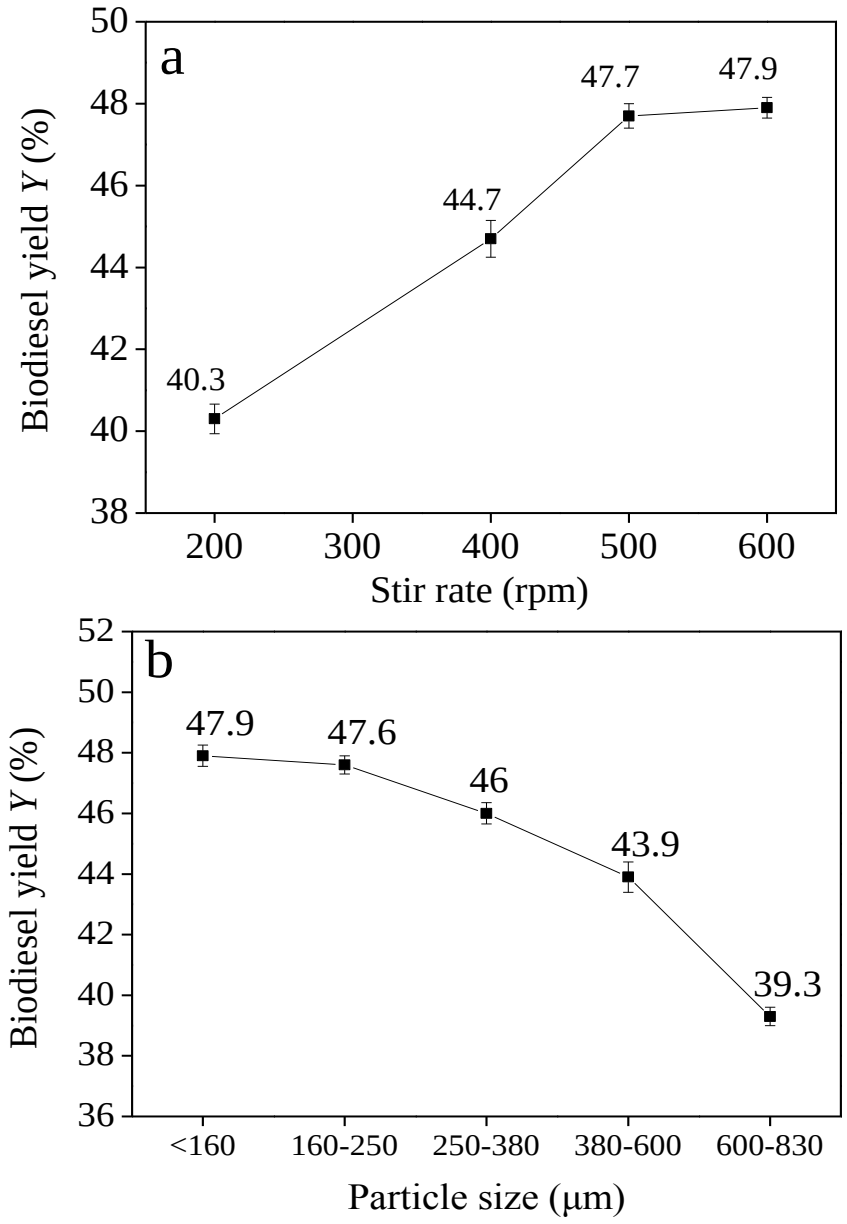

Figure 5-6 Biodiesel yields with varied stir rates (a) and catalyst particle sizes (b)

5.2.2 Biodiesel yield

In examining the effect of reaction temperature, M/O and catalyst loading on biodiesel yield, the transesterification reactions were carried out at five temperatures, 50 ℃, 55 ℃, 60°C, 65°C and 70°C, four M/O's in the range of 6:1 to 15:1 and four catalyst loadings from 1.0 wt% to 2.5 wt%. The biodiesel yield as a function of reaction time under different conditions is plotted in Figure 5-7. The equilibrium conversions X_e are

summarised in Table 5-5. Both biodiesel yield and equilibrium conversion X_e increased at higher temperatures, M/Os and catalyst loadings within the tested ranges.

Table 5-5 Rate constants obtained at varied temperatures, M/Os and catalyst loadings

Reaction variables		*Xe* (%)	k_1 ($Lmol^{-1}min^{-1}g^{-1}$)	k_{-1} ($Lmol^{-1}min^{-1}g^{-1}$)	R^2
Temperature (℃)[a]	50	72.7	0.082	0.062	0.959
	55	78.6	0.092	0.046	0.952
	60	83.0	0.098	0.035	0.969
	65	86.4	0.116	0.027	0.942
	70	91.9	0.138	0.016	0.951
M/O[b]	6:1	61.5	0.085	0.057	0.939
	9:1	82.9	0.114	0.028	0.988
	12:1	91.9	0.138	0.016	0.951
	15:1	92.3	0.133	0.018	0.959
Catalyst loading (wt%)[c]	1.0	78.9	0.135	0.052	0.946
	1.5	85.8	0.139	0.036	0.923
	2.0	91.9	0.138	0.016	0.951
	2.5	93.3	0.115	0.010	0.908

Note: [a] Reactions were carried out with M/O of 12:1 and catalyst loading of 2.0 wt%; [b] reaction temperature was kept as 70 ℃ and catalyst loading 2.0 wt%; [c] reaction temperature 70 ℃ and M/O 12:1

Biodiesel yield increased consistently with increasing reaction temperature. A biodiesel yield of 61.1% was obtained under 50 ℃ in 180 min, while under 70 ℃, it reached 80.3% and X_e finally arrived at 91.9% (Table 5-5). Similar results were observed under different M/Os and catalyst loading ratios. Higher biodiesel yield and X_e were observed at increased M/Os and catalyst loadings. The stoichiometry of the transesterification reactions requires 3M methanol to 1M triglyceride. However, excess methanol was normally favoured in order to achieve higher biodiesel yields (Gemma Vicente 2005).

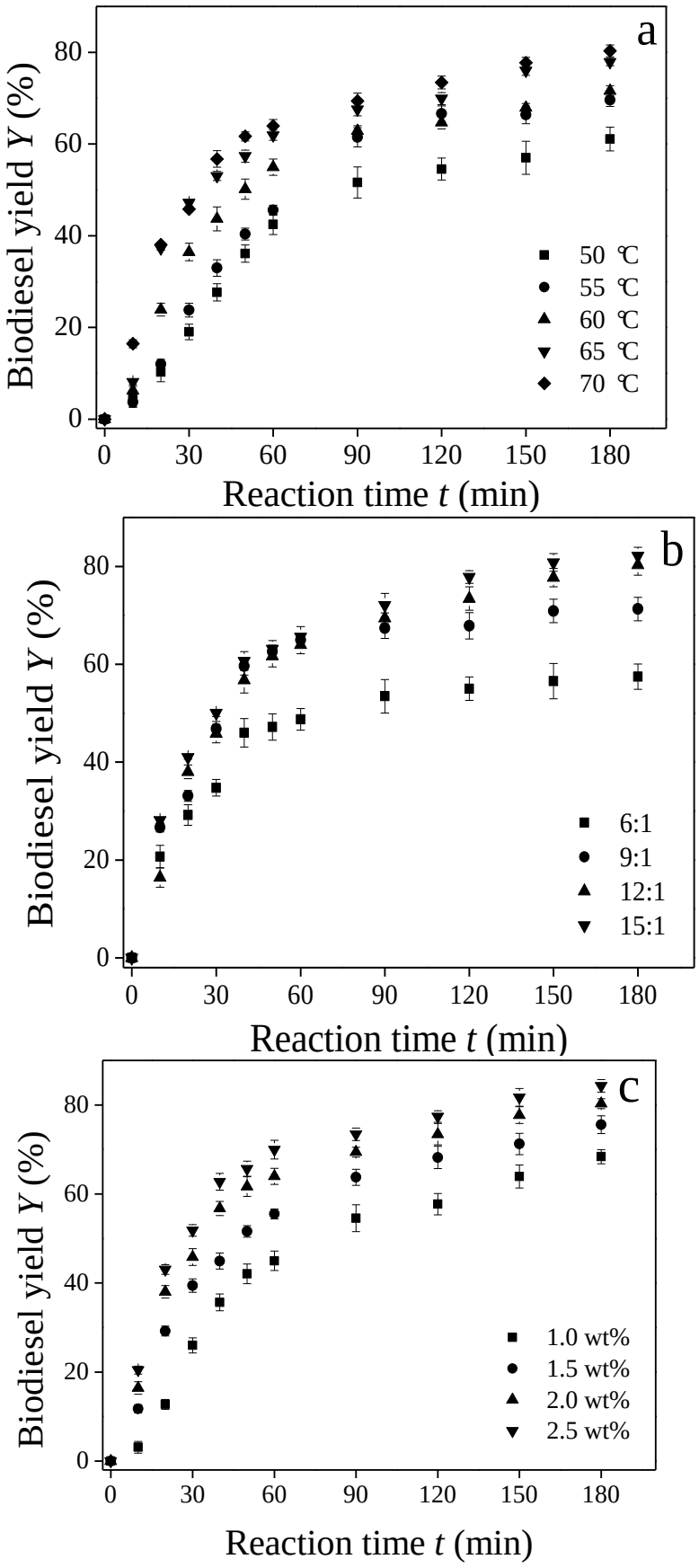

Figure 5-7 Effect of (a) reaction temperature, (b) M/O and (c) catalyst loading on biodiesel yield

Herein, in this heterogeneous reaction system, the immiscible oil, methanol and solid MAK catalyst has to be well stirred and mixed in order to increase the oil-methanol interface and consequently increase the reaction rate per volume of the mixture, leading to a higher biodiesel yield (D. Darnoko 2000). The equilibrium conversion X_e increased from only 61.5% of M/O 6:1 to 92.3% of M/O 15:1. Likewise, in terms of the effect of catalyst loading, with increasing addition of MAK catalyst, a higher reaction equilibrium conversion was reached because of the increase in the total number of available active catalytic sites for the reaction (Xuejun Liu 2008). The equilibrium conversion X_e increased from 78.9% at catalyst loading of 1.0 wt% to 93.3% at 2.5 wt%.

5.2.3 Kinetics

In the present study, a model built on the Eley-Rideal mechanism was employed to perform the kinetic study. Kinetic parameters were determined by fitting the model to the experimental data. The forward step was treated as a pseudo first order reaction, while the reverse reaction was second order (Sanjib Kumar Karmee 2004; Singh *et al.* 2007). The Eley-Rideal mechanism, as illustrated in Figure 5-8, assumes that methanol is adsorbed on the basic site of the catalyst surface as the first step (Dossin *et al.* 2006; Xuejun Liu 2008; Xiao *et al.* 2010; Chantrasa *et al.* 2011; Agarwal *et al.* 2012), forming methoxide anion. This is followed by the surface reaction between methoxide anion and triglyceride from the liquid phase to form a tetrahedral intermediate (Chantrasa *et al.* 2011). The intermediate releases one methyl ester and one diglyceride from the catalyst surface(Xiao *et al.* 2010; Agarwal *et al.* 2012). The diglyceride formed then reacts with a methoxide anion along a similar process to generate one more methyl ester and one monoglyceride, which is finally converted into the final methyl ester as the biodiesel product and glycerol as a by-product. The glycerol formed eventually desorbs from the catalyst surface (Xiao *et al.* 2010; Agarwal *et al.* 2012) to complete a reaction cycle.

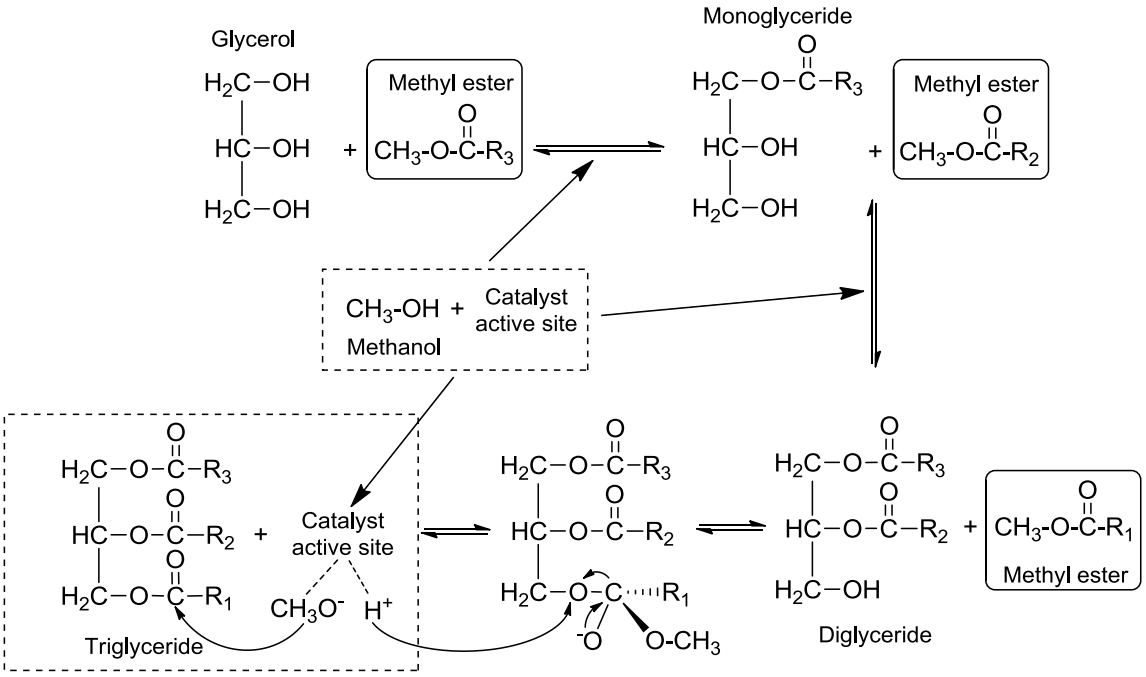

Figure 5-8 A schematic of the Eley–Rideal mechanism

Herein, by knowing the biodiesel yield *Y* (Figure 5-7) and the equilibrium conversion X_e (Table 5-5), f(*Y*) as a function of reaction time under different conditions can be estimated based on the kinetic model and the results are presented in Figure 5-9. It was found that the calculated xagreed with the experimental data very well under all conditions tested, suggesting the suitability of the model for describing he kinetics of the transesterification reactions.

From known f(*Y*), k_{-1} and k_1 can be calculated using Eq. (3-7) and Eq. (3-9) and the results are summarised in Table 5-5. As can be seen, the forward rate constant k_1 increased at higher temperatures, M/Os and catalyst loadings, while the reverse rate constant k_{-1} decreased accordingly within the tested ranges. The forward rate constant k_1 increased consistently from 0.082 $Lmol^{-1}min^{-1}g^{-1}$ at 50 ℃ to 0.138 $Lmol^{-1}min^{-1}g^{-1}$ at 70 ℃, while the reverse rate constant k_{-1} decreased correspondingly from 0.062 $Lmol^{-1}min^{-1}g^{-1}$ to 0.016 $Lmol^{-1}min^{-1}g^{-1}$ and, consequently, resulting in substantially higher biodiesel yields. These observations as shown in Figure 5-9a were in accordance with the literature reports (Gemma Vicente 2005; Xiao *et al.* 2010).

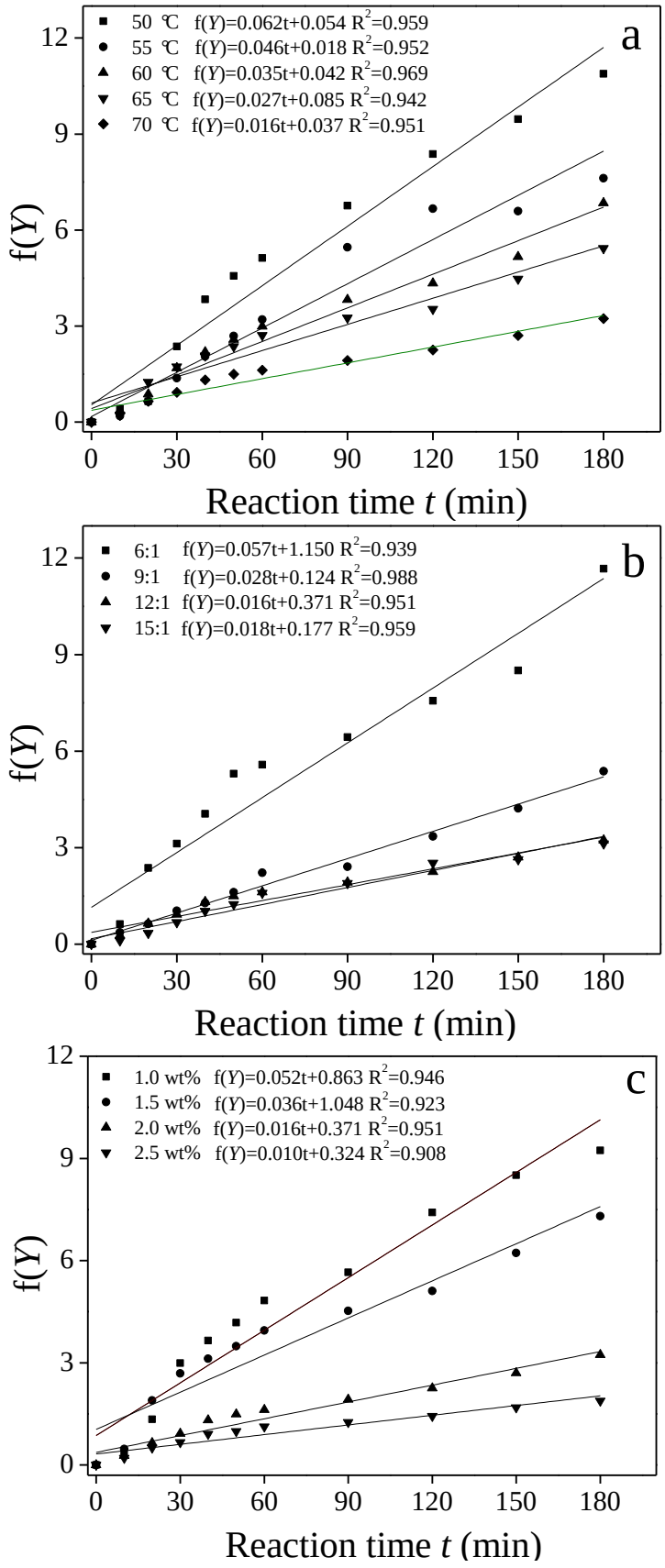

Figure 5-9 Prediction of f(*Y*) as a function of reaction time under different: (a) reaction temperatures, (b) M/Os and (c) catalyst loadings

Table 5-6 Activation energy and pre-exponential factor obtained by fitting the experimental data with the Arrhenius equation

Reaction variables		k_1 obtained over different temperatures ($Lmol^{-1}min^{-1}$)					E_a ($kJmol^{-1}$)	Pre-exponential factor k_0	R^2
		50 ℃	55 ℃	60 ℃	65 ℃	70 ℃			
M/O[a]	6:1	0.049	0.057	0.060	0.068	0.085	22.8	236.5	0.962
	9:1	0.067	0.076	0.083	0.090	0.114	22.6	295.3	0.949
	12:1	0.082	0.092	0.098	0.116	0.138	23.4	492.3	0.962
	15:1	0.082	0.087	0.102	0.110	0.133	22.0	290.9	0.964
Catalyst loading (wt%)[b]	1.0	0.086	0.092	0.096	0.116	0.135	20.9	195.5	0.926
	1.5	0.082	0.095	0.107	0.111	0.139	22.3	336.5	0.958
	2.0	0.082	0.092	0.098	0.116	0.138	23.4	492.3	0.962
	2.5	0.070	0.078	0.086	0.101	0.115	23.2	390.8	0.989

Note: [a] Reactions were carried out with catalyst loading 2.0 wt%; [b] M/O was kept as 12:1

Likewise, in the case of higher M/Os, higher biodiesel yields and the forward rate constant k_1 were also demonstrated. As seen from Table 5-6, k_1 increased from 0.085 at M/O of 6:1 to 0.138 at M/O of 12:1 and then slightly dropped to 0.133 $Lmol^{-1}min^{-1}g^{-1}$ at M/O of 15:1. For different catalyst loadings, k_1 initially kept steady as the amount of the catalyst in the reaction mixture increased from 1.0 wt% to 2.0 wt%, maintaining a value in the order of 0.140 $Lmol^{-1}min^{-1}g^{-1}$, but substantially decreased to 0.115 $Lmol^{-1}min^{-1}g^{-1}$ when the catalyst was further increased to 2.5 wt%. This observation can be reliably attributed to the excessive catalyst addition. Assuming 0.5 wt% of the catalyst in the case of 2.5 wt% catalyst addition did not contribute to the catalysing of the transesterification reaction, the rate constant should have been calculated based on 2.0 wt% catalyst that was active, yielding 0.143 $Lmol^{-1}min^{-1}g^{-1}$, consistent with the rate constant data obtained for lower catalyst addition amounts.

The k_1 values obtained over the four M/Os and four catalyst loadings at different reactions temperatures are also summarised in Table 5-6. The results confirm that k_1 increased at elevated temperatures, M/Os and catalyst loadings (in the rage of 1.0 wt% to 2.0 wt%). As k_1 at varied temperatures from 50 ℃ to 70 ℃ under different M/Os and catalyst loadings were determined, the activation energy E_a could be obtained using the Arrhenius equation Eq. (3-11). In this way, the plots of the natural logarithms of the calculated rate constants for the MAK catalysed reactions versus the reciprocals of reaction temperatures are shown in Figure 5-10. The activation energy E_a and pre-exponential factor k_0 are summarised in Table 5-6.

Results show that the activation energies obtained at different M/Os and catalyst loadings were quite stable, within a range from 20.9 $kJmol^{-1}$ to 23.4 $kJmol^{-1}$, owing to the use of the same catalyst (Xie *et al.* 2009). However, the pre-exponential factor k_0 varied significantly, increasing from 236.5 at M/O of 6:1 to 492.3 at M/O of 12:1 and slightly dropped to 290.9 at M/O of 15:1, or raised from 195.5 at catalyst loading of 1.0

wt% to 390.8 at 2.5 wt%. The increase in k_0 indicated the facilitated contact of reactant molecules in increased M/O and catalyst loading conditions could contribute to higher reaction rate (Xie *et al.* 2009; Kuan *et al.* 2013).

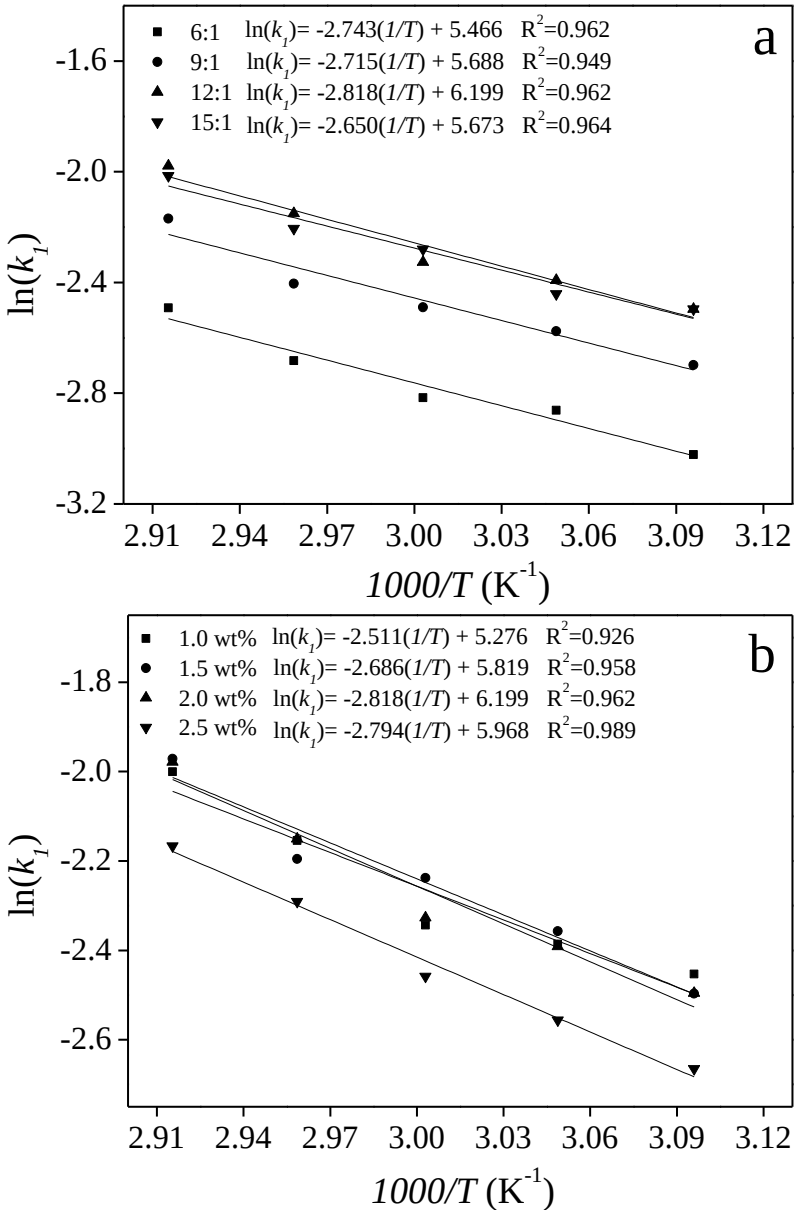

Figure 5-10 Arrhenius plots for determining the activation energy and pre-exponential factor

The literature values of the activation energy E_a for alkali-catalysed homogeneous and heterogeneous transesterification of oil with methanol ae usually in the range of 20.0 to 81.1 kJmol^{-1} (D. Darnoko 2000; Gemma Vicente 2005; Xuejun Liu 2008; Singh *et al.* 2009; Pugnet *et al.* 2010; Xuejun Liu 2010; Zhang *et al.* 2010; Chantrasa *et al.* 2011).

The obtained activation energy in this study is within but at the lower end of this range. This is expected as the MAK catalyst employed in this study possessed a strong basicity amongst the catalysts compared.

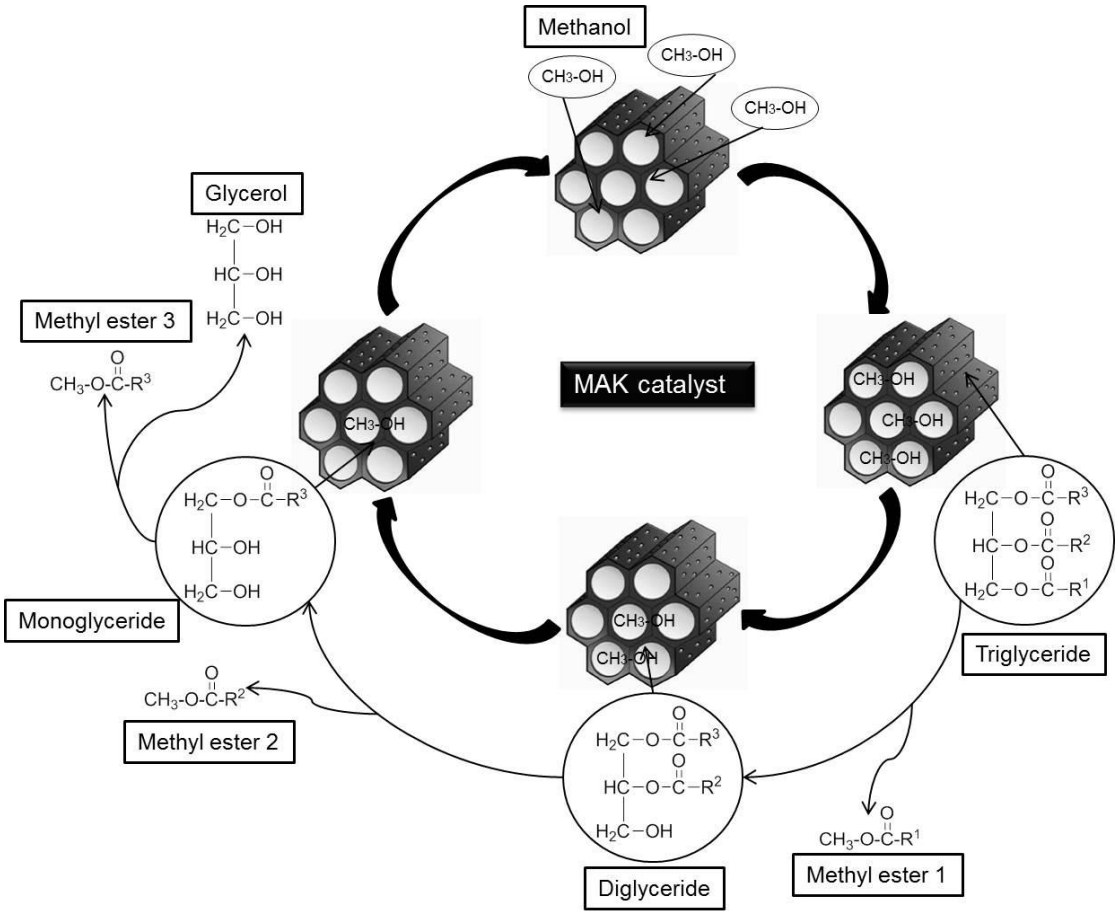

Figure 5-11 A schematic representing the reaction pathway of the MAK catalysed transesterification

The kinetic model built on the Eley–Rideal mechanism has been shown to reproduce the experimental data very well. A reaction pathway of the MAK catalysed transesterification of canola oil with methanol was therefore proposed in this study, as shown in Figure 5-11. The adsorption of methanol on the active sites of the MAK catalyst leads to the formation of methoxide anions. This is then followed by the surface reaction between the methoxide anions and triglyceride molecules to form three methyl esters and one glycerol.

5.3 Summary

Mesoporous alumina supported potassium catalysts were synthesised following the one-pot synthesis pathway via self-assembly of potassium precursor KNO_3 and aluminium isopropoxide. The MAK materials were used as the heterogeneous alkaline catalysts for biodiesel production by transesterification of canola oil with methanol. The effect of potassium loading and P123 addition on the structural properties of the catalysts and thus on the catalytic activity was investigated.

While the K incorporation has reduced the BET surface area and pore volume of the MA, it has increased the pore size significantly. When applied in catalysis, by introducing 20% molar fraction of K species to MA, a very high yield of biodiesel of 92.2% was achieved. Moreover, higher surface area, pore volume and greater pore size of the catalyst reduced the mass transfer limitation in catalysis, thus leading to the higher biodiesel yields over the MAK series catalysts with the same 20% molar fraction of K species to MA but different structural properties by modulating the usage of P123 in the synthesis. The MA1P20K catalyst showed a good reusability, only a slight drop in the biodiesel yield was observed after five successive cycles.

An experimental and kinetic study of the MAK catalysed transesterification for biodiesel synthesis was performed on the MA1P20K catalyst. The activation energy of the MAK catalysed transesterification ranged from 20.9 to 23.4 $kJmol^{-1}$. This transesterification process was shown to follow the Eley–Rideal mechanism, suggesting that the reaction started with methanol adsorption on the active sites of MAK catalyst surface, followed by surface reaction between methoxide anions formed on the surface and triglyceride from the bulk liquid phase to produce methyl esters as the biodiesel product and glycerol as the by-product.

Chapter 6: MA Supported Lipase as the Enzymatic Catalysts for Biodiesel Production

Enzymatic transesterification of canola oil with methanol for biodiesel production was studied in this chapter using pseudomonas fluorescens lipase immobilised on MA as catalyst. MAs with tunable structural properties were used as supports for lipase immobilisation and their performance was compared to that of free lipase and lipase immobilised on a commercial alumina.

The effect of reaction temperature (30 ℃ to 50 ℃), water addition (0 to 8 wt% relative to the weight of oil) and catalyst loading (2 wt% to 6 wt% relative to the weight of oil) was appraised over the MA4P15AlN supported lipase catalyst using a central composite experimental design strategy to determine the significant parameters and the optimal conditions for biodiesel production. A highest biodiesel yield of 88.9% was achieved in 24 h under the reaction conditions of 41 ℃, 3.9 wt% water addition and 5.0 wt%.catalyst loading ratio, which compared favourably with other transesterification systems.

6.1 Effect of Structural Properties of Support on Catalysis

6.1.1 Structural Properties and the Nano-scale Morphology of Supports

Structural properties of a support would play an important role in determining lipase adsorption. A group of MAs were selected as the supports and the structural properties are summarised in Table 6-1. Nitrogen physisorption isotherms are plotted in Figure 6-1 (a, c, e) while the PSD curves are shown in Figure 6-1 (b, d, f). As discussed in Chapter 4, the addition of template P123 induced a great impact on the structural properties of the resulting MAs. From MA0A to MA4P, an increasing trend in the BET surface area (from 236 m^2g^{-1} to 325 m^2g^{-1}), V_p (from 0.4 cm^3g^{-1} to 1.8 cm^3g^{-1}), D_a (from 5.2 nm to

19.3 nm) and D_p (from 7.0 to 28.2 nm) were evident. Further increasing P123 addition led the MA synthesised to possess larger surface areas, pore sizes and pore volumes.

Table 6-1 Adsorption parameters of MAs and a commercial alumina

Samples	BET Surface Area (m^2g^{-1})	Pore Volume V_p (cm^3g^{-1})	D_a (nm)	D_p (nm)
MA0A	236	0.4	5.2	7.0
MA2P	295	1.2	13.7	11.0
MA4P	325	1.8	19.3	28.2
MA4P15AlN	287	2.8	38.6	60.2
MA4P2AlS	335	1.7	18.3	28.1
MA4P30AlCl	244	1.7	27.5	64.1
MA4F	358	1.9	20.8	30.1
MA20C	319	1.1	10.2	13.4
MA20S	260	0.5	6.7	8.6
Commercial alumina	152	0.9	21.5	-

Furthermore, for MA4P*y*AlB, compared to MA4P, though the BET surface area decreased, MA4P15AlN and MA4P30AlCl showed substantial increases in the pore volume and pore diameter, respectively, from 1.8 cm^3g^{-1} and 28.2 nm of MA4P to 2.8 cm^3g^{-1} and 60.2 nm of MA4P15AlN and 1.7 cm^3g^{-1} and 64.1 nm of MA4P30AlCl. However, for MA4P2AlS, the variations in the structural properties were only marginal, with the BET surface area increasing from 325 m^2g^{-1} of MA4P to 335 m^2g^{-1} of MA4P2AlS while pore size slightly decreasing from 28.2 nm to 28.1 nm. In addition, MA4F, MA20C and MA20S were also used as the supports, among which MA4F shows a highest BET surface area of 358 m^2g^{-1}. A commercial alumina was used as a

reference, whose the nitrogen sorption isotherm and PSD curve shown in Figure 6-1e and Figure 6-1f, suggest a low BET surface area of 152 m^2g^{-1} and pore volume of 0.9 cm^3g^{-1} with very broad and irregular PSD.

Figure 6-2 shows TEM images of the MAs. MA0A (Figure 6-2a) exhibited a dense structure with closely packed adjacent nanoparticles. In contrast, a lath-like or a scaffold-like configuration with no significant structural ordering in the pore arrangement was observed over MA2P, MA4P, MA4F, MA20C and MA20S, which was believed to arise from the entanglement of nanolaths (Bleta *et al.* 2012). Doping of inorganic aluminium precursors did not change the nano-scale morphology of the resulting MAs, MA4P15AlN, MA4P2AlS and MA4P30AlCl also showed a similar lath-like or scaffold-like configuration as illustrated in Figure 6-2.

6.1.2 Effect of the Support Structural Properties on Lipase Adsorption

Time dependence of lipase adsorption on MAs and the commercial alumina is shown in Figure 6-3 and Table 6-2. As can be seen, in all of the cases, most of the adsorption took place in the initial 30 minutes and gradually approached equilibrium in 60 minutes. From the MA synthesised free of template (MA0A) to the one synthesised with 4 g of P123 per 10 mmol of MA (MA4P), the amount of lipase adsorption increased consistently, due to the correspondingly higher surface area, larger pore volume and bigger pore size.

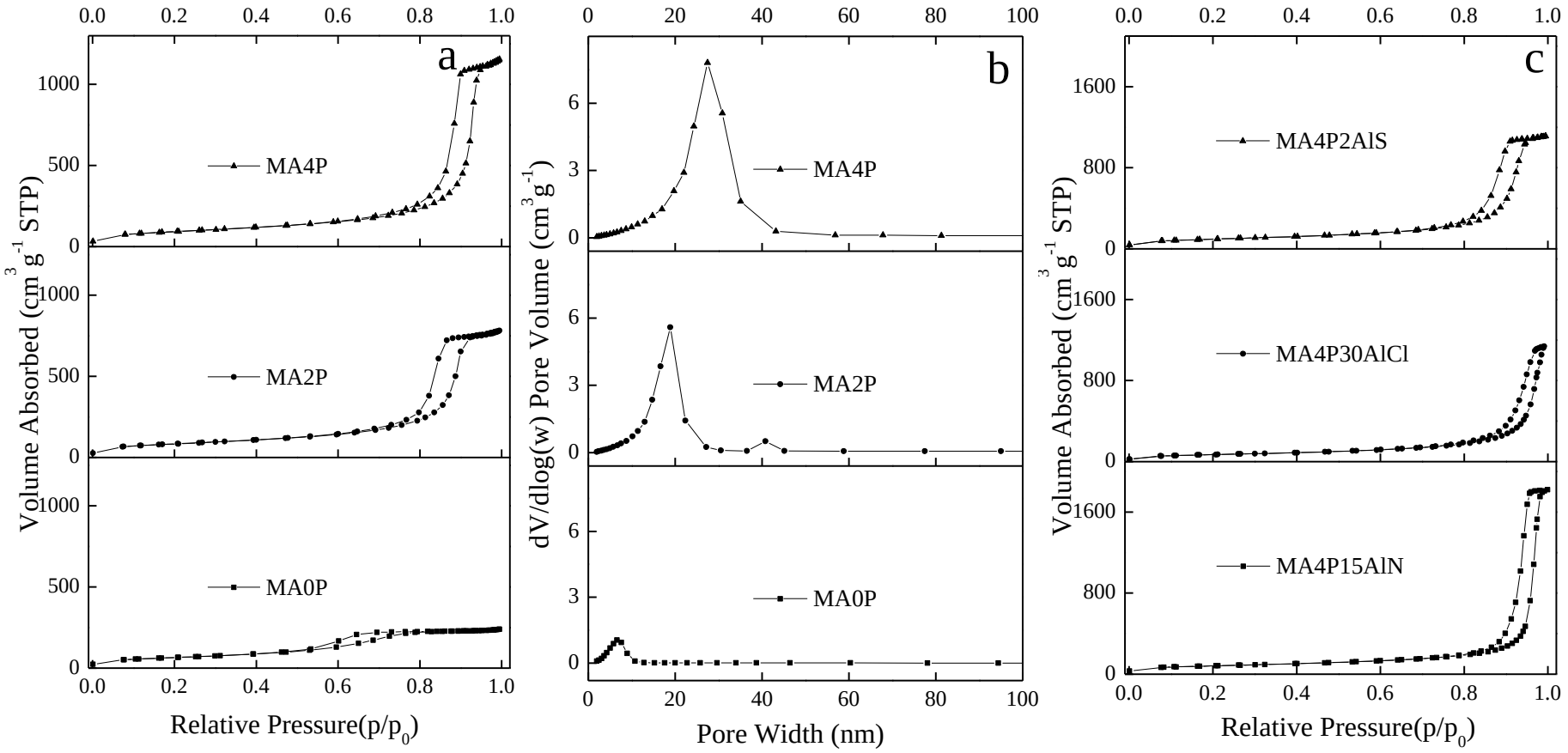

Figure 6-1 Nitrogen physisorption isotherms (a, c, e) and corresponding pore size distributions (b, d, f) of the supports

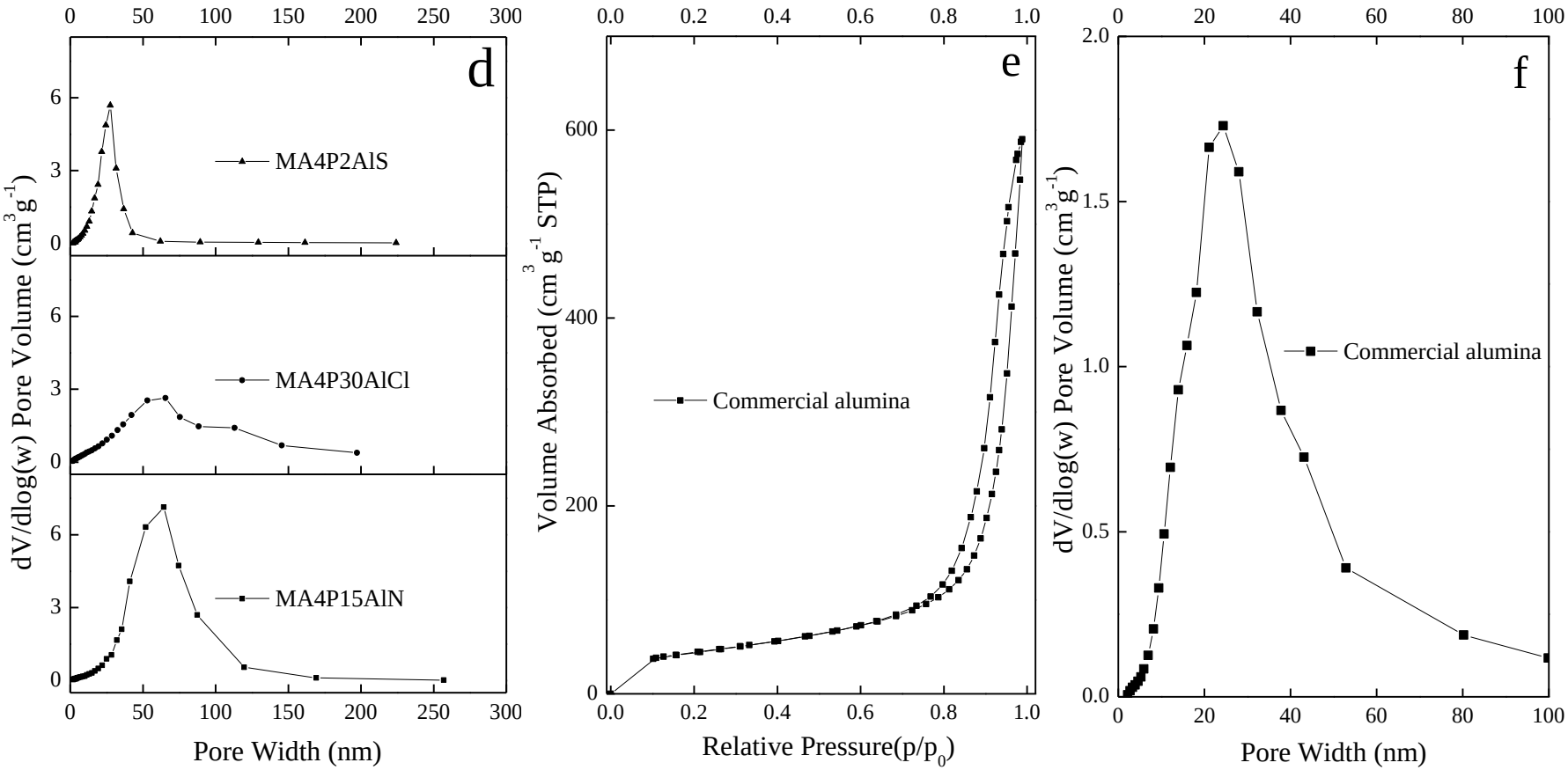

Figure 6-1 Nitrogen physisorption isotherms (a, c, e) and corresponding pore size distributions (b, d, f) of the supports (to be continued)

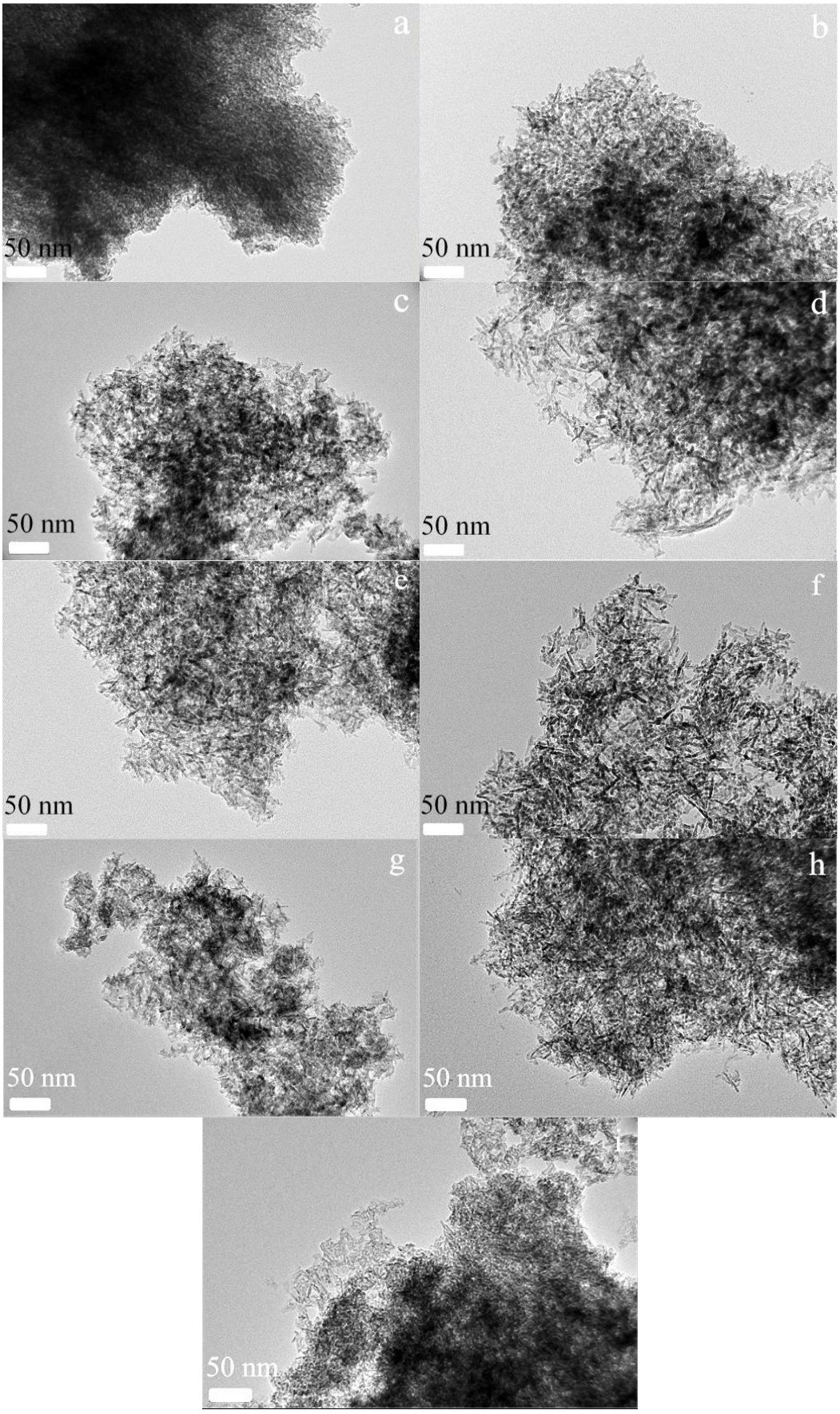

Figure 6-2 TEM images of (a) MA0A, (b) MA2P, (c) MA4P, (d) MA4P15AlN, (e) MA4P2AlS, (f) MA4P30AlCl, (g) MA4F, (h) MA20C and (i) MA20S

This indicates that MA with larger contact interface and more accessible porous channels were very important for lipase adsorption. This was also confirmed by the high lipase adsorption capabilities of MA4P15AlN and MA4P30AlCl, reaching 142.9 mgg^{-1} and 131.8 mgg^{-1} in 120 min, much higher than the other MAs and the commercial alumina. The variations in lipase adsorption capability may be attributed to the further expansion of pore volume and pore size in MA4P15AlN and MA4P30AlCl as compared to MA4P, giving more accessible porous channels and larger pore space, would allow quicker lipase transfer and greater adsorption.

Table 6-2 Time dependence of lipase adsorption on MAs and a commercial alumina

Samples	Lipase adsorbed amounts in the specified time (mgg^{-1})			
	10 min	30 min	60 min	120 min
MA0A	12.9	17.8	18.7	19.0
MA2P	51.4	67.2	71.8	72.9
MA4P	79.1	95.6	98.3	100.5
MA4P15AlN	114.3	135.7	139.4	142.9
MA4P2AlS	84.9	105.3	108.2	111.4
MA4P30AlCl	97.2	121.8	127.6	131.8
MA4F	80.9	100.2	113.5	116.2
MA20C	25.4	42.1	45.8	48.6
MA20S	14.9	19.1	21.7	23.3
Commercial alumina	94.2	115.2	119.6	121.7

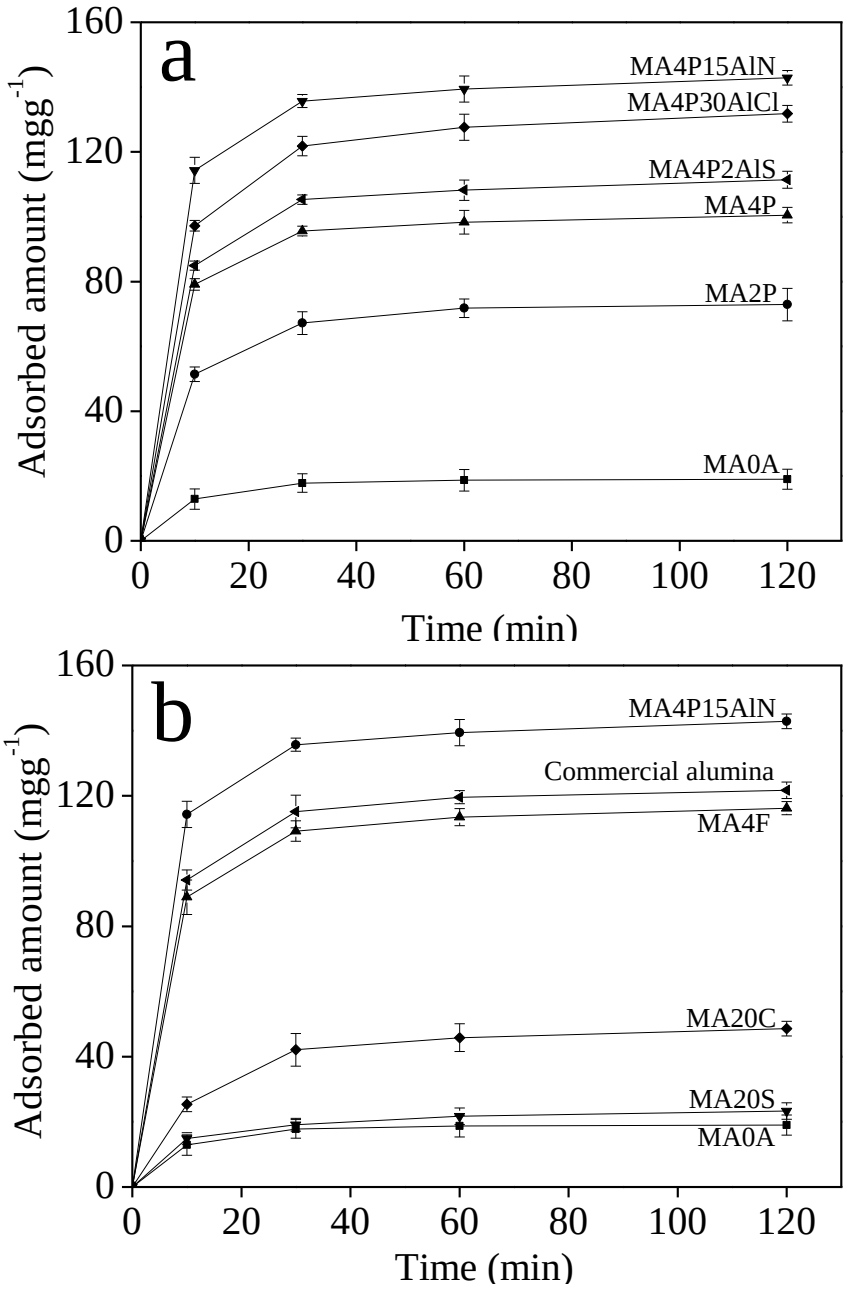

Figure 6-3 Adsorption amount of lipase as a function of time on different supports

6.1.3 Effect of the Support Structural Properties on Lipase Activity

Table 6-3 and Figure 6-4 compare the biodiesel yields over different catalysts. The free lipase and commercial alumina supported lipase were also included for comparison. As seen in Table 6-3, the highest biodiesel yield was achieved over MA4P15AlN (49.6%), higher than that of free lipase (30.6%) and commercial alumina (41.6%) as well as other MAs under the same reaction conditions. Lipase catalytic activity was then calculated

based on the biodiesel yield and lipase adsorption amount on the supports and the results are presented in Figure 6-4. It was found that, regardless of the type of support, the immobilisation of lipase profoundly improved the lipase activity. As can be seen in Table 6-3, the lipase catalytic activity substantially increased from 12.8 μmolh^{-1}g^{-1} of the free lipase to 166.5 μmolh^{-1}g^{-1} of MA4P30AlCl. This observation was in accordance with the (Yan *et al.* 2009; Yan *et al.* 2011), which reported significant increases in the catalytic activity after lipase immobilisation. This was thought to be attributed to the largely alleviated lipase aggregation and consequently the reduced mass transfer limitation in catalysis.

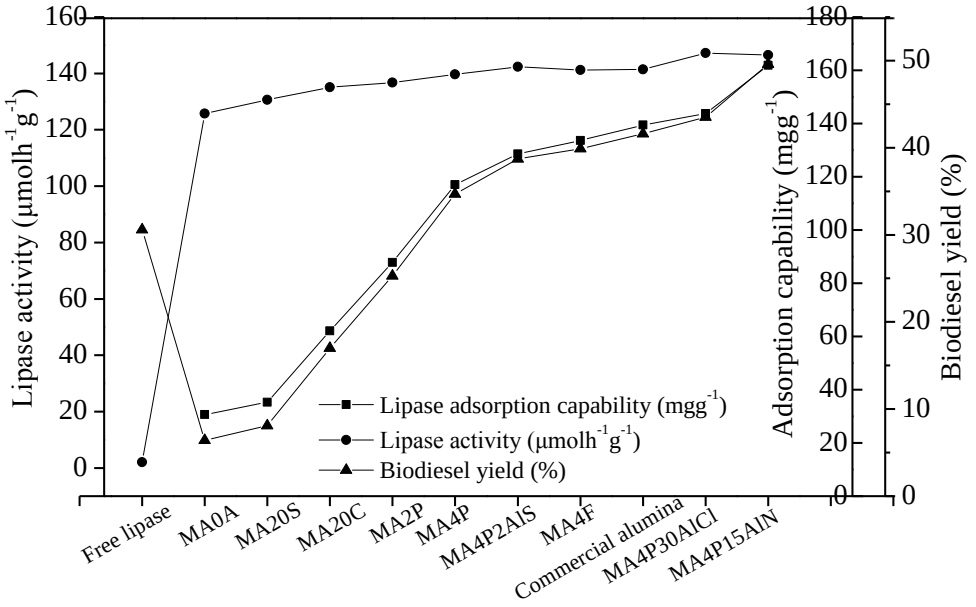

Figure 6-4 Comparisons of lipase adsorption capability, lipase activity and the resulting biodiesel yield on different supports

In addition, the differences in the enhancement of lipase activity induced by different supports were also observed. An increase in the lipase activity was demonstrated from MA0A to MA4P30AlCl, started from 143.7 μmolh^{-1}g^{-1} of MA0A to 166.5 μmolh^{-1}g^{-1} of MA4P30AlCl, relatively improved by 15.9%. This increase was thought to be ascribed to the improved structural properties (larger pore volume and pore size, higher surface area), afforded reduced mass transfer resistance of the triglycerides within the pores of

catalyst. The immobilisation of lipase on MA4P30AlCl and MA4P15AlN showed similar transesterification activity (166.5 $\mu molh^{-1}g^{-1}$ and 165.7 $\mu molh^{-1}g^{-1}$, respectively). However, as seen in Table 6-3, under the reaction conditions, owing to its superior lipase adsorption capability, MA4P15AlN supported lipase gave a higher biodiesel yield than MA4P30AlCl. Likewise, the biodiesel yield obtained over MA4P15AlN was 19.2% higher than that over the commercial alumina. This was also mainly attributed to the higher lipase adsorption capability of MA4P15AlN, as shown in Figure 6-4.

Table 6-3 Comparison of lipase adsorption capability, lipase activity and resulting biodiesel yield on different supports

Support	Amount of adsorbed lipase in 120 min (mgg^{-1})	Biodiesel yield (%)	Lipase activity ($\mu molh^{-1}g^{-1}$)
Free lipase	-	30.6	12.8
MA0A	19.0	6.4	143.7
MA2P	72.9	25.3	155.4
MA4P	100.5	34.7	158.5
MA4P15AlN	142.9	49.6	165.7
MA4P2AlS	111.4	38.7	161.3
MA4P30AlCl	131.8	43.5	166.5
MA4F	116.2	39.9	160.1
MA20C	48.6	17.0	153.6
MA20S	23.3	8.1	148.9
Commercial alumina	121.7	41.6	160.3

6.2 Optimisation of Reaction Conditions using RSM

6.2.1 Effect of the Studied Reaction Variables

Since the MA4P15AlN was found to achieve the highest lipase adsorption and the MA4P15AlN supported lipase showed a high transesterification activity, as discussed in Section 6.2.2 and 6.2.3, respectively, an experimental design using RSM based on the three-variable central composite design (CCD) method was applied to MA4P15AlN to determine the significant parameters and the optimal conditions for biodiesel production. The key variables investigated included water addition, reaction temperature and catalyst loading. The reaction parameters such as water addition (nil to 8 wt%), reaction temperature (30 ℃ to 50 ℃) and catalyst loading (2 wt% to 6 wt%) were varied with an aim to obtain the optimal reaction conditions. The ranges and levels of the three variables studied are shown in Table 3-2. A total of 14 factorial points and 5 centre points were used for fitting a second-order response surface. Table 6-4 shows the design matrix of experiments and the corresponding responses.

Using the response surface methodology for the analysis of experimental parameters, including X_1 reaction temperature, X_2 water addition and X_3 catalyst loading, a quadratic polynomial equation Eq. (6-1) in terms of the coded factors when using MA4P15AlN supported lipase catalyst for biodiesel production was generated to fit the experimental data:

$$Y = 86.69 + 0.94X_1 - 0.37X_2 + 4.19X_3 - 0.027X_1X_2 + 0.069X_1X_3 - 0.092X_2X_3 - 3.64X_1^2 - 3.63X_2^2 - 2.07X_3^2 \quad (6\text{-}1)$$

A statistical analysis of variance (ANOVA) was carried out to study the fitness of the model as well as the effect of significant individual terms and their interactions on the chosen response (Kafuku *et al.* 2010).

Table 6-4 Design matrix of experiments and the corresponding biodiesel yields

Standard order	Reaction parameters			Yield (%)
	Temperature (℃)	Water (wt%)	Catalyst loading (wt%)	
1	35	6	3	68.8
2	40	4	4	87.3
3	40	8	4	75.6
4	45	2	3	74.2
5	50	4	4	75.1
6	40	4	2	71.8
7	35	2	5	80.4
8	40	4	4	86.4
9	30	4	4	72.5
10	45	2	5	83.1
11	45	6	3	71.1
12	45	6	5	79.5
13	40	4	6	88.3
14	40	4	4	88.2
15	40	4	4	87.7
16	40	4	4	97.1
17	35	6	5	77.0
18	40	0	4	72.0
19	35	2	3	71.9

From Table 6-5, it can be seen that at 95% confidence level, the fitting of the experimental data to the quadratic polynomial equation (3-11) was found significant, as confirmed by the high *F* value of 11.81 and very low probability value ("Prob > F") of 0.0005 (Rashid *et al.* 2011; Ghosh *et al.* 2012). The low "Lack of fit F-value" of 1.211 implied that the lack of fit was not significant relative to the pure error (Ghosh *et al.* 2012). In addition, the high regression coefficient (R^2) of 0.9219 was an indication that the fitted model could be used for prediction with confidence (Kafuku *et al.* 2010). "Adeq Precision" measures the signal to noise ratio. A ratio greater than 4 is desirable

(Rashid *et al.* 2011). Herein, the ratio of 8.408 indicated an adequate signal to noise ratio. On the other hand, a low value of coefficient of variation (CV = 3.48%) revealed a better precision and reliability of the experimental results of the fitted model (Ghosh *et al.* 2012). Noticeably, the ANOVA parameters, including model *F* value, coefficient of variation and squared regression all indicated a good fitness of experimental values. Moreover, the data related to the statistical significance of individual parameters in Table 6-5 revealed that the linear term of X_3 and the quadratic terms of X_1, X_2 and X_3 had a profound effect on biodiesel yield due to the high F-values and the corresponding low *p*-values. Accordingly, the linear terms of X_1, X_2 and the interaction terms of X_1X_2, X_1X_3 and X_2X_3 were considered insignificant.

Table 6-5 Analysis of variance (ANOVA) for response surface quadratic model

Source of variation	Sum of squares	Degrees of freedom	Mean squares	*F* value	Prob > F *p*-value
Model	801.71	9	89.08	11.81	0.0005
X_1	14.18	1	14.18	1.88	0.2036
X_2	2.23	1	2.23	0.30	0.6000
X_3	280.73	1	280.73	37.21	0.0002
X_1X_2	0.0057	1	0.0057	0.00076	0.9787
X_1X_3	0.038	1	0.038	0.005	0.9449
X_2X_3	0.068	1	0.068	0.0091	0.9262
X_1^2	313.00	1	313.00	41.48	0.0001
X_2^2	311.65	1	311.65	41.30	0.0001
X_3^2	101.62	1	101.62	13.47	0.0052
Residual	67.91	9	7.55		
Lack of fit	66.10	5	13.22	1.211	0.0030
Pure error	1.81	4	0.45		
Total	869.62	18			

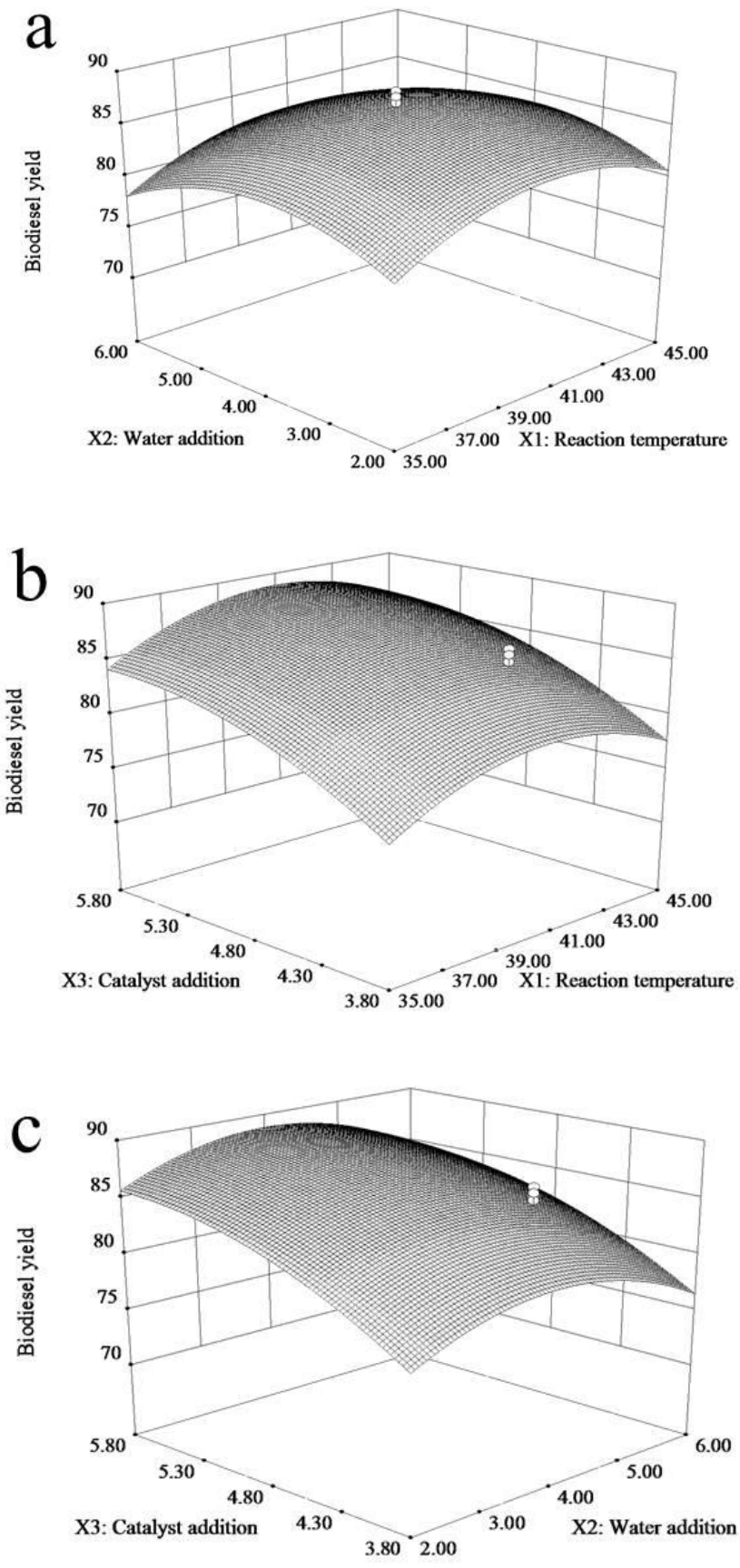

Figure 6-5 Three-dimensional response surface plots

Three-dimensional response surfaces were plotted on the basis of the model equation, to investigate the interaction among the three variables and to determine the optimum condition of each variable for maximum biodiesel production. Figure 6-5a, Figure 6-5b and Figure 6-5c show the interaction between X_1 reaction temperature and X_2 water addition, X_1 reaction temperature and X_3 catalyst loading, X_2 water addition and X_3 catalyst loading, respectively. The curvature nature and clear elongated diagonals of the 3-dimensional surface seen in Figure 6-5a were indicative of the significant interactive effect on biodiesel yield between X_1 reaction temperature and X_2 water addition (Rashid *et al.* 2011; Ghosh *et al.* 2012). The biodiesel yield initially increased with increasing reaction temperature and water addition and then decreased. Peak biodiesel yields were obtained at reaction temperature around 40 ℃ and water addition around 4 wt%, respectively. In contrast, in Figure 6-5b and Figure 6-5c, catalyst loading was the dominant factor, showing great influence on biodiesel yield. This was accordant with the much larger F value of X_3 catalyst loading seen in Table 6-5, implying a stronger effect of catalyst loading on biodiesel yield. In Figure 6-5b and Figure 6-5c, at any designated reaction temperature from 35 ℃ to 45 ℃ and water addition from 2 wt% to 6 wt%, biodiesel yield increased progressively with increased catalyst loading. The optimal reaction temperature and water addition were also attained to be around 40 ℃ and 4 wt%, consistent with the observations in Figure 6-5a.

Actually, for the enzymatic transesterification process, as the temperature increases, the reaction rate initially increases, mainly due to an enhancement in rate constants and partly due to less mass transfer limitations, but decreases sharply at the onset of denaturation of the lipase at higher temperatures (Gog *et al.* 2012). Therefore, there must be a particular optimum temperature for each lipase, giving a peak value to the biodiesel yield and every critical temperature is determined by the interaction between the operational stability of the lipase and the rate of transesterification reaction (Gog *et*

al. 2012). In addition, the lipase-catalysed biodiesel production is also heavily affected by water content. Some essential water is indispensable to activate lipase at the oil-water interface and the availability of the interface assists to maintain lipase activity (Al-Zuhair 2007). The transesterification efficiency depends on the size of interfacial area which can be aptly increased by the addition of certain amount of water (Al-Zuhair 2007). However, because of the hydrolases nature of lipases, excess water will stimulate the unintended side-reaction hydrolysis, thus causing the decrease of transesterification yield. Therefore, the optimum water content is actually a compromise between maximising lipase activity by enhancing the interfacial area and also the minimisation of hydrolysis (Tan *et al.* 2010; Gog *et al.* 2012). In this study, the optimum temperature and water addition for the MA4P15AlN immobilised pseudomonas fluorescens lipase was around 40 ℃ and 4 wt%, respectively.

6.2.2 Optimisation Study

As the fitted model presented in Eq. (6-1) offered a good estimate of the experimental conditions, it was employed to predict the best transesterification process variables for obtaining a maximum biodiesel yield. It was observed that the biodiesel yield up to 88.9% could be obtained with the following conditions: temperature 41 ℃, water addition 3.9 wt% and catalyst loading 5.0 wt%. This result compares favourably well with the other reactions systems using the commercial homogeneous catalysts reported in the literature (~ 95%) (G. Vicente 1998; Rashid *et al.* 2008) and the heterogeneous MAK catalyst (92.2 %) found in Chapter 4.

6.3 Summary

Immobilised enzymatic catalysts for the transesterification of canola oil with methanol were prepared by the adsorption of pseudomonas fluorescens lipase on MAs and a commercial alumina. The immobilised lipase significantly improved the lipase activity

in transesterification. The adsorption of lipase on a support prevented lipase aggregation and reduced mass transfer limitations due to the larger surface area and pore volume of the support. Moreover, the improved structural properties of MA also enhanced lipase adsorption capability. Owing to the high lipase activity and superior lipase adsorption capability, a tailor-designed support MA4P15AlN exhibited higher biodiesel yield than the other MAs and the reference commercial alumina.

An experimental design was performed using RSM with MA4P15AlN supported lipase as the catalyst to explore the impact of reaction conditions. The highest biodiesel yield of 88.9% was achieved in 24 h of reaction time with the following reaction conditions: temperature 41 ℃, water addition 3.9 wt% and catalyst loading ratio 5.0 wt%.

Chapter 7 Evaluation and Practical Implications

In this chapter, the findings from the main body of the present research as detailed in Chapters 4 to 6 are integrated and evaluated, and the potential implications are also assessed, with reference to the gaps identified and the objectives set out in Chapter 2. In evaluating the present work, the results from the present study are compared with the literature data. The evaluation can identify and highlight new gaps in knowledge and practical implications to which future research should be directed.

7.1 MA Synthesis and Control of Structural Properties

In the present research, mesoporous aluminas with controllable structural properties, viz. BET surface area, pore volume and pore size, were successfully synthesised based on a sol-gel self-assembly process via the hydrolysis of aluminium isopropoxide associated with a SDA as the template in an acidic aqueous system. The key synthetic conditions tested in this study included nitric acid addition amount, template type, template addition amount, inorganic aluminium precursor doping and calcination temperature.

As reviewed in Chapter 2, MA are commonly synthesised by three pathways: (1) by solvent-deficient synthesis without the SDAs and templates (Huang *et al.* 2013; Huang *et al.* 2013), (2) by adopting the nanocasting method with polymers and carbon molds as hard templates (Wu *et al.* 2010), and (3) a pathway based on a modified sol-gel self-assembly process in the presence of a soft template such as a cationic, anionic, or nonionic surfactant as the SDAs (Čejka 2003; Kim *et al.* 2004; Maekawa 2004; Xu *et al.* 2006; C Márquez‐Alvarez 2008; Kondo *et al.* 2008; Paul *et al.* 2012; Ghosh *et al.* 2014). Compared to the former two pathways, the soft template pathway has attracted great attention as its easily accessible and reproducible manner in fabricating MA with differed structural properties of the obtained MAs. The present findings agree well with

the literature and the resulting structural properties can be modulated by fine-tuning the synthetic conditions.

A step further on the current recipes for the synthesis of MA using ethanol as the solvent, a major improvement has been made by using water as the synthesis medium. Upon the hydrolysis of aluminium precursor in the presence of a surfactant, the formation of an intermediate boehmite/surfactant nano-composite was identified to occur. This study was the first attempt, which systematically investigated the effect of a group of synthetic conditions and realised the control of the structural properties of the obtained MAs over very wide ranges. Table 7-1 summarises the differences in the structural properties of MAs synthesised following different pathways and by manipulating different synthesis conditions.

From Table 7-1, it can be concluded that compared with literature, the structural properties of the synthesised MAs in the present study could be controlled in much wider ranges, especially in the pore volume and pore size. Herein, the pore volume could be expanded from 0.4 to 2.8 cm^3g^{-1} while the pore size could be adjusted within the range from 5.5 to 64.1 nm. The fine tuning of the mesoporosity features was realised by the rather strict control of the synthesis conditions such as acid, template, aluminium precursor composition and crystallization temperature.

Moreover, the hard template pathway has long been criticised for its complexity and time-consuming synthesis process (Wu *et al.* 2010). And also, due to the lack of a template, the modulation of the structural properties following the surfactant free pathway was not continuous, only particular values can be obtained. The aqueous phase synthesis route developed in this study is therefore recommended as an efficient and facile approach for MA synthesis.

Table 7-1 Summary and comparison of the structural properties of MAs synthesised following different pathways

Synthesis pathway	Template	Solvent	BET Surface Area (m^2g^{-1})	Pore Volume V_p (cm^3g^{-1})	Pore size (nm)	Reference
Surfactant free pathway	-	Ethylenediamine *tetra*-acetic acid (EDTA)-ethylenediamine (ED)-water	323	0.5	6.1	(Mathew *et al.* 2012)
Surfactant free pathway	-	*Iso*-propanol-toluene-water	121~365	0.4~0.8	5.4~10.8	(Gan *et al.* 2007)
Surfactant free pathway	-	Alcohol-toluene mixed system	186~641	0.2~1.3	2.3~22.8	(Li *et al.* 2013)
Surfactant free pathway	-	ethanol, *iso*-propanol, *sec*-butanol and *n*-hexanol	180~260	0.8~1.4	7~37	(Huang *et al.* 2013)
Surfactant free pathway	-	Aqueous medium	240~320	0.4~1.6	4~18	(Huang *et al.* 2014)
Surfactant free pathway	-	Aqueous medium	210~320	0.4~1.7	3~4	(Huang *et al.* 2013)
Hard template pathway	A pristine mesoporous carbon (PMC) and a functionalized mesoporous	Ethanol	141~357	0.2~0.9	3.6~8.0	(Zhangxiong Wu 2010)

	carbon (FMC)					
Hard template pathway	Carbon aerogels	Aqueous medium	275~335	0.8~1.6	7.7~22.9	(Li *et al.* 2005)
Nonionic surfactant pathway	Pluronic P123	Ethanol	206~410	0.4~0.8	3.9~15.0	(Niesz *et al.* 2005)
Nonionic surfactant pathway	Pluronic P123	Ethanol	178~300	0.4	2.9~3.4	(Li *et al.* 2009)
Nonionic surfactant pathway	Pluronic P123 and F127	Ethanol	116~480	0.2~0.8	3.1~7.3	(A.-X.Y. Q. Yuan 2008)
Nonionic surfactant pathway	Pluronic P123	Ethanol	10~292	0.1~0.6	0~9.0	(Stacy M. Morris *et al.* 2008)
Nonionic surfactant pathway	Pluronic P123	Ethanol	307~530	0.3~0.6	4.1~11.1	(Cai *et al.* 2011)
Nonionic surfactant pathway	Pluronic P123	Ethanol, *sec*-butanol, *tert*-butanol	156~432	0.4~0.8	3.4~8.0	(Pérez *et al.* 2013)
Nonionic surfactant pathway	Pluronic P123	Ethanol	26~583	0.1~0.7	3.7~12.4	(Grant *et al.* 2012)
Nonionic surfactant pathway	Brij®78, F108 and B50-6600	Ethanol	300~433	0.3~1.1	2.7~11.5	(Cai *et al.* 2011)
Nonionic surfactant pathway	Pluronic P123	Aqueous medium	463	2.6	17.8	(Liu *et al.*

						2008)
Nonionic surfactant pathway	Brij30	Aqueous medium	285	2.3	15.4	(Liu *et al.* 2008)
Cationic surfactant pathway	CTAB	Aqueous medium	413	1.9	12.4	(Liu *et al.* 2008)
Cationic surfactant pathway	Pluronic P123, Brij56 and CTAB	Ethanol in diluted aqueous HCl	238~306	-	7.0~8.3	(Suzuki *et al.* 2010)
Cationic surfactant pathway	CTAB	Ethanol-water mixture	407	0.9	5-25	(Zhang *et al.* 2004)
Cationic surfactant pathway	CTAB	Aqueous medium	158~382	0.1~0.3	3.5~4.2	(Liu *et al.* 2007)
Anionic surfactant pathway	SDS	Aqueous medium	338~528	0.3~0.4	3.1~3.3	(Liu *et al.* 2007)
Anionic surfactant pathway	SDS	Aqueous medium	368	1.3	11.7	(Liu *et al.* 2008)
Anionic surfactant pathway	AOT	Aqueous medium	382	1.5	13.3	(Liu *et al.* 2008)
Nonionic surfactant pathway	Pluronic P123	Aqueous medium	104~409[a] 104~335[b]	0.4~2.5[a] 0.4~2.8[b]	7.0~36.5[a] 7.0~64.1[b]	The present study
Nonionic surfactant	Pluronic	Aqueous medium	236~358	0.4~1.9	7.0~30.1	The present

pathway	F127					study
Cationic surfactant pathway	CTAB	Aqueous medium	236~319	0.4~1.1	7.0~13.4	The present study
Anionic surfactant pathway	SDS	Aqueous medium	236~260	0.4~0.5	5.5~8.6	The present study

Note: [a] The MAs were obtained by modulating the P123 addition amount and calcination temperature, shown in Table 4-2. [b] The MAs were synthesised by modulating the P123 addition amount and the inorganic aluminium precursors summarised in Table 4-3.

7.2 Alkaline MAK Catalyst for Biodiesel Production

The effectiveness of the as-synthesised heterogeneous alkaline mesoporous alumina supported potassium catalyst in catalysing the transesterification of canola oil with methanol for biodiesel production was measured. The MAK catalysts were synthesised following the one-pot synthesis pathway via the self-assembly of potassium precursor KNO_3 and aluminium isopropoxide simultaneously. The incorporation of K species has reduced the BET surface area and pore volume of the MA, but significantly increased the pore size. The structural properties of the obtained catalyst were also modulated by adjusting the usage of template P123. On the basis of the reduced level of mass transfer limitation in catalysis as a result of the improved structural properties, MA1P20K showed a high yield of biodiesel of 92.2% under the conditions as: 2 wt% catalyst loading, 12:1 molar ratio of methanol to oil at 70 ℃ with 5 h of reaction time under stirring. In addition, the MA1P20K exhibited good reusability, biodiesel yield only slightly decreased from 92.2 % to 86.8% after five successive cycles.

Up to now, Alamu and the co-authors reported a maximum biodiesel yield of 95.8 % from palm kernel oil using KOH as the catalyst under the reaction conditions of 60 ℃, KOH concentration of 1.0 wt% within 2 h (OJ Alamu 2007). A high biodiesel yield of 96.2% was demonstrated by Refaat and the co-authors by using NaOH as the catalyst under M/O of 6:1 and temperature of 65 ℃ (A. A. Refaat 2008). Data in Chapter 5 has confirmed that the MAK catalysts synthesised in the present study showed comparable activity to the extensively used homogeneous catalysts.

Moreover, most literature reports only focused on the performance of homogeneous alkaline catalysts like the aforementioned KOH and NaOH (Sharma *et al.* 2011). Despite favourable effectiveness and relatively low cost, these homogeneous catalysts may cause environmental problems that militate against the implementation of easy

separation and product purification procedures, thus leading to the increased production cost and severe environmental issues. Combined with the high catalytic activity, favourable reusability and the heterogeneous nature, the MAK series catalysts were efficient in producing biodiesel, and would be of great value for practical industrial implications.

Activation energy of the MA1P20K catalysed transesterification was found ranging from 20.2 $kJmol^{-1}$ to 23.6 $kJmol^{-1}$, indicating its high effectiveness in catalysing the transesterification reaction. The activation energy E_a for the alkali-catalysed homogeneous and heterogeneous transesterification of oils with methanol were reported in the range of 20.0 $kJmol^{-1}$-81.1 $kJmol^{-1}$ (D. Darnoko 2000; Gemma Vicente 2005; Xuejun Liu 2008; Singh *et al.* 2009; Pugnet *et al.* 2010; Xuejun Liu 2010; Zhang *et al.* 2010; Chantrasa *et al.* 2011). The activation energy obtained in this study was found lower than most of the studies, probably owing to the strong basicity of MA1P20K catalyst.

7.3 MA Immobilised Lipase as the Enzymatic Catalyst for Biodiesel Production

Enzymatic transesterification for biodiesel production was also studied using the immobilised pseudomonas fluorescens lipase on MAs as the catalysts. The MAs supported lipase catalysts were assessed for their lipase adsorption and catalytic activity in biodiesel production. Significantly improved lipase catalytic activity in transesterification was demonstrated by the immobilisation on a support, possibly due to the largely alleviated lipase aggregation and consequently the reduced mass transfer limitation in catalysis. The structural properties of MAs were found an important factor in affecting the lipase activity and lipase adsorption capacity. Generally, MA with larger contact interface and more accessible porous channels showed enhanced lipase activity

and adsorption capacity, leading to higher biodiesel yield in transesterification. In the present study, transesterification process using a catalyst based on the tailor-designed MA4P15AlN with high surface area, large pore volume and pore size was optimised and exhibited the highest biodiesel yield of 88.9%. The reaction conditions were kept as: 24 h of reaction time, temperature 41 ℃, water 3.9 wt% and catalyst loading ratio 5.0 wt%. This result compares favourably well with the other reaction systems using the commercial homogeneous catalysts reported in the literature (~ 95%) (G. Vicente 1998; OJ Alamu 2007; Rashid *et al.* 2008; Mathew *et al.* 2012) and the heterogeneous MAK catalyst (92.2 %) found in Chapter 5 of the present study.

On the other hand, the stability of the adsorbed lipase on a support is of great importance, which may affect the reusability of the synthesised catalyst. In addition to the currently studied catalysts synthesised by physically adsorbing lipase onto the supports MAs, other immobilisation techniques like covalent bonding and encapsulation need to be trialled, in particular pay attention to the effect on the activity, stability and reusability of the prepared catalysts in future studies.

7.4 Process Design and Options Analysis for Biodiesel Production

As part of the effort to evaluate the practical implications of the present study, a total of five process design alternatives for biodiesel production were proposed and analysed. The five process design options considered in this study include: (1) a heterogeneous MAK-catalysed transesterification process using a virgin vegetable oil as the feedstock in a batch reactor; (2) an MAK-catalysed transesterification process using the virgin vegetable oil in a continuous stirred tank reactor (CSTR); (3) an MAK-catalysed transesterification process fed with animal tallow in a batch reactor; (4) an MAK-catalysed transesterification process using waste cooking oil in a batch reactor and; (5) the conventional homogeneous NaOH catalysed transesterification process using the

virgin vegetable oil in a batch reactor. The nominal plant production capacity was specified at 10,000 tonne/year based on 300 operating days per year.

Table 7-2 Upstream operations according to the type of feedstock

Type of feedstock	Features	Upstream operations				
		Oil extraction	Melting	Filtration	Pre-esterification	Water removal
Virgin vegetable oil	Vegetable oil with minor FFA and water	-	-	-	-	-
Animal tallow	Various FFA with water and insoluble particles	√	-	√	√	√
Waste cooking oil	Over 10 wt% FFA, with water and insoluble particles	-	√	√	√	√

The main production steps could be broadly divided into upstream and downstream processing, which included all the operation units prior or subsequent to the transesterification reaction step, respectively. As stated in Chapter 2 Literature Review, it was concluded that the upstream processing mainly relied on the type of feedstock whereas the downstream processing depended largely on the type of catalyst chosen for the transesterification reaction. The necessary unit operations for the pre-treatment of each type of feedstock and the downstream processing are shown in Table 7-2 and Table 7-3, respectively. The schematics of the five processes are represented in Figure 7-1. These processes all followed the same general scheme: the extraction, filtration and

esterification of the oil (if applicable) followed by the transesterification unit, and then the downstream processing, including the methanol recovery, catalyst neutralisation and removal, water washing, glycerol separation, and methyl esters' purification by distillation (West et al. 2008). The corrosion of equipment due to the alkali or acid catalysts and the reaction taking place in pipelines were not considered. Moreover, the theoretical reaction intermediates such as diglycerides and monoglycerides were ignored because of the high methanol to oil ratios used in this study (Zhang 2003). Piping and instrumentation diagrams were drawn using Visio 2013.

Table 7-3 Downstream operations according to the type of catalyst chosen for the transesterification reaction.

Type of catalyst	Glycerol removal	Catalyst recovery	Catalyst neutralisation	Alcohol removal	Water washing	Vacuum distillation
MAK	√	√	-	√	√	√
NaOH	√	-	√	√	√	√

7.4.1 Process 1 MAK catalysed transesterification of virgin vegetable oil with methanol in a batch reactor

The detailed piping and instrumentation diagram (PID) of Process 1 is shown in Figure 7-2. The main processing units included reactors, distillation columns, extraction columns, heat exchangers, pumps and separators. Parameters for the calculations of mass balance are summarised in Table 7-4. As investigated in Section 5.2, the reaction conditions for the MAK-catalysed transesterification were suggested as: temperature 70 ℃, catalyst loading 2.0 wt%, M/O 12:1 and reaction time 5 h, under which a biodiesel yield of 92.2 % could be obtained. A virgin vegetable oil containing 0.5 wt% FFA and 0.5 wt% water was used as the feedstock oil (Morais et al. 2010).

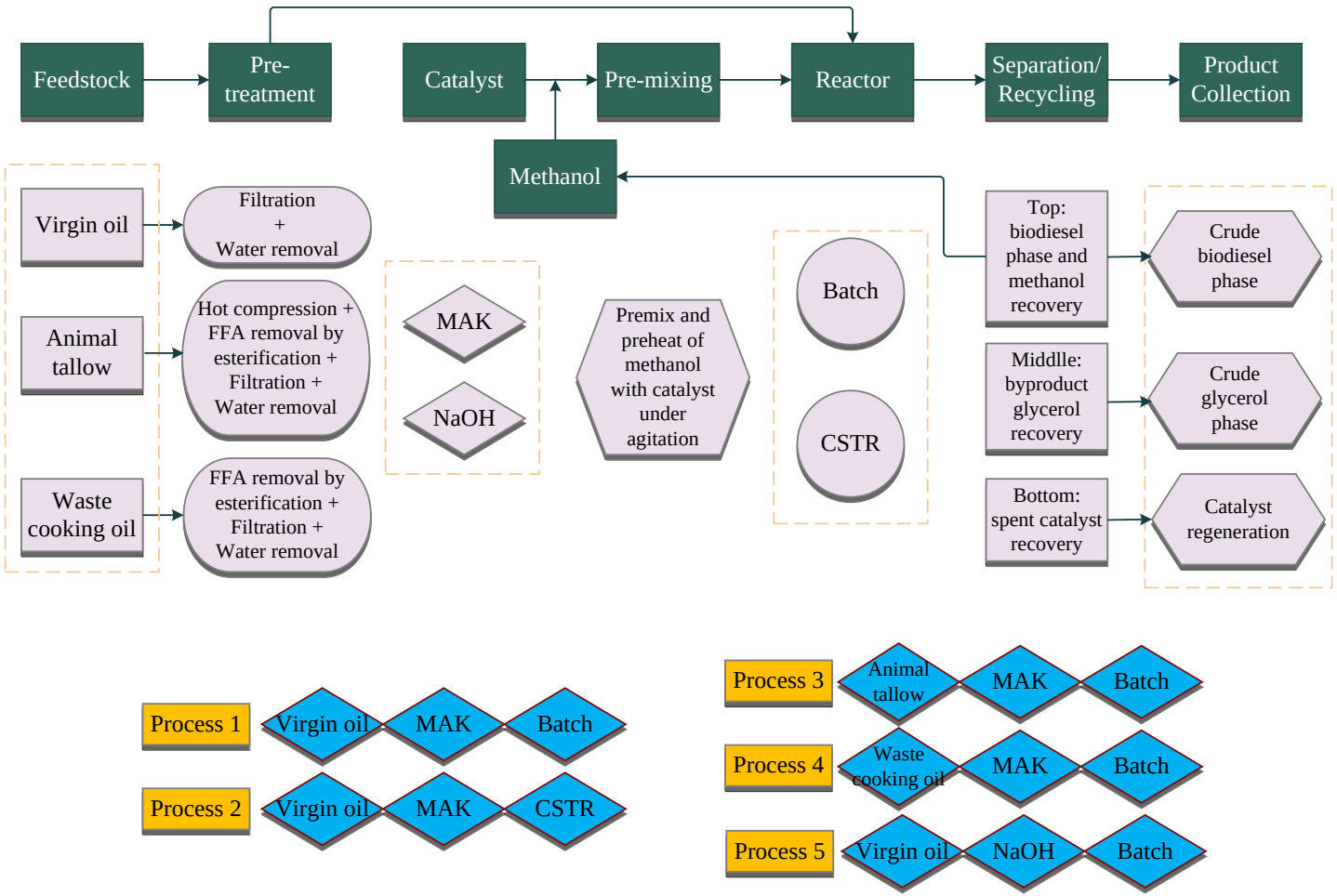

Figure 7-1 Schematics of the five studied processes

The properties of the main streams of Process 1 are shown in Table 7-6. In detail, before entering the reactor R201, fresh methanol (stream 101) was premixed with MAK catalyst in a mixer M101 while virgin vegetable oil (stream 103) was preheated in a heat exchanger H101. Transesterification reaction was conducted in a stirred tank reactor R201. In addition to biodiesel containing FAME, the product stream 203 was rich in unreacted methanol and the by-product glycerol.

Table 7-4 Parameters for the mass balance calculations of Process 1 (Zhang 2003; West et al. 2008; Morais et al. 2010; Santana et al. 2010)

Molecular mass ($gmol^{-1}$)		MAK catalysed transesterification		Other parameters	
Triglyceride[a]	884	Temperature	70 ℃	Annual output	10,000.0 t
Methanol	32	M/O	12:1	Daily output	33.3 t
Methyl ester[a]	296	Catalyst loading	2.0 wt%	Water usage for product purification per batch	1.0 t
Glycerol	92			Feedstock conversion by the MAK catalysed transesterification	92.2%
Virgin vegetable oil (Morais et al. 2010)					
FFA	0.5 wt%	Reaction time per batch	5 h	Methanol reclaim	100%
Water content	0.5 wt%			FAME separation from unconverted oil	99.2%
Triglyceride	99.0 wt%			Water separation from glycerol	99.5%

Note: [a] Calculated in average

In the downstream processing, multi-stage distillation was used for methanol recovery as well as purification of both FAME and glycerol (Zhang 2003; Morais et al. 2010; Santana et al. 2010; Lee et al. 2011). As the boiling point of methanol (65 ℃) was much

lower than that of FAME (approximately 320 ℃) or glycerol (300 ℃), an absolute recovery of methanol was assumed in this study by using a distillation column S301 with three stages and a reflux ratio of two (Santana et al. 2010). For the separations of FAME from unconverted oil and water removal from glycerol, distillation columns with five theoretical stages were required and a 99.2 % separation of FAME from the unconverted oil and a 99.5% recovery of water from glycerol were assumed (Zhang 2003).

Table 7-5 Parameters for the energy input calculations

Specific heat capacity C ($kJkg^{-1}$ $℃^{-1}$)		Power setting W (kW)	
Feedstock oil	2.09	Mixer	$12.0^a/2.0^b$
FAME	2.93	Pump	$16.0^a/2.5^b$
Methanol	2.51	Reactor	$36.0^a/8.0^b$
Glycerol	2.43	Distillation tower	$6.0^c/12.0^d$
Water	4.19	Heat loss coefficient of recovered methanol e	
MAK catalyst	0.75		
NaOH	1.49	0.3	
CaO	0.59		
H_2SO_4	1.47	Initial temperature T (℃)	
H_3PO_4	3.13	20	

Note: [a] Power setting of mixers, pumps and reactors for batch reactors in Process 1, 4, 5, 6. [b] Power setting of mixers, pumps and reactors for continuous reactors in Process 2. [c] Power setting of the vacuum distillation towers for methanol recovery and water separation. [d] Power setting of the vacuum distillation tower for FAME purification from the unconverted oil.

Methanol distillate (stream 302) leaving the distillation column S301 was stored in a tanker T301 for next batch of reaction to be mixed with fresh methanol. Bottom stream 301 was sent to a cyclone C301 for MAK catalyst recovery followed by water washing in S302, enhancing the separation of glycerol and the leached catalyst ions from FAME (Morais et al. 2010). Leaving the water wash column S302, phase separation between the FAME and glycerol could be achieved by the following decanter S303 by gravitational separation. Afterwards, the top stream 307A was subjected to FAME separation from the un-reacted oil in S304. FAME product was obtained in stream 308 as a liquid distillate while the un-reacted oil remained at the bottom. Although the un-reacted oil was not considered in this study, this oil stream could be considered for further recycling and conversion within this process. The bottom stream 307B leaving decanter S303 was fed to water distillation in S305 to separate water from the by-product glycerol.

Parameters for the energy input calculations are shown in Table 7-5 while the summary of energy input is presented in Table 7-7. The energy input was divided into three sectors: to heat up the feedstocks, the electricity for transmission equipment like mixer, pump and reactor, and the electricity for distillations. The initial temperature of feedstocks was set as 20 ℃ and the heat loss coefficient of the recovered methanol *e* was 0.3. As seen in Table 7-7, for a daily output of biodiesel of 33,333.3 kg, the energy input was 9,716,201.7 kJ and the energy input per kilogram of the produced biodiesel was 291.5 kJ.

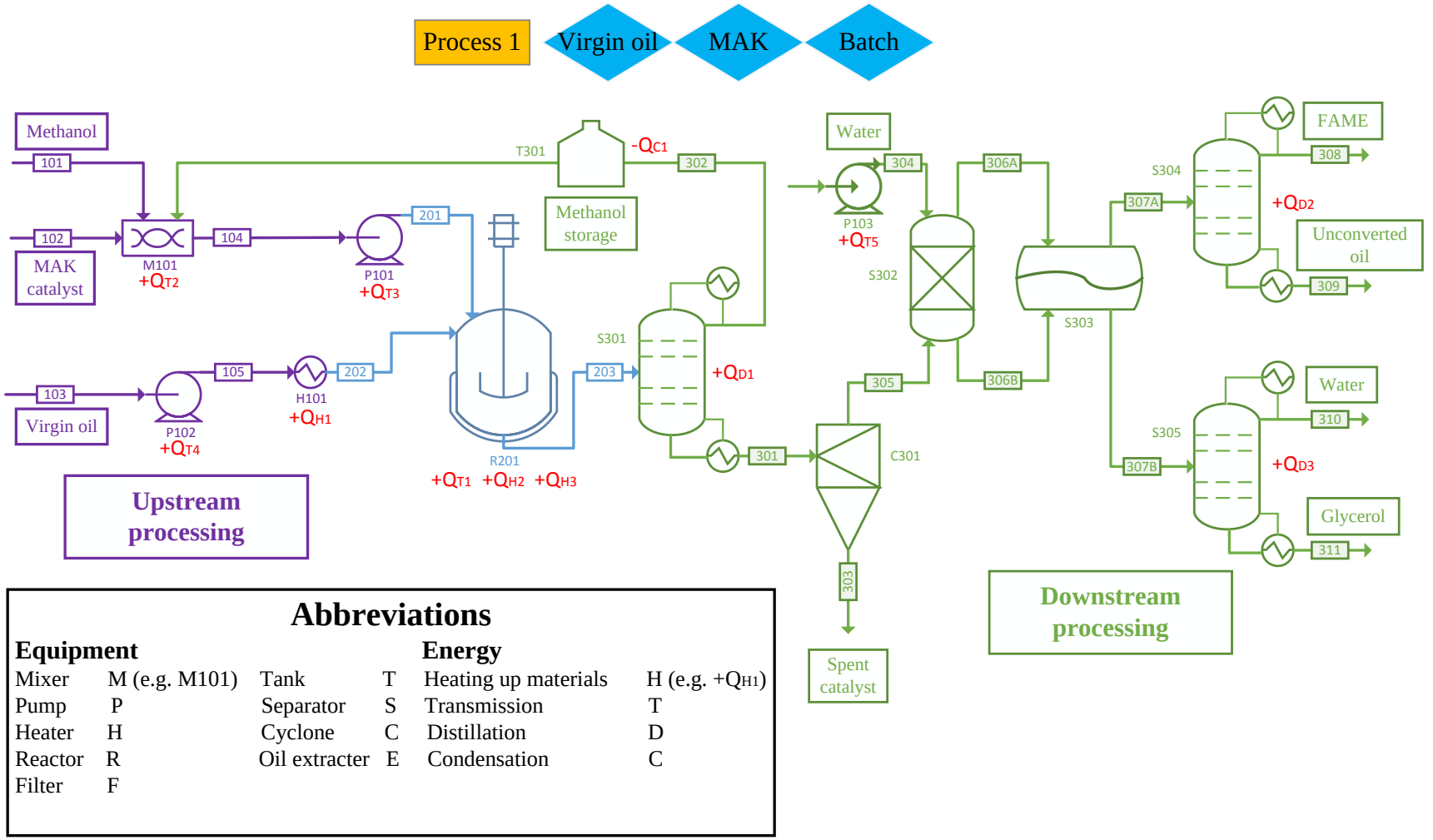

Figure 7-2 Piping and instrumentation diagram of Process 1

Table 7-6 Properties of main streams of Process 1

Inventory	Stream name						
	Feed streams				104/201	203	301
	101	102	103/105/202	304			
Mass fraction (kg per batch)							
Triglyceride	-	-	12,094.8	-	-	943.4	943.4
Methanol	1211.0	-	-	-	5253.8	4042.8	-
MAK	-	241.9	-	-	241.9	241.9	241.9
FAME	-	-	-	-	-	11,201.8	11,201.8
Glycerol	-	-	-	-	-	1160.6	1160.6
Water	-	-	-	1000.0	-	-	-

Table 7-6 Properties of main streams of Process 1 (to be continued)

Inventory	Stream name							
				Product streams				
	305	307A	307B	303	308	309	310	311
Mass fraction (kg per batch)								
Triglyceride	943.4	943.4	-	-	-	943.4	-	-
Methanol	-	-	-	-	-	-	-	-
MAK	-	-	-	241.9	-	-	-	-
FAME	11,201.8	11,201.8	-	-	11,111.1	90.7	-	-
Glycerol	1160.6	-	1160.6	-	-	-	-	1160.6
Water	-	-	1000.0	-	-	-	995.0	5.0

Table 7-7 Energy input calculations of Process 1

Heating up materials per batch (Q_{Hx})			
$Q_{H1} = C_{oil} \times \Delta T \times m_{oil}$ =2.09 ×50 ×12216.9 kJ=1,276,668.7 kJ		$Q_{H3} = Q_{C1} = C_{MtOH} \times \Delta T \times m_{MtOH2} \times e$ =2.51 ×50 ×4042.8 ×0.3 kJ=152,212.6 kJ	
$Q_{H2} = Q_{MtOH1} + Q_{MAK} = C_{MtOH} \times \Delta T \times m_{MtOH1} + C_{MAK} \times \Delta T \times m_{MAK}$ =2.51 ×50 ×1211.0+0.75 ×50 ×241.9 kJ=161,052.6 kJ			
Sum	1,589,933.9 kJ		
Transmission per batch (Q_{Tx})			
$Q_{T1} = P_{R201} \times t_1$ =36 ×5 kWh=648,000.0 kJ		$Q_{T2} = P_{M101} \times t_2$ =12 ×1.5 kWh=64,800.0 kJ	
$Q_{T3} + Q_{T4} = P_{P101} \times t_2 \times 2$ =16 ×1.5 ×2 kWh=172,800.0 kJ		$Q_{T5} = P_{P103} \times t_3$ =2.5 ×8 kWh=72,000.0 kJ	
Sum	957,600.0 kJ		
Distillation per batch (Q_{Dx})			
$Q_{D1} + Q_{D3} = P_{S301} \times t_3 \times 2$ =6 ×8 ×2 kWh=345,600.0 kJ		$Q_{D2} = P_{S304} \times t_3$ =12 ×8 kWh=345,600.0 kJ	
Sum	691,200.0 kJ		
Total energy input per batch	3,238,733.9 kJ	Total energy input per day	9,716,201.7 kJ
Energy input per kilogram of produced biodiesel		291.5 kJ	

7.4.2 Process 2 MAK catalysed transesterification of virgin vegetable oil with methanol in a continuous stirred tank reactor (CSTR)

Compared to Process 1, the major difference in Process 2 was the employment of a CSTR instead of the batch reactor. A CSTR is an ideal steady-state flow reactor, in which the feedstock oil and the premixed methanol and catalyst are introduced while the reaction effluent is steadily removed (Santana et al. 2010). The contents in the reactor are well stirred and uniform throughout, which is identically represented by the exiting stream. In this study, the transesterification reaction was conducted in three CSTRs in series. The three reactors had the same volume of 10.3 m^3. Transesterification reaction conditions and the downstream processing were kept identical as in Process 1.

Table 7-8 Parameters for the mass balance calculations of Process 2 (West *et al.* 2008)

Virgin vegetable oil		MAK catalysed transesterification		Other parameters	
FFA	0.5 wt%	Temperature	70 ℃	Annual output	10,000.0 t
Water content	0.5 wt%	M/O	12:1	Daily output	33.3 t
Triglyceride	99.0 wt%	Catalyst loading	2.0 wt%	Water usage for product purification	2.5 $kgmin^{-1}$
Equal-size mixed flow reactors in series		Kinetics parameters		Flow rate of oil	25.3 $kgmin^{-1}$
Number of reactor	3	Rate constant k_1 of the forward reaction	0.138 $Lmol^{-1}min^{-1}g^{-1}$	Flow rate of methanol	10.9 $kgmin^{-1}$
Reactor volume	10.3 m^3			Methanol reclaim	100%
Fill factor of a reactor	0.8	Rate constant k_{-1} of the reverse reaction	0.016 $Lmol^{-1}min^{-1}g^{-1}$	FAME separation from unreacted oil	99.2%
Filled volume of a reactor V	8.3 m^3			Water separation from glycerol	99.5%

Figure 7-3 shows the PID of Process 2 while Table 7-8 presents the parameters for mass balance calculations. The first reactor R201 was continuously fed with virgin vegetable oil and the premixed methanol and MAK catalyst. The stream 203 leaving the first reactor was fed into the second reactor R202 and afterwards the third reactor R203 at a rate equal to the rate of charging with reactants and catalyst.

As shown in Section 3.2.5, in a transesterification reaction, the stoichiometric relationship between reactants and products is:

$$A + 3B \xrightarrow{Catalyst} 3C + D \tag{3-3}$$

where A stands for triglyceride, B methanol, C methyl ester and D glycerol. For CSTR, the general mass balance equation for the specific reactor *i* is:

$$v_o(c_{A,i-1} - c_{A,i}) = (-r_A)_i V \tag{7-1}$$

where v_0 is the feed flow rate, V is the filled volume of the reactor, $(-r_A)_i$ is the disappearance of triglyceride A by reaction in reactor i, $C_{A,i-1}$ and $C_{A,i}$ are the concentration of triglyceride in reactor *i-1* and *i*, respectively. The space time of the reactor *i* is:

$$\tau_i = V / v_o = (c_{A,i-1} - c_{A,i})/(-r_A)_i \tag{7-2}$$

For the MAK catalysed transesterification, the general rate equation is shown in Eq. (3-3):

$$-dC_A/mdt = k_1 C_A - k_{-1} C_C C_D \tag{3-4}$$

where m, k_1 and k_{-1} are the mass of catalyst (g), rate constants of the forward and reverse reaction, respectively. In addition:

$$C_A = C_{A0}(1-Y) \tag{3-5}$$

$$C_C = 3C_{A0}Y \tag{7-3}$$

$$C_D = C_{A0}Y \tag{7-4}$$

C_{A0} is the initial concentration of triglyceride, Y is the biodiesel yield. So, the disappearance of triglyceride A ($-r_A$) can be derived as:

$$-(r_A) = m[k_1 C_{A0}(1-Y) - 3k_{-1}C_{A0}^2 Y^2] \tag{7-5}$$

Therefore, for the first reactor:

$$\tau_1 = V/\mathrm{v}_0 = (c_{A0} - c_{A1})/(-r_A)_1 = c_{A0}Y_1/m[k_1 C_{A0}(1-Y_1) - 3k_{-1}C_{A0}^2 Y_1^2] \tag{7-6}$$

By following the Eq. (7-6), biodiesel yield Y_1 from the first reactor was 67.4%. Follow the same method, the ultimate biodiesel yield leaving the third reactor achieved 92.7%. The detailed stream information is presented in Table 7-9. In addition, the summary of energy input calculations are shown in Table 7-10. To achieve a daily biodiesel output of 33,333.3 kg, the total energy input was 9,739,005.6 kJ and the energy input per kilogram of produced biodiesel was 292.2 kJ.

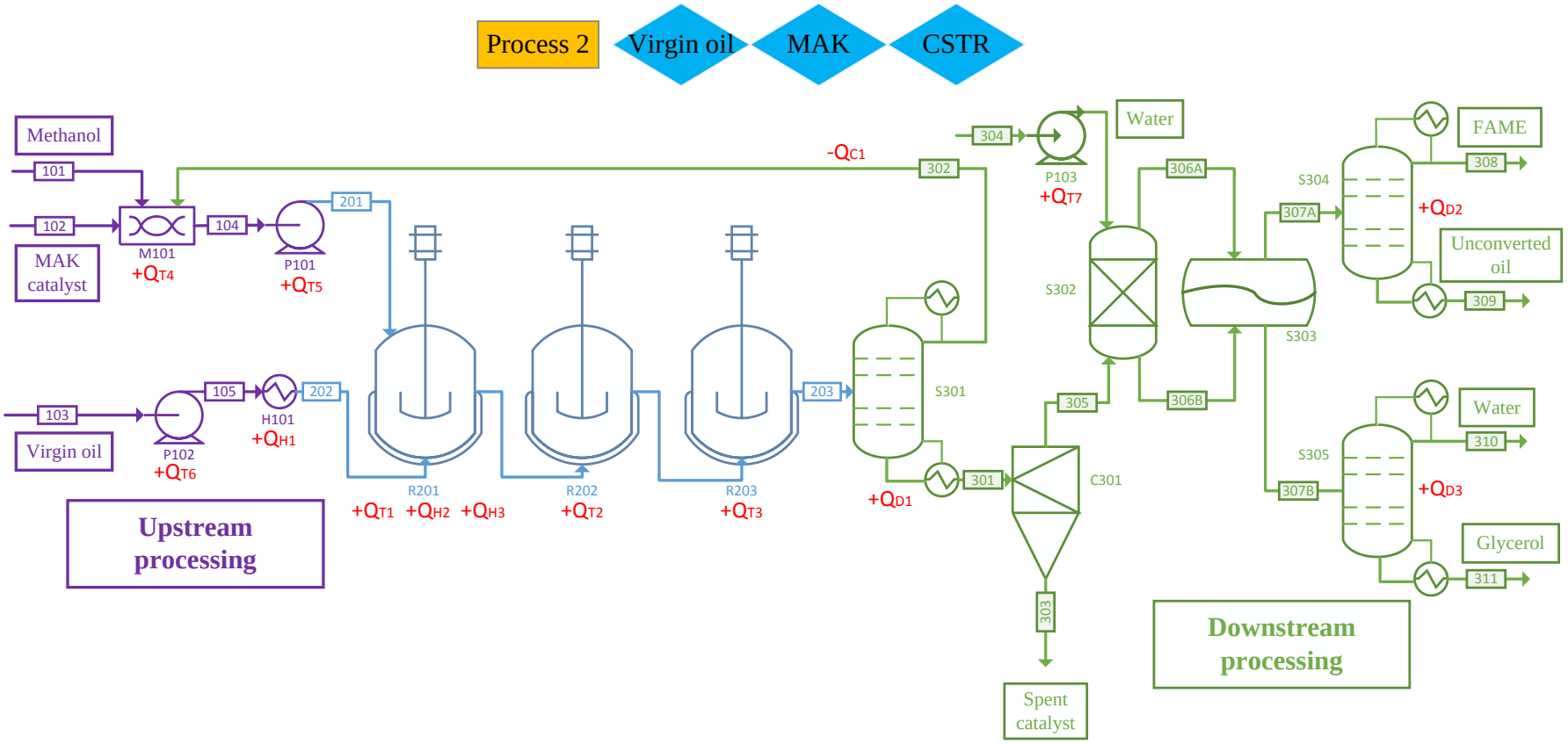

Figure 7-3 Piping and instrumentation diagram of Process 2

Table 7-9 Properties of main streams of Process 2

Inventory	Stream name						
	Feed streams				104/201	203	301
	101	102	103/105/202	304			
Mass flow ($kgmin^{-1}$)							
Triglyceride	-	-	25.3	-	-	1.8	1.8
Methanol	2.7	-	-	-	10.9	8.2	-
MAK	-	0.5	-	-	0.5	0.5	0.5
FAME	-	-	-	-	-	23.3	23.3
Glycerol	-	-	-	-	-	2.4	2.4
Water	-	-	-	2.5	-	-	-

Table 7-9 Properties of main streams of Process 2 (to be continued)

Inventory	Stream name								
					Product streams				
	302	305	307A	307B	303	308	309	310	311
Mass flow ($kgmin^{-1}$)									
Triglyceride	-	1.8	1.8	-	-	-	1.8	-	-
Methanol	8.2	-	-	-	-	-	-	-	-
MAK	-	-	-	-	0.5	-	-	-	-
FAME	-	23.3	23.3	-	-	23.1	0.2	-	-
Glycerol	-	2.4	-	2.4	-	-	-	-	2.4
Water	-	-	-	2.5	-	-	-	2.5	Trace

Table 7-10 Energy input calculations of Process 2

Heating up materials per hour (Q_{Hx})			
$Q_{H1} = C_{oil} \times \Delta T \times m_{oil}$ =2.09 ×50 ×25.3 ×60 kJ=158,725.1 kJ		$Q_{H3} = Q_{C1} = C_{MtOH} \times \Delta T \times m_{MtOH2} \times e$ =2.51 ×50 ×4042.8 ×0.3 kJ=152,212.6 kJ	
$Q_{H2} = Q_{MtOH1} + Q_{MAK} = C_{MtOH} \times \Delta T \times m_{MtOH1} + C_{MAK} \times \Delta T \times m_{MAK}$ =2.51 ×50 ×2.7 ×60+0.75 ×50 ×0.5 ×60 kJ=21,624.4 kJ			
Sum	198,791.9 kJ		
Transmission per hour (Q_{Tx})			
$Q_{T1} + Q_{T2} + Q_{T3} = P_{R201} \times \mathrm{t} \times 3$ =8 ×1 ×3 kWh=864,000.0 kJ		$Q_{T4} = P_{M101} \times \mathrm{t}$ =2 ×1 kWh=7,200.0 kJ	
$Q_{T5} + Q_{T6} + Q_{T7} = P_{P101} \times \mathrm{t} \times 3$ =2.5 ×1 ×3 kWh=27,000.0 kJ			
Sum	120,600.0 kJ		
Distillation per hour (Q_{Dx})			
$Q_{D1} + Q_{D3} = P_{S301} \times \mathrm{t} \times 2$ =6 ×1 ×2 kWh=43,200.0 kJ		$Q_{D2} = P_{S304} \times \mathrm{t}$ =12 ×1 kWh=43,200.0 kJ	
Sum	86,400.0 kJ		
Total energy input per hour	405,791.9 kJ	Total energy input per day	9,739,005.6 kJ
Energy input per kilogram of produced biodiesel		292.2 kJ	

7.4.3 Process 3 MAK catalysed transesterification of animal tallow with methanol in a batch reactor

This process dealt with the conversion of an animal tallow containing 10.0 wt% FFA, 5.0 wt% water and 5.0 wt% solid into biodiesel. Due to the high concentration of FFA, an acid-catalysed esterification process to eliminate the FFA must be applied prior to the alkali-catalysed transesterification reaction (Santana et al. 2010). Figure 7-4 shows the PID of Process 3, in particular the pretreatment steps, including the oil extraction by hot compression, esterification of FFA, methanol recovery and glycerol washing. Table 7-11 summarises the parameters for the mass balance calculations. The H_2SO_4-catalysed esterification reaction was performed at 70 ℃, methanol to FFA molar ratio of 20:1, H_2SO_4 loading 2.0 wt% and reaction time 3 h. It showed a 99.5% conversion of FFA into methyl esters (Morais et al. 2010).

As can be seen in Figure 7-4, animal tallow was firstly preheated in a heat exchanger H101 and then subjected to hot compression for oil extraction. The extracted oil (stream 109) was filtered in F101 to remove solid and then mixed with fresh (stream 104) and recycled (stream 117) methanol and sulfuric acid (stream 105) before entering the reactor R101. Water and catalyst H_2SO_4 contained in the effluent stream 112 must be removed before proceeding to transesterification unit. Therefore, after esterification, the effluent stream 112 was forwarded to a glycerol washing column S101, where glycerol was used (stream 124) to wash out H_2SO_4 and water through a three theoretical washing stage (Morais et al. 2010). The treated oil leaving the glycerol washing column from the top stream 115 was sent to the downstream transesterification unit. The remaining components in the bottom stream 116, mainly glycerol, water and H_2SO_4 were then charged into a distillation column S102, where the non-reacted methanol (stream 117) to be recycled and fed back to the esterification reactor R101.

Table 7-11 Parameters for the mass balance calculations of Process 3 (West *et al.* 2008; Santana *et al.* 2010)

Molecular mass ($gmol^{-1}$)		MAK catalysed transesterification		Other parameters	
FFA	282	Temperature	70 ℃	Annual output	10,000.0 t
Sulphuric acid H_2SO_4	98	M/O	12:1	Daily output	33.3 t
Calcium oxide CaO	56	Catalyst loading	2.0 wt%	Water usage for product purification per batch	1.0 t
Calcium sulphate $CaSO_4$	136	Reaction time per batch	5 h	FFA removal by H_2SO_4 catalysed esterification	99.5%
Animal tallow (Morais *et al.* 2010)		H_2SO_4 catalysed esterification for FFA removal		Methanol reclaim	100%
FFA	10.0 wt%	Temperature	70 ℃	FAME separation from unconverted oil	99.2%
Water content	5.0 wt%	Molar ratio of methanol to FFA	20:1		
Solid content	5.0 wt%	Catalyst loading (relative to the mass of FFA)	5.0 wt%	Water separation from glycerol	99.5%
Triglyceride	80.0 wt%	Reaction time per batch	3 h		

After methanol recovery, the glycerol and H_2SO_4 leaving the distillation column S102 in the bottom stream 118 was fed to a neutralisation reactor R102 with calcium oxide. An absolute removal of sulfuric acid was assumed. The precipitated calcium sulphate was removed in a gravity separator S103. The glycerol stream 122 leaving the gravity separator was then purified in an evaporator S104 to remove water. Glycerol in the bottom stream 124 was then recycled in the glycerol washing column S101 to be mixed with the fresh glycerol makeup stream 113. The following transesterification unit and downstream processing steps were identical with the details as illustrated in Process 1. Properties of main streams on the basis of 11,111.1 kg of biodiesel production capacity per batch are shown in Table 7-12. Table 7-13 summarises the energy input calculations. Due to the added esterification unit and the followed glycerol washing and H_2SO_4 neutralisation steps, the energy input per kilogram of the produced biodiesel reached 526.0 kJ.

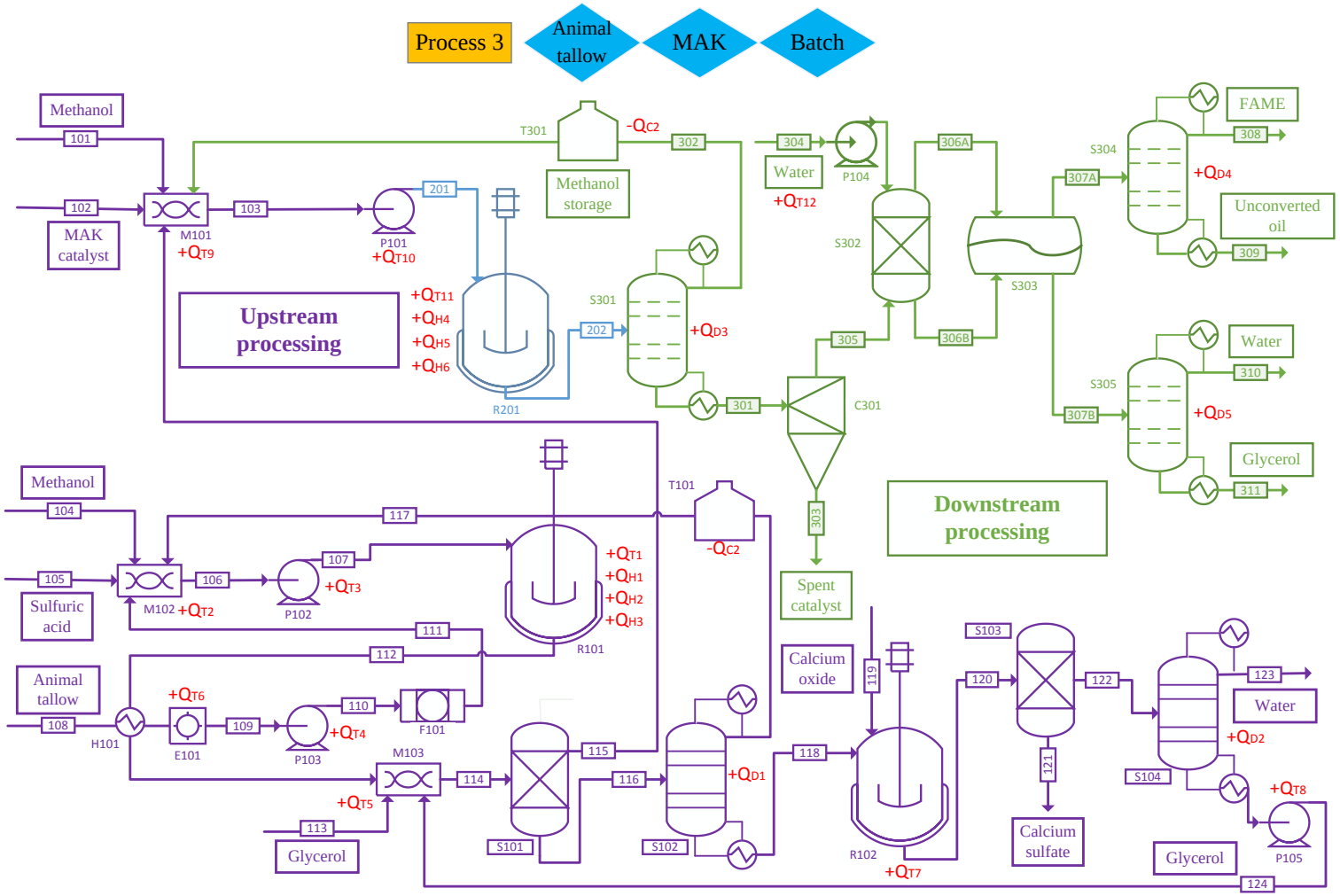

Figure 7-4 Piping and instrumentation diagram of Process 3

Table 7-12 Properties of main streams of Process 3

Inventory	Stream name								
	Feed streams							103/201	202
	101	102	104	105	108	119	304		
Mass fraction (kg per batch)									
Triglyceride	-	-	-	-	10,600.5	-	-	10,600.5	826.8
Methanol	1151.5	-	150.4	-	-	-	-	4604.6	3453.1
MAK	-	212.0	-	-	-	-	-	212.0	212.0
FAME	-	-	-	-	-	-	-	1383.9	11,201.8
Glycerol	-	-	-	-	-	-	-	-	1017.1
Water	-	-	-	-	662.5	-	1000.0	-	-
FFA	-	-	-	-	1325.1	-	-	-	-
CaO	-	-	-	-	-	37.9	-	-	-
H_2SO_4	-	-	-	66.3	-	-	-	-	-
$CaSO_4$	-	-	-	-	-	-	-	-	-

Table 7-12 Properties of main streams of Process 3 (to be continued)

Inventory	Stream name									
	301	305	307A	307B	111	106/107	112	115	116	118
Mass fraction (kg per batch)										
Triglyceride	826.8	826.8	826.8	-	10,600.5	10,600.5	10,600.5	10,600.5	-	-
Methanol	-	-	-	-	-	3007.9	2857.5	-	2857.5	-
MAK	212.0	-	-	-	-	-	-	-	-	-
FAME	11,201.8	11,201.8	11,201.8	-	-	-	1383.9	1383.9	-	-
Glycerol	1017.1	1017.1	-	1017.1	-	-	-	-	1000.0	1000.0
Water	-	-	-	1000.0	662.5	662.5	746.7	-	746.7	746.7
FFA	-	-	-	-	1325.1	1325.1	-	-	-	-
CaO	-	-	-	-	-	-	-	-	-	-
H_2SO_4	-	-	-	-	-	66.3	66.3	-	66.3	66.3
$CaSO_4$	-	-	-	-	-	-	-	-	-	-

Table 7-12 Properties of main streams of Process 3 (to be continued)

Inventory	Stream name									
	120	122	Product streams							
			303	308	309	310	311	121	123	124
Mass fraction (kg per batch)										
Triglyceride	-	-	-	-	826.8	-	-	-	-	-
Methanol	-	-	-	-	-	-	-	-	-	-
MAK	-	-	212.0	-	-	-	-	-	-	-
FAME	-	-	-	11,111.1	90.7	-	-	-	-	-
Glycerol	1000.0	1000.0	-	-	-	-	1017.1	-	-	1000.0
Water	758.9	758.9	-	-	-	995.0	5.0	-	755.1	3.8
FFA	-	-	-	-	-	-	-	-	-	-
CaO	-	-	-	-	-	-	-	-	-	-
H_2SO_4	-	-	-	-	-	-	-	-	-	-
$CaSO_4$	91.9	-	-	-	-	-	-	91.9	-	-

Table 7-13 Energy input calculations of Process 3

Heating up materials per batch (Q_{Hx})

$Q_{H1} = C_{oil} \times \Delta T \times m_{oil1}$=2.09×50×12588.1 kJ=1,315,459.6 kJ

$Q_{H3} = Q_{C1} = C_{MtOH} \times \Delta T \times m_{MtOH2} \times e$=2.51×50×2857.5×0.3 kJ=107,585.3 kJ

$Q_{H2} = Q_{MtOH1} + Q_{H_2SO_4} = C_{MtOH} \times \Delta T \times m_{MtOH1} + C_{H_2SO_4} \times \Delta T \times m_{H_2SO_4}$=2.51×50×150.4+1.47×50×66.3 kJ=23,743.9 kJ

$Q_{H4} = Q_{FAME} + Q_{oil2} = C_{FAME} \times \Delta T \times m_{FAME} + C_{oil} \times \Delta T \times m_{oil2}$=2.93×50×1383.9+2.09×50×10600.5 kJ=1,310,496.7 kJ

$Q_{H5} = Q_{MtOH3} + Q_{MAK} = C_{MtOH} \times \Delta T \times m_{MtOH3} + C_{MAK} \times \Delta T \times m_{MAK}$=2.51×50×1151.5+0.75×50×212.0 kJ=152,461.4 kJ

$Q_{H6} = Q_{C2} = C_{MtOH} \times \Delta T \times m_{MtOH4} \times e$=2.51×50×3453.1×0.3 kJ=130,010.0 kJ

Sum 3,039,756.9 kJ

Transmission per batch (Q_{Tx})

$Q_{T1} = P_{R101} \times t_1$=36×3 kWh=388,800.0 kJ

$Q_{T3} + Q_{T4} + Q_{T10} = P_{P101} \times t_2 \times 3$=16×1.5×3 kWh=259,200.0 kJ

$Q_{T2} + Q_{T5} + Q_{T9} = P_{M101} \times t_2 \times 3$=12×1.5×3 kWh=194,400.0 kJ

$Q_{T6} = P_{E101} \times t_2$=12×1.5 kWh=64,800.0 kJ

$Q_{T7} = P_{R102} \times t_3$=8×6 kWh=172,800.0 kJ

$Q_{T8} = P_{P105} \times t_3$=2.5×6 kWh=54,000.0 kJ

$Q_{T11} = P_{R201} \times t_4$=36×5 kWh=648,000.0 kJ

$Q_{T12} = P_{P104} \times t_5$=2.5×8 kWh=72,000.0 kJ

Sum	1,854,000.0 kJ		
Distillation per batch (Q_{Dx})			
$Q_{D1} + Q_{D2} = P_{S102} \times t_3 \times 2 = 6 \times 6 \times 2$ kWh=259,200.0 kJ		$Q_{D4} = P_{S304} \times t_5 = 12 \times 8$ kWh=345,600 kJ	
$Q_{D3} + Q_{D5} = P_{S301} \times t_5 \times 2 = 6 \times 8 \times 2$ kWh=345,600.0 kJ			
Sum	950,400.0 kJ		
Total energy input per batch	5,844,156.9 kJ	Total energy input per day	17,532,470.7 kJ
Energy input per kilogram of produced biodiesel		526.0 kJ	

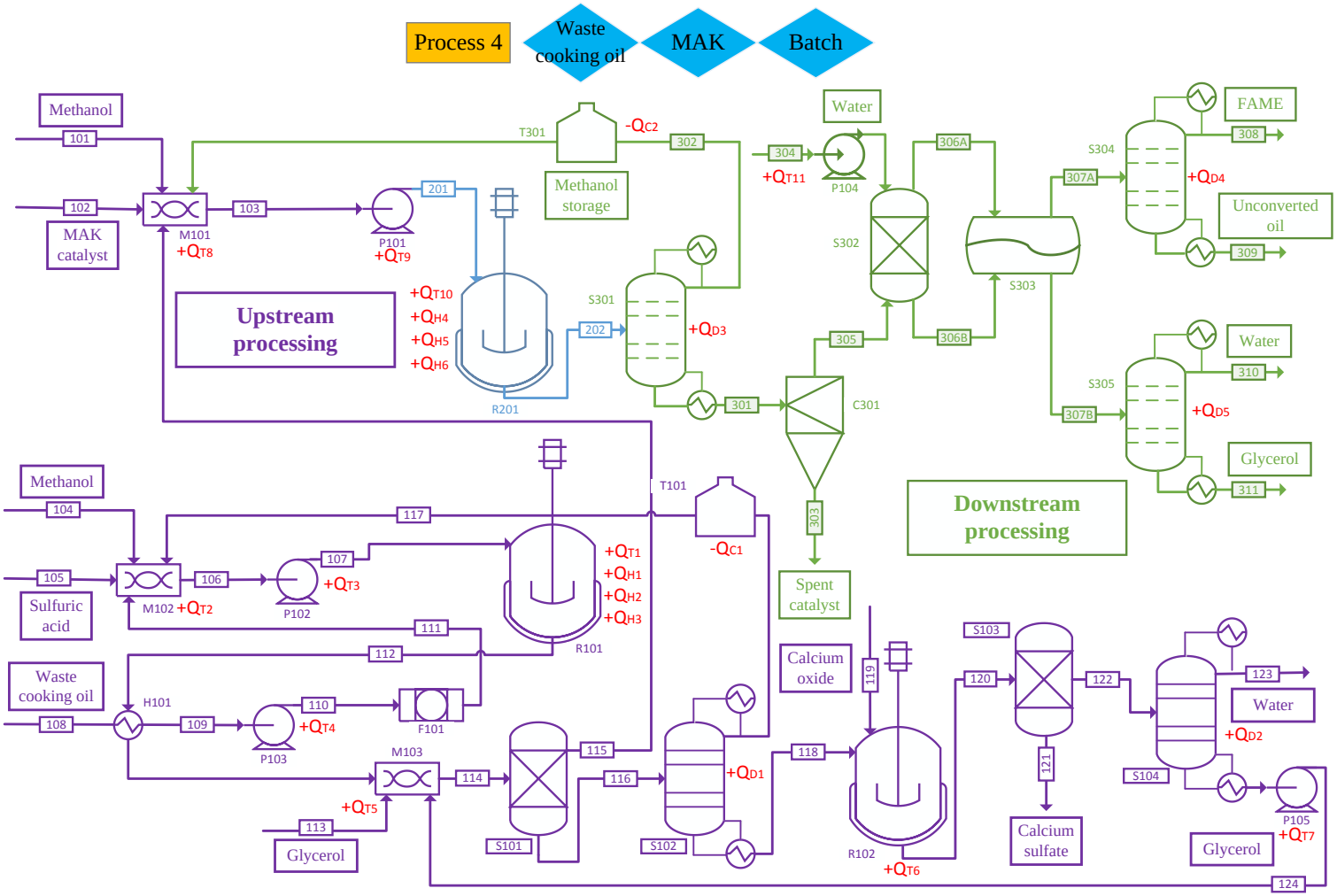

Figure 7-5 Piping and instrumentation diagram of Process 4

Table 7-14 Properties of main streams of Process 4

Inventory	Stream name								
	Feed streams							103/201	202
	101	102	104	105	108	119	304		
Mass fraction (kg per batch)									
Triglyceride	-	-	-	-	10,036.9	-	-	10,036.9	782.9
Methanol	1090.0	-	207.1	-	-	-	-	4359.9	3269.9
MAK	-	200.7	-	-	-	-	-	200.7	200.7
FAME	-	-	-	-	-	-	-	1905.9	11,201.8
Glycerol	-	-	-	-	-	-	-	-	963.1
Water	-	-	-	-	121.7	-	1000.0	-	-
FFA	-	-	-	-	1824.9	-	-	-	-
CaO	-	-	-	-	-	52.2	-	-	-
H_2SO_4	-	-	-	91.2	-	-	-	-	-
$CaSO_4$	-	-	-	-	-	-	-	-	-

Table 7-14 Properties of main streams of Process 4 (to be continued)

Inventory	Stream name									
	301	305	307A	307B	111	106/107	112	115	116	118
Mass fraction (kg per batch)										
Triglyceride	782.9	782.9	782.9	-	10,036.9	10,036.9	10,036.9	10,036.9	-	-
Methanol			-	-	-	4141.6	3934.6	-	3934.6	-
MAK	200.7		-	-	-	-	-	-	-	-
FAME	11,201.8	11,201.8	11,201.8	-	-	-	1905.9	1905.9	-	-
Glycerol	963.1	963.1	-	963.1	-	-	-	-	1000.0	1000.0
Water	-	-	-	1000.0	121.7	121.7	237.6	-	237.6	237.6
FFA	-	-	-	-	1824.9	1824.9	-	-	-	-
CaO	-	-	-	-	-	-	-	-	-	-
H_2SO_4	-	-	-	-	-	91.2	91.2	-	91.2	91.2
$CaSO_4$	-	-	-	-	-	-	-	-	-	-

Table 7-14 Properties of main streams of Process 4 (to be continued)

Inventory	Stream name									
	120	122	Product streams							
			303	308	309	310	311	121	123	124
Mass fraction (kg per batch)										
Triglyceride	-	-	-	-	782.9	-	-	-	-	-
Methanol	-	-	-	-	-	-	-	-	-	-
MAK	-	-	200.7	-	-	-	-	-	-	-
FAME	-	-	-	11,111.1	90.7	-	-	-	-	-
Glycerol	1000.0	1000.0	-	-	-	-	963.1	-	-	1000.0
Water	254.3	254.3	-	-	-	995.0	5.0	-	253.0	1.3
FFA	-	-	-	-	-	-	-	-	-	-
CaO	-	-	-	-	-	-	-	-	-	-
H_2SO_4	-	-	-	-	-	-	-	-	-	-
$CaSO_4$	126.5	-	-	-	-	-	-	126.5	-	-

Table 7-15 Energy input calculations of Process 4

Heating up materials per batch (Q_{Hx})	
$Q_{H1} = C_{oil} \times \Delta T \times m_{oil1}$ =2.09 ×50 ×11983.5 kJ=1,250,074.1 kJ	$Q_{H3} = Q_{C1} = C_{MtOH} \times \Delta T \times m_{MtOH2} \times e$ =2.51 ×50 ×3934.6 ×0.3 kJ=148,135.8 kJ
$Q_{H2} = Q_{MtOH1} + Q_{H_2SO_4} = C_{MtOH} \times \Delta T \times m_{MtOH1} + C_{H_2SO_4} \times \Delta T \times m_{H_2SO_4}$ =2.51 ×50 ×207.1+1.47 ×50 ×91.2 kJ=32,693.2 kJ	
$Q_{H4} = Q_{FAME} + Q_{oil2} = C_{FAME} \times \Delta T \times m_{FAME} + C_{oil} \times \Delta T \times m_{oil2}$ =2.93 ×50 ×1905.9+2.09 ×50 ×10036.9 kJ=1,328,076.6 kJ	
$Q_{H5} = Q_{MtOH3} + Q_{MAK} = C_{MtOH} \times \Delta T \times m_{MtOH3} + C_{MAK} \times \Delta T \times m_{MAK}$ =2.51 ×50 ×1090.0+0.75 ×50 ×200.7 kJ=144,321.5 kJ	
$Q_{H6} = Q_{C2} = C_{MtOH} \times \Delta T \times m_{MtOH4} \times e$ =2.51 ×50 ×3269.9 ×0.3 kJ=123,113.2 kJ	
Sum	3,028,614.4 kJ
Transmission per batch (Q_{Tx})	
$Q_{T1} = P_{R101} \times t_1$ =36 ×3 kWh=388,800.0 kJ	$Q_{T3} + Q_{T4} + Q_{T9} = P_{P101} \times t_2 \times 3$ =16 ×1.5 ×3 kWh=259,200.0 kJ
$Q_{T2} + Q_{T5} + Q_{T8} = P_{M101} \times t_2 \times 3$ =12 ×1.5 ×3 kWh=194,400.0 kJ	$Q_{T6} = P_{R102} \times t_3$ =8 ×6 kWh=172,800.0 kJ
$Q_{T7} = P_{P105} \times t_3$ =2.5 ×6 kWh=54,000.0 kJ	$Q_{T10} = P_{R201} \times t_4$ =36 ×5 kWh=648,000.0 kJ
$Q_{T11} = P_{P104} \times t_5$ =2.5 ×8 kWh=72,000.0 kJ	

Sum	1,789,200.0 kJ		
Distillation per batch (Q_{Dx})			
$Q_{D1}+Q_{D2}=P_{S102}\times t_3\times 2$ =6×6×2 kWh=259,200.0 kJ		$Q_{D4}=P_{S304}\times t_5$ =12×8 kWh=345,600 kJ	
$Q_{D3}+Q_{D5}=P_{S301}\times t_5\times 2$ =6×8×2 kWh=345,600.0 kJ			
Sum	950,400.0 kJ		
Total energy input per batch	5,768,214.4 kJ	Total energy input per day	17,304,643.3 kJ
Energy input per kilogram of produced biodiesel		519.1 kJ	

7.4.4 Process 4 MAK catalysed transesterification of waste cooking oil with methanol in a batch reactor

Comparing to Process 3, the major difference for Process 4 was the use of waste cooking oil as the feedstock oil instead of animal tallow. The FFA, water and solid content in waste cooking oil were specified as 15.0 wt%, 1.0 wt% and 1.5 wt%, respectively. There was no hot compression and oil extraction unit in the PID as seen in Figure 7-5. The waste cooking oil (stream 108) was directly introduced to the heat exchanger H101, and then filtered in F101 before entering the esterification reactor R101. All the remaining procedures were the same as described in Process 3. Properties of main streams are shown in Table 7-14. Table 7-15 summarises the energy input calculations. Under the assumed conditions, to achieve a daily biodiesel output of 33,333.3 kg, the total energy input was 17,304,643.3 kJ and the energy input per kilogram of the produced biodiesel was 519.1 kJ.

7.4.5 Process 5 NaOH catalysed transesterification of virgin vegetable oil with methanol in a batch reactor

In this process, a homogeneous catalyst NaOH was used. The reaction conditions were: temperature 70 ℃, NaOH loading 2.0 wt%, M/O 6:1 and reaction time 5 h, under which a biodiesel yield of 96.2 % was reported (A. A. Refaat 2008). In the PID as shown in Figure 7-6, there was no cyclone required for solid catalyst recovery, instead, the catalyst NaOH was neutralised with phosphoric acid in R301 and an absolute removal of NaOH was assumed. The resulting Na_3PO_4 was removed in a gravity separator S305. All the remaining procedures were the same as Process 1. Table 7-16 shows the properties of main streams while the corresponding energy input calculations are shown in Table 7-17. A daily energy input of 9,927,008.7 kJ was required and the energy input per kilogram of the produced biodiesel was 297.8 kJ.

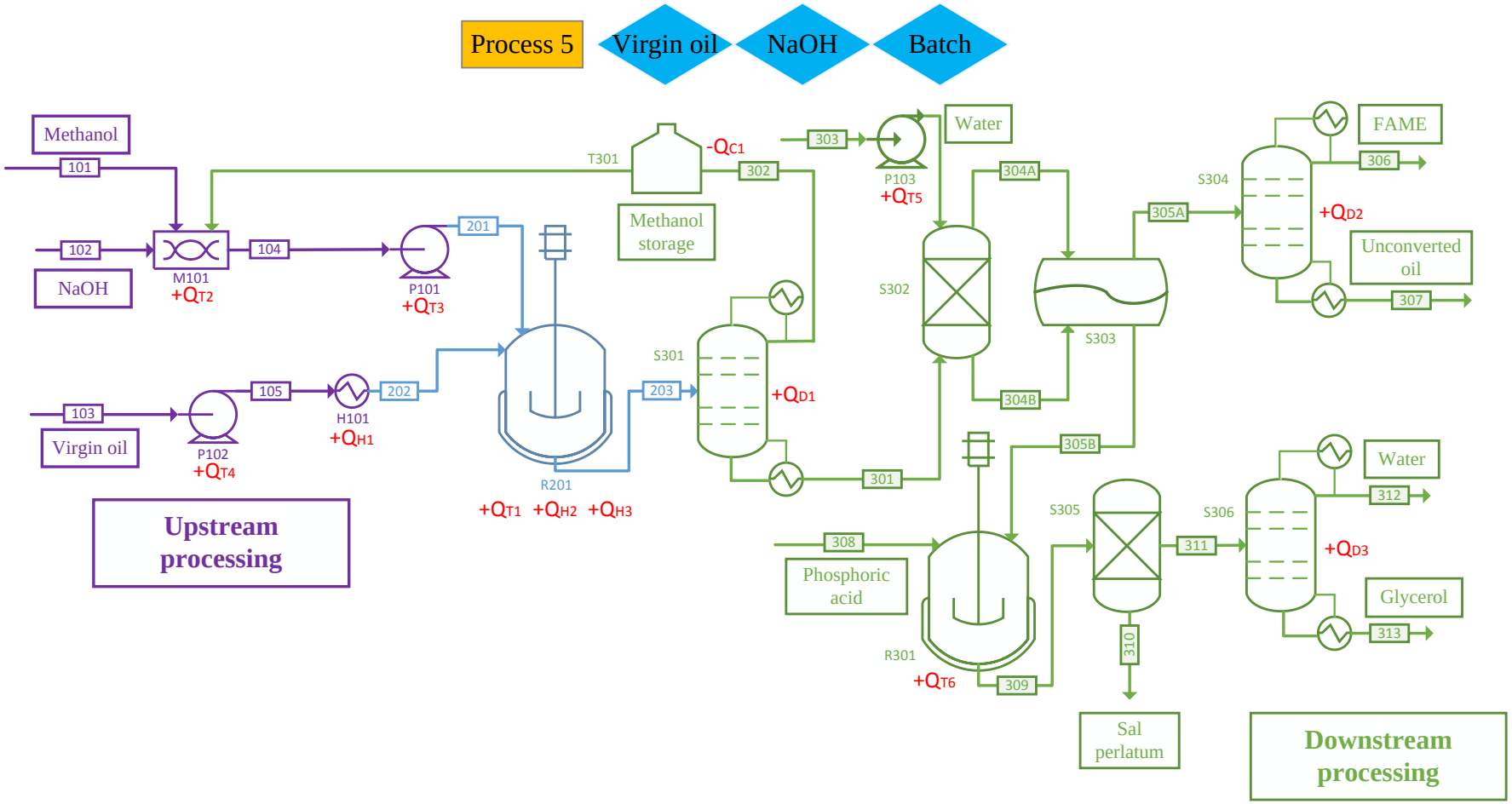

Figure 7-6 Piping and instrumentation diagram of Process 5

Table 7-16 Properties of main streams of Process 5

Inventory	Stream name								
	Feed streams								
	101	102	103/105/202	303	308	104/201	203	301	305A
Mass fraction (kg per batch)									
Triglyceride	-	-	11,591.9	-	-	-	440.5	440.5	440.5
Methanol	1211.0	-	-	-	-	2517.7	1306.7	-	-
NaOH	-	231.8	-	-	-	231.8	231.8	231.8	-
FAME	-	-	-	-	-	-	11,201.8	11,201.8	11,201.8
Glycerol	-	-	-	-	-	-	1160.6	1160.6	-
Water	-	-	-	5000.0	-	-	-	-	-
Phosphoric acid	-	-	-	-	189.3	-	-	-	-
Sal perlatum	-	-	-	-	-	-	-	-	-

Table 7-16 Properties of main streams of Process 5 (to be continued)

Inventory	Stream name							
				Product streams				
	305B	309	311	306	307	312	313	310
Mass fraction (kg per batch)								
Triglyceride	-	-	-	-	440.5	-	-	-
Methanol	-	-	-	-	-	-	-	-
NaOH	231.8	-	-	-	-	-	-	-
FAME	-	-	-	11,111.1	90.7	-	-	-
Glycerol	1160.6	1160.6	1160.6	-	-	-	1160.6	-
Water	5000.0	5104.3	5104.3	-	-	5078.8	25.5	-
Phosphoric acid	-	-	-	-	-	-	-	-
Sal perlatum	-	316.7	-	-	-	-	-	316.7

Table 7-17 Energy input calculations of Process 5

Heating up materials per batch (Q_{Hx})			
$Q_{H1} = C_{oil} \times \Delta T \times m_{oil}$=2.09×50×11591.9 kJ=1,211,352.7 kJ		$Q_{H3} = Q_{C1} = C_{MtOH} \times \Delta T \times m_{MtOH2} \times e$=2.51×50×1306.7×0.3 kJ=49,196.8 kJ	
$Q_{H2} = Q_{MtOH1} + Q_{NaOH} = C_{MtOH} \times \Delta T \times m_{MtOH1} + C_{NaOH} \times \Delta T \times m_{NaOH}$ =2.51×50×1211.0+1.49×50×231.8 kJ=169,253.4 kJ			
Sum	1,429,802.9 kJ		
Transmission per batch (Q_{Tx})			
$Q_{T1} = P_{R201} \times t_1$=36×5 kWh=648,000.0 kJ		$Q_{T2} = P_{M101} \times t_2$=12×1.5 kWh=64,800.0 kJ	
$Q_{T3} + Q_{T4} + Q_{T5} = P_{P101} \times t_2 \times 2 + P_{P103} \times t_3$=16×1.5×2+2.5×8 kWh=244,800.0 kJ		$Q_{T6} = P_{R309} \times t_3$=8×8 kWh=230,400.0 kJ	
Sum	1,188,000.0 kJ		
Distillation per batch (Q_{Dx})			
$Q_{D1} + Q_{D3} = P_{S301} \times t_3 \times 2$=6×8×2 kWh=345,600.0 kJ		$Q_{D2} = P_{S304} \times t_3$=12×8 kWh=345,600.0 kJ	
Sum	691,200.0 kJ		
Total energy input per batch	3,309,002.9 kJ	Total energy input per day	9,927,008.7 kJ
Energy input per kilogram of produced biodiesel		297.8 kJ	

7.4.6 Summary of process designs and analysis

In this study, for an annual biodiesel production capacity of 10,000.0 t, five transesterification process design options using virgin vegetable oil, animal tallow or waste cooking oil as the feedstock oils were analysed. The heterogeneous MAK and the conventional homogeneous NaOH were used the catalysts. Batch reactor and CSTRs in series were considered as the reaction reactors. Detailed PIDs showing the upstream and downstream processing were presented. Mass balance and energy input were calculated. Table 7-18 shows the daily material and energy inventory of the five options.

There were a number of differences amongst the options. The first difference was with regard to the feedstock oil, which determined the pretreatment steps. The use of animal tallow and waste cooking oil in Process 3 and 4 necessitated an extra H_2SO_4-catalysed esterification prior to the transesterification. This resulted in an increase in the process complexity and energy consumption (Morais et al. 2010). As seen in Table 7-18, the energy input per kilogram of the produced biodiesel was almost doubled in Process 3 and 4 than other options using virgin vegetable oil (~520 kJ vs ~290 kJ).

The second difference was from the use of different catalysts, either heterogeneous or homogeneous. The use of heterogeneous MAK catalyst avoided the neutralisation unit for catalyst removal and allowed a relatively facile catalyst recovery and enabled potential reuse of the catalyst in practical applications. Another advantage of the heterogeneous MAK-catalysed process was the much less water usage required for biodiesel purification. Under the assumed conditions in this study, water usage per kilogram of the produced biodiesel was much lower than that in NaOH-catalysed process (~0.10 vs 0.45 kg). This advantage might contribute to relieve the environment concerns (Morais et al. 2010). The process designs in the present thesis could be part of the effort providing deeper insight of the implication of the MAK catalyst in the future.

Table 7-18 Daily material and energy inventory data for the five processes

Inventory	Process 1	Process 2	Process 3	Process 4	Process 5
Feeds (kg)					
Virgin vegetable oil	36,650.8	36,453.6	-	-	34,775.7
Animal tallow	-	-	39,752.1	-	-
Waste cooking oil	-	-	-	36,497.9	-
Methanol	3633.0+4042.8[a]	3919.7+11756.2[a]	3905.6+6310.6[a]	3891.2+7204.5[a]	3633.0+1306.7[a]
MAK	725.7	721.7	636.0	602.2	-
NaOH	-	-	-	-	695.5
CaO	-	-	113.6	156.5	-
H_2SO_4	-	-	198.8	273.7	-
H_3PO_4	-	-	-	-	567.8
Water	3000.0	3600.0	3000.0	3000.0	15,000.0
Water usage per kilogram of produced biodiesel (kg)	0.09	0.11	0.09	0.09	0.45

Products (kg)					
Biodiesel	33,333.3	33,333.3	33,333.3	33,333.3	33,333.3
Glycerol	3481.7	3481.9	3051.4	2889.3	3481.7
Unconverted triglyceride	2830.2	2633.8	2480.5	2348.6	1321.6
$CaSO_4$	-	-	275.6	379.6	-
Na_3PO_4	-	-	-	-	950.2
Energy input					
Total energy input (kJ)	9,716,201.7	9,739,005.6	17,532,470.7	17,304,643.3	9,927,008.7
Energy input per kilogram of produced biodiesel (kJ)	291.5	292.2	526.0	519.1	297.8

Note: [a] Indicates the recycled methanol

Chapter 8 Conclusions and Recommendations

The evaluations in Chapter 7 enabled the new and significant findings to be ascertained, which were consolidated into conclusions in this final chapter. In the meantime, the evaluations and conclusions of the present work have also led to new gaps and recommendations for future studies in this area.

8.1 Conclusions

8.1.1 MA Synthesis and the Structural Properties Control

- A facile sol-gel self-assembly route for the aqueous phase synthesis of mesoporous alumina with tunable structural properties was successfully demonstrated in this study by adjusting the amount of nitric acid addition, type of template, amount of template addition, doping of inorganic aluminium precursors and calcination temperature.
- HNO_3 addition between 1N (0.097 mL HNO_3 per 20 mmol of Al) and 3N (0.291 mL HNO_3 per 20 mmol of Al) was conducive for the formation of organised MAs. Increasing HNO_3 addition in the range of 1N~3N led to larger pores while further increasing HNO_3 addition beyond 3N resulted in disordered pores with broad PSD.
- With a given surfactant concentration, nonionic surfactants P123 and F127 were shown to more strongly influence the structural properties compared to CTAB and SDS, exhibiting in a descending order of F127 > P123 > CTAB > SDS. F127 showed superior capability in controlling the structural properties of the resulting MA, owing to its larger hydrophile-lipophile balance HLB value than that of P123.
- With increasing template addition, the resulting MA showed continuously increased surface area, pore volume and pore size, maintained sufficiently narrow PSD.

- The optimal doping ratios of $Al(NO_3)_3$ and $AlCl_3$ were 15% and 30%, respectively, at which much larger pore volumes and pore sizes with narrow PSDs could be obtained, while higher ratios of doping above 15% and 30% brought about broader PSDs as well as a significant reduction in the surface area and pore volume because of the collapse of mesoporosity.
- The introduction of $Al(NO_3)_3$ into the synthesis system improved the overall acidity, increased the micelle size, and resulted in larger pore size and pore volume. The impact of the doped $AlCl_3$ on the structural properties of MA was determined by a combination of factors such as the coordination of Cl^- with Al^{3+} and the evaporation of the generated HCl. In case of $Al_2(SO_4)_3$, the high precipitating capacity of SO_4^{2-} was the dominant factor, which resulted in a low doping ratio of $Al_2(SO_4)_3$ (2%) and a compact structure.
- Increasing the calcination temperature from 500 ℃ to 1100 ℃ caused an increase in pore size, but significantly decreased surface area and pore volume. The crystallinity of MA was improved upon high-temperature treatment. Calcination at 1100 ℃ resulted in a phase transition from γ-alumina to θ-Al_2O_3.
- By carefully considering the synthetic conditions on the structural properties of the resulting MA, the BET surface area, pore volume and pore size of MAs could be adjusted in the wide ranges of 178 m^2g^{-1} ~ 409 m^2g^{-1}, 0.4 cm^3g^{-1} ~ 2.8 cm^3g^{-1} and 5.5 nm ~ 60.2 nm, respectively.

8.1.2 Alkaline MAK Catalyst for Biodiesel Production

- MAK catalysts synthesised following the one-pot synthesis pathway via the self-assembly of potassium precursor KNO_3 and aluminium isopropoxide were effective catalysts for biodiesel production by transesterification of canola oil with methanol.

- The incorporation of potassium species has reduced the BET surface area and pore volume of the MA, but could significantly increase the pore size.
- By introducing 20% molar fraction of K species to MA, a high yield of biodiesel of 92.2% could be achieved.
- Higher surface area, pore volume and greater pore size of the catalyst reduced the mass transfer limitation in catalysis, thus leading to the higher biodiesel yield.
- MAK catalyst showed good reusability, biodiesel yield obtained using MA1P20K catalyst slightly decreased from 92.2 % to 86.8% after five successive cycles.
- The activation energy of the MA1P20K catalysed transesterification ranged from 20.9 to 23.4 $kJmol^{-1}$.
- The MA1P20K catalysed transesterification process was shown to follow the Eley–Rideal mechanism.
- The MAK catalysed transesterification starts with methanol adsorption on the active sites of MAK catalyst surface, followed by surface reaction between methoxide anions formed on the surface and triglyceride from the bulk liquid phase to produce methyl esters as the biodiesel product and glycerol as the by-product.
- When evaluated through the biodiesel plant design, the MAK-catalysed transesterification process showed comparable catalytic reactivity and energy efficiency to the conventional homogeneous NaOH. While its advantages including being free of a catalyst neutralisation unit, facile recovery and potential reuse of the catalyst and the reduced operation complexity would make the MAK catalyst more attractive for future development and commercial applications.

8.1.3 MA Immobilised Lipase as the Enzymatic Catalyst for Biodiesel Production

- Enzymatic catalysts for the transesterification of canola oil with methanol for biodiesel production were successfully synthesised via immobilising pseudomonas fluorescens lipase on MAs by physical adsorption.
- Lipase adsorption on a support greatly improved the lipase catalytic activity in transesterification, owing to the largely alleviated lipase aggregation. The support MA with improved structural properties was preferred, owing to the reduced mass transfer resistance of the triglycerides within the pores of catalyst, and thus leading to an increase in the lipase activity.
- Lipase adsorption capacity enhanced with improved structural properties of MA. The larger contact interface and more accessible porous channels allow quicker lipase transfer and greater adsorption.
- RSM was applied to identify the optimised conditions for biodiesel production using the tailor-designed MA4P15AlN supported lipase as the catalyst. The highest biodiesel yield of 88.9% was achieved in 24 h of reaction time with the following reaction conditions: temperature 41 ℃, water 3.9 wt% and catalyst loading ratio 5.0 wt%.

8.2 Recommendations

In the present thesis work, two types of novel heterogeneous catalysts, namely, the alkaline catalyst MAK and enzymatic catalyst MA immobilised with lipase, were investigated. Although the overall objectives of this research have been achieved, a number of new gaps have also been identified following the evaluations of the findings from the present research, leading to the recommendations for future research as follows:

- In this study, a combined manipulation of a group of synthetic factors has been

developed and investigated to control the structural properties of MA following the aqueous phase synthesis pathway. Three inorganic aluminium precursors including $Al(NO_3)_3$, $AlCl_3$ and $Al_2(SO_4)_3$ were doped as the substitutions to the extensively used organic aluminium precursor aluminium isopropoxide. Extending the present work, it would be worthwhile to employ the inorganic aluminium precursors to completely replace the organic aluminium precursors as the means to reduce synthesis cost.

- In this work the MAs were synthesised in an aqueous medium instead of the generally used ethanol as the solvent following the standard evaporation induced self-assembly (EISA) pathway. There has been no systematic investigation on the comparison of the EISA pathway and the aqueous phase pathway in fabricating MA, in particular in the resulting structural properties and nano-morphology. In these two processes, the solvent type and water amount can play major roles in determining the hydrolysis rate of aluminium precursors. The fundamental understanding of how different alcohols and water content affect the copolymer/nanoparticle interactions and consequently the variations in textural characteristics of the mesoporous alumina synthesised needs to be studied.
- In this study, a good reusability of the MAK catalyst in transesterification reaction was demonstrated since only a slight decrease in the biodiesel yield was observed after five successive cycles. The drop of the biodiesel yield after recycled use could be attributed to the leaching of the K species from the catalyst to the alcoholic phase. In the future, a detailed study to quantitatively measure the dissolution of the K species is recommended.
- In the present study, a process design excise was carried out to evaluate the practical implications of the MAK catalyst by comparing with the widely used

commercial homogeneous catalyst NaOH in terms of energy input, water usage and catalyst reuse. However, a complete and separate cost analysis is recommended in the future.

- Regarding the enzymatic catalyst, in addition to the currently studied catalysts synthesised by physically adsorbing lipase onto the supports MAs, other immobilisation techniques like covalent bonding and encapsulation can be trialled, in particular pay attention to the effect on the activity, stability and reusability of the prepared catalysts.

References

A.-X.Y. Q. Yuan C.L., L.-D. Sun, Y.-W. Zhang, W.-T. Duan, H.-C. Liu and C.-H. Yan 2008, Facile Synthesis for Ordered Mesoporous γ-Aluminas with High Thermal Stability. *J. Am. Chem. Soc.*, 130, (11), 3465–3472.

A. A. Refaat N.K.A., H. A. Sibak, S. T. El Sheltawy, G. I. ElDiwani 2008, Production optimization and quality assessment of biodiesel from waste vegetable oil *International Journal of Environmental Science & Technology*, 5, (1), 75-82.

Abdullah A.Z., Sulaiman N.S. & Kamaruddin A.H. 2009, Biocatalytic esterification of citronellol with lauric acid by immobilized lipase on aminopropyl-grafted mesoporous SBA-15. *Biochemical Engineering Journal*, 44, (2-3), 263-270.

Agarwal M., Singh K. & Chaurasia S.P. 2012, Kinetic modeling for biodiesel production by heterogeneous catalysis. *Journal of Renewable and Sustainable Energy*, 4, (1), 74-81.

Al-Zuhair S. 2007, Production of biodiesel: possibilities and challenges. *Biofuels, Bioproducts and Biorefining*, 1, (1), 57-66.

Alonso D.M., Mariscal R., Moreno-Tost R., Poves M.D.Z. & Granados M.L. 2007, Potassium leaching during triglyceride transesterification using K/γ-Al2O3 catalysts. *Catalysis Communications*, 8, (12), 2074-2080.

Alphonse P. & Faure B. 2013, Synthesis of highly porous alumina-based materials. *Microporous and Mesoporous Materials*, 181, 23-28.

Arzamendi G., Campo I., Arguiñarena E., Sánchez M., Montes M. & Gandía L.M. 2007, Synthesis of biodiesel with heterogeneous NaOH/alumina catalysts: Comparison with homogeneous NaOH. *Chemical Engineering Journal*, 134, (1-3), 123-130.

Atabani A.E., Silitonga A.S., Badruddin I.A., Mahlia T.M.I., Masjuki H.H. & Mekhilef S. 2012, A comprehensive review on biodiesel as an alternative energy resource and its characteristics. *Renewable and Sustainable Energy Reviews*, 16, (4), 2070-2093.

Bai P., Wu P., Yan Z. & Zhao X.S. 2009, Cation–anion double hydrolysis derived mesoporous γ-Al2O3 as an environmentally friendly and efficient aldol reaction catalyst. *Journal of Materials Chemistry*, 19, (11), 1554-1563.

Bai P., Wu P., Yan Z. & Zhao X.S. 2009, Cation–anion double hydrolysis derived mesoporous γ-Al2O3 as an environmentally friendly and efficient aldol reaction catalyst. *Journal of Materials Chemistry*, 19, (11), 1554-1563.

Bai P., Wu P., Zhao G., Yan Z. & Zhao X.S. 2008, Cation–anion double hydrolysis derived mesoporous γ-Al2O3as an environmentally friendly and efficient aldol reaction catalyst. *Journal of Materials Chemistry*, 18, (1), 74-76.

Bai Y.-X., Li Y.-F., Yang Y. & Yi L.-X. 2006, Covalent immobilization of triacylglycerol lipase onto functionalized nanoscale SiO2 spheres. *Process Biochemistry*, 41, (4), 770-777.

Balat M. & Balat H. 2010, Progress in biodiesel processing. *Applied Energy,* 87, (6), 1815-1835.

Benjapornkulaphong S., Ngamcharussrivichai C. & Bunyakiat K. 2009, Al2O3-supported alkali and alkali earth metal oxides for transesterification of palm kernel oil and coconut oil. *Chemical Engineering Journal,* 145, (3), 468-474.

Bleta R., Alphonse P., Pin L., Gressier M. & Menu M.J. 2012, An efficient route to aqueous phase synthesis of nanocrystalline gamma-Al2O3 with high porosity: from stable boehmite colloids to large pore mesoporous alumina. *J Colloid Interface Sci,* 367, (1), 120-128.

Bo X., Guomin X., Lingfeng C., Ruiping W. & Lijing G. 2007, Transesterification of Palm Oil with Methanol to Biodiesel over a KF/Al2O3 Heterogeneous Base Catalyst. *Energy & Fuels,* 21, (6), 3109–3112.

Borges M.E. & Díaz L. 2012, Recent developments on heterogeneous catalysts for biodiesel production by oil esterification and transesterification reactions: A review. *Renewable and Sustainable Energy Reviews,* 16, (5), 2839-2849.

Brito A., Borges M.E. & Otero N. 2007, Zeolite Y as a Heterogeneous Catalyst in Biodiesel Fuel Production from Used Vegetable Oil. *Energy & Fuels,* 21, (6), 3280-3283.

Bussemaker M.J., Xu F. & Zhang D. 2013, Manipulation of ultrasonic effects on lignocellulose by varying the frequency, particle size, loading and stirring. *Bioresour Technol,* 148, 15-23.

C Márquez-Alvarez, N.Ž. J.P.P. & Čejkab J. 2008, Synthesis, characterization and catalytic applications of organized mesoporous aluminas. *Catalysis Reviews Science and Engineering,* 50, (2), 222-286.

Cai W., Hu Y., Chen J., Zhang G. & Xia T. 2012, Synthesis of nanorod-like mesoporous γ-Al2O3 with enhanced affinity towards Congo red removal: Effects of anions and structure-directing agents. *CrystEngComm,* 14, (3), 972-977.

Cai W., Yu J., Anand C., Vinu A. & Jaroniec M. 2011, Facile Synthesis of Ordered Mesoporous Alumina and Alumina-Supported Metal Oxides with Tailored Adsorption and Framework Properties. *Chemistry of Materials,* 23, (5), 1147-1157.

Cai W., Yu J. & Jaroniec M. 2011, Effect of nonionic structure-directing agents on adsorption and structural properties of mesoporous alumina. *Journal of Materials Chemistry,* 21, (25), 9066-9072.

Čejka J. 2003, Organized mesoporous alumina: synthesis, structure and potential in catalysis. *Applied Catalysis A: General,* 254, (2), 327-338.

Chantrasa A., Phlernjai N. & Goodwin J.G. 2011, Kinetics of hydrotalcite catalyzed transesterification of tricaprylin and methanol for biodiesel synthesis. *Chemical Engineering Journal,* 168, (1), 333-340.

Chen X., Du W. & Liu D. 2008, Effect of several factors on soluble lipase-mediated biodiesel preparation in the biphasic aqueous-oil systems. *World Journal of Microbiology and Biotechnology,* 24, (10), 2097-2102.

Chen Y., Xiao B., Chang J., Fu Y., Lv P. & Wang X. 2009, Synthesis of biodiesel from waste cooking oil using immobilized lipase in fixed bed reactor. *Energy Conversion and Management,* 50, (3), 668-673.

Chen Y., Yang C., Ching C. & Xu R. 2008, Immobilization of Lipases on Hydrophobilized Zirconia Nanoparticles Highly Enantioselective and Reusable Biocatalysts. *Langmuir,* 24, (16), 8877-8884.

Chouhan A.P.S. & Sarma A.K. 2011, Modern heterogeneous catalysts for biodiesel production: A comprehensive review. *Renewable and Sustainable Energy Reviews,* 15, (9), 4378-4399.

D. Darnoko M.C. 2000, Kinetics of Palm Oil Transesterification in a Batch Reactor. *Journal of the American Oil Chemists' Society*, 77, (12), 1263-1267.

Demirbas A. 2009, Progress and recent trends in biodiesel fuels. *Energy Conversion and Management,* 50, (1), 14-34.

Dossin T.F., Reyniers M.-F., Berger R.J. & Marin G.B. 2006, Simulation of heterogeneously MgO-catalyzed transesterification for fine-chemical and biodiesel industrial production. *Applied Catalysis B: Environmental,* 67, (1-2), 136-148.

Dossin T.F., Reyniers M.F. & Marin G.B. 2006, Kinetics of heterogeneously MgO-catalyzed transesterification. *Applied Catalysis B: Environmental,* 62, (1-2), 35-45.

Elena Bikou A.L., Nikos Papayannakos 1999, The Effect of Water on the Transesterification Kinetics of Cotton Seed Oil with Ethanol. *Chemical Engineering & Technology,* 22, (1), 70-75.

Endalew A.K., Kiros Y. & Zanzi R. 2011, Inorganic heterogeneous catalysts for biodiesel production from vegetable oils. *Biomass and Bioenergy,* 35, (9), 3787-3809.

Fishman A. & Cogan U. 2003, Bio-imprinting of lipases with fatty acids. *Journal of Molecular Catalysis B: Enzymatic,* 22, (3-4), 193-202.

Fjerbaek L., Christensen K.V. & Norddahl B. 2009, A review of the current state of biodiesel production using enzymatic transesterification. *Biotechnol Bioeng,* 102, (5), 1298-1315.

Foresti M.L., Alimenti G.A. & Ferreira M.L. 2005, Interfacial activation and bioimprinting of Candida rugosa lipase immobilized on polypropylene: effect on

the enzymatic activity in solvent-free ethyl oleate synthesis. *Enzyme and Microbial Technology*, 36, (2-3), 338-349.

G. Vicente A.C., M. Martinez, J. Aracil 1998, Application of the factorial design of experiments and response surface methodology to optimize biodiesel production. *Industrial Crops and Products,* 8, (1), 29-35.

Gan Z., Ning G., Lin Y. & Cong Y. 2007, Morphological control of mesoporous alumina nanostructures via template-free solvothermal synthesis. *Materials Letters,* 61, (17), 3758-3761.

Gemma Vicente M.M.n., Jose´Aracil, Alfredo Esteban 2005, Kinetics of Sunflower Oil Methanolysis. *Industrial & Engineering Chemistry Research,* 44, (15), 5447-5454.

Ghosh D., Sobro I.F. & Hallenbeck P.C. 2012, Stoichiometric conversion of biodiesel derived crude glycerol to hydrogen: Response surface methodology study of the effects of light intensity and crude glycerol and glutamate concentration. *Bioresour Technol,* 106, 154-160.

Ghosh S., Naskar M.K. & Troczynski T. 2014, Understanding the Role of Triblock Copolymers for the Synthesis of Mesoporous Alumina, and Its Adsorption Efficiency for Congo Red. *Journal of the American Ceramic Society,* 97, (1), 100-106.

Gog A., Roman M., Toşa M., Paizs C. & Irimie F.D. 2012, Biodiesel production using enzymatic transesterification – Current state and perspectives. *Renewable Energy,* 39, (1), 10-16.

González-Peña V., Márquez-Alvarez C., Díaz I., Grande M., Blasco T. & Pérez-Pariente J. 2005, Sol–gel synthesis of mesostructured aluminas from chemically modified aluminum sec-butoxide using non-ionic surfactant templating. *Microporous and Mesoporous Materials,* 80, (1-3), 173-182.

Grant S.M. & Jaroniec M. 2012, Effect of acid concentration on pore size in polymer-templated mesoporous alumina. *Journal of Materials Chemistry,* 22, (1), 86-92.

Grant S.M. & Jaroniec M. 2012, Effect of acid concentration on pore size in polymer-templated mesoporous alumina. *Journal of Materials Chemistry,* 22, (1), 86-92.

Guncheva M., Dimitrov M. & Zhiryakova D. 2011, Nanosized tin dioxide — Unexplored carrier for lipase immobilization. *Catalysis Communications,* 16, (1), 205-209.

Gustafsson H., Johansson E.M., Barrabino A., Oden M. & Holmberg K. 2012, Immobilization of lipase from Mucor miehei and Rhizopus oryzae into mesoporous silica--the effect of varied particle size and morphology. *Colloids Surf B Biointerfaces,* 100, 22-30.

H Noureddini D.Z. 1997, Kinetics of Transesterification of Soybean Oil. *Journal of the American Oil Chemists' Society,* 74, (11), 1457–1463.

H. Y. Zhu J.D.R., and J. C. Barry 2002, γ-Alumina Nanofibers Prepared from Aluminum Hydrate with Poly(ethylene oxide) Surfactant. *Chemistry of Materials,* 14, (5), 2086–2093.

Helwani Z., Othman M.R., Aziz N., Kim J. & Fernando W.J.N. 2009, Solid heterogeneous catalysts for transesterification of triglycerides with methanol: A review. *Applied Catalysis A: General,* 363, (1-2), 1-10.

Hilal N., Nigmatullin R. & Alpatova A. 2004, Immobilization of cross-linked lipase aggregates within microporous polymeric membranes. *Journal of Membrane Science,* 238, (1-2), 131-141.

Huang B., Bartholomew C.H., Smith S.J. & Woodfield B.F. 2013, Facile solvent-deficient synthesis of mesoporous γ-alumina with controlled pore structures. *Microporous and Mesoporous Materials,* 165, 70-78.

Huang B., Bartholomew C.H. & Woodfield B.F. 2013, Facile structure-controlled synthesis of mesoporous γ-alumina: Effects of alcohols in precursor formation and calcination. *Microporous and Mesoporous Materials,* 177, 37-46.

Huang B., Bartholomew C.H. & Woodfield B.F. 2013, Facile structure-controlled synthesis of mesoporous< i> γ</i>-alumina: Effects of alcohols in precursor formation and calcination. *Microporous and Mesoporous Materials,* 177, 37-46.

Huang B., Bartholomew C.H. & Woodfield B.F. 2014, Facile synthesis of mesoporous γ-alumina with tunable pore size: The effects of water to aluminum molar ratio

in hydrolysis of aluminum alkoxides. *Microporous and Mesoporous Materials,* 183, 37-47.

Izrael-Zivkovic L., Zivkovic L., Jokic B., Savic A. & Karadzic I. 2015, Adsorption of Candida rugosa lipase onto alumina: Effect of surface charge. *Journal of the Serbian Chemical Society,* 80, (9), 1113-1125.

Jaeger K. & Eggert T. 2002, Lipases for biotechnology. *Current opinion in Biotechnology,* 13, (4), 390–397.

Kafuku G., Lam M.K., Kansedo J., Lee K.T. & Mbarawa M. 2010, Heterogeneous catalyzed biodiesel production from Moringa oleifera oil. *Fuel Processing Technology,* 91, (11), 1525-1529.

Kahveci D. & Xu X. 2011, Enhancement of activity and selectivity of Candida rugosa lipase and Candida antarctica lipase A by bioimprinting and/or immobilization for application in the selective ethanolysis of fish oil. *Biotechnology Letters,* 33, (10), 2065-2071.

Kaieda M., Samukawa T., Kondo A. & Fukuda H. 2001, Effect of methanol and water contents on production of biodiesel fuel from plant oil catalyzed by various lipases in a solvent-free system. *Journal of Bioscience and Bioengineering,* 91, (1), 12-15.

Karel Komers F.s.S., Radek Stloukal, Jaroslav Machek 2002, Kinetics and mechanism of the KOH — catalyzed methanolysis of rapeseed oil for biodiesel production. *European Journal of Lipid Science and Technology,* 104, (11), 728-737.

Kawakami K., Urakawa T., Oda Y. & Iwai Y. 2009, Activation of lipase by sol-gel coating with hydrophobic alkyl-substituted silicates in supercritical carbon dioxide. *Journal of Chemical Technology & Biotechnology,* 84, (9), 1412-1417.

Kim H.-J.,Kang B.-S.,Kim M.-J.,Park Y.M.,Kim D.-K.,Lee J.-S. ,Lee K.-Y. 2004, Transesterification of vegetable oil to biodiesel using heterogeneous base catalyst. *Catalysis Today,* 93-95, 315-320.

Kim P., Kim Y., Kim H., Song I.K. & Yi J. 2004, Synthesis and characterization of mesoporous alumina with nickel incorporated for use in the partial oxidation of methane into synthesis gas. *Applied Catalysis A: General,* 272, (1-2), 157-166.

Kiss A.A., Dimian A.C. & Rothenberg G. 2006, Solid Acid Catalysts for Biodiesel Production –-Towards Sustainable Energy. *Advanced Synthesis & Catalysis,* 348, (1-2), 75-81.

Kondo J. & Domen K. 2008, Crystallization of Mesoporous Metal Oxides. *Chemistry of Materials,* 20, (3), 835-847.

Kuan W.H., Huang Y.F., Chang C.C. & Lo S.L. 2013, Catalytic pyrolysis of sugarcane bagasse by using microwave heating. *Bioresour Technol,* 146, 324-329.

Lam M.K., Lee K.T. & Mohamed A.R. 2010, Homogeneous, heterogeneous and enzymatic catalysis for transesterification of high free fatty acid oil (waste cooking oil) to biodiesel: a review. *Biotechnol Adv,* 28, (4), 500-518.

Lapis A.A., de Oliveira L.F., Neto B.A. & Dupont J. 2008, Ionic liquid supported acid/base-catalyzed production of biodiesel. *ChemSusChem,* 1, (8-9), 759-762.

Lee D.-G., Ponvel K.M., Kim M., Hwang S., Ahn I.-S. & Lee C.-H. 2009, Immobilization of lipase on hydrophobic nano-sized magnetite particles. *Journal of Molecular Catalysis B: Enzymatic,* 57, (1-4), 62-66.

Lee D.-W., Park Y.-M. & Lee K.-Y. 2009, Heterogeneous Base Catalysts for Transesterification in Biodiesel Synthesis. *Catalysis Surveys from Asia,* 13, (2), 63-77.

Li G., Liu Y. & Liu C. 2013, Solvothermal synthesis of gamma aluminas and their structural evolution. *Microporous and Mesoporous Materials,* 167, 137-145.

Li L.L., Duan W.T., Yuan Q., Li Z.X., Duan H.H. & Yan C.H. 2009, Hierarchical gamma-Al2O3 monoliths with highly ordered 2D hexagonal mesopores in macroporous walls. *Chem Commun (Camb),* (41), 6174-6176.

Li W.C., Lu A.H., Schmidt W. & Schuth F. 2005, High surface area, mesoporous, glassy alumina with a controllable pore size by nanocasting from carbon aerogels. *Chemistry,* 11, (5), 1658-1664.

Li Y., Zhou G., Li C., Qin D., Qiao W. & Chu B. 2009, Adsorption and catalytic activity of Porcine pancreatic lipase on rod-like SBA-15 mesoporous material. *Colloids and Surfaces A: Physicochemical and Engineering Aspects,* 341, (1-3), 79-85.

Li Y., Zhou G., Qiao W. & Wang Y. 2009, Immobilization of Porcine pancreas lipase on fiber-like SBA-15 mesoporous material. *Materials Science and Engineering: B,* 162, (2), 120-126.

Lin L., Cunshan Z., Vittayapadung S., Xiangqian S. & Mingdong D. 2011, Opportunities and challenges for biodiesel fuel. *Applied Energy,* 88, (4), 1020-1031.

Liu Q., Wang A., Wang X., Gao P., Wang X. & Zhang T. 2008, Synthesis, characterization and catalytic applications of mesoporous γ-alumina from boehmite sol. *Microporous and Mesoporous Materials,* 111, (1-3), 323-333.

Liu Q., Wang A., Wang X. & Zhang T. 2007, Morphologically controlled synthesis of mesoporous alumina. *Microporous and Mesoporous Materials,* 100, (1-3), 35-44.

Liu T., Liu Y., Wang X., Li Q., Wang J. & Yan Y. 2011, Improving catalytic performance of Burkholderia cepacia lipase immobilized on macroporous resin NKA. *Journal of Molecular Catalysis B: Enzymatic,* 71, (1-2), 45-50.

López-Serrano P., Cao L., Rantwijk F.v. & Sheldon R.A. 2002, Cross-linked enzyme aggregates with enhanced activity application to lipases. *Biotechnology Letters,* 24, (16), 1379-1383.

Lü Y.,Guo Y.,Wang Y.,Liu X.,Wang Y.,Guo Y.,Zhang Z. ,Lu G. 2008, Immobilized penicillin G acylase on mesoporous silica: The influence of pore size, pore volume and mesophases. *Microporous and Mesoporous Materials,* 114, (1-3), 507-510.

Lukic I., Krstic J., Jovanovic D. & Skala D. 2009, Alumina/silica supported K2CO3 as a catalyst for biodiesel synthesis from sunflower oil. *Bioresour Technol,* 100, (20), 4690-4696.

Luque R., Lovett J.C., Datta B., Clancy J., Campelo J.M. & Romero A.A. 2010, Biodiesel as feasible petrol fuel replacement: a multidisciplinary overview. *Energy & Environmental Science,* 3, (11), 1706.

MacArio A.,Giordano G.,Setti L.,Parise A.,Campelo J.M.,Marinas J.M. ,Luna D. 2007, Study of lipase immobilization on zeolitic support and transesterification reaction in a solvent free-system. *Biocatalysis and Biotransformation,* 25, (2-4), 328-335.

Maekawa H. 2004, Size-dependent ionic conductivity observed for ordered mesoporous alumina-LiI composite. *Solid State Ionics,* 175, (1-4), 281-285.

Marszewski M. & Jaroniec M. 2013, Toward tunable adsorption properties, structure, and crystallinity of titania obtained by block copolymer and scaffold-assisted templating. *Langmuir,* 29, (40), 12549-12559.

Martín A., Morales G., Martínez F., van Grieken R., Cao L. & Kruk M. 2010, Acid hybrid catalysts from poly(styrenesulfonic acid) grafted onto ultra-large-pore SBA-15 silica using atom transfer radical polymerization. *Journal of Materials Chemistry,* 20, (37), 8026-8035.

Mathew T., Sivaranjani K., Gnanakumar E.S., Yamada Y., Kobayashi T. & Gopinath C.S. 2012, γ-Al2−xMxO3±y (M = Ti4+ through Ga3+): potential pseudo-3D mesoporous materials with tunable acidity and electronic structure. *Journal of Materials Chemistry,* 22, (27), 13484-13493.

Melero J.A., Bautista L.F., Morales G., Iglesias J. & Sánchez-Vázquez R. 2010, Biodiesel production from crude palm oil using sulfonic acid-modified mesostructured catalysts. *Chemical Engineering Journal,* 161, (3), 323-331.

Miao S. & Shanks B.H. 2009, Esterification of biomass pyrolysis model acids over sulfonic acid-functionalized mesoporous silicas. *Applied Catalysis A: General,* 359, (1-2), 113-120.

Mondal K., Mehta P., Mehta B.R., Varandani D. & Gupta M.N. 2006, A bioconjugate of Pseudomonas cepacia lipase with alginate with enhanced catalytic efficiency. *Biochim Biophys Acta,* 1764, (6), 1080-1086.

Mootabadi H., Salamatinia B., Bhatia S. & Abdullah A.Z. 2010, Ultrasonic-assisted biodiesel production process from palm oil using alkaline earth metal oxides as the heterogeneous catalysts. *Fuel*, 89, (8), 1818-1825.

Nie K., Xie F., Wang F. & Tan T. 2006, Lipase catalyzed methanolysis to produce biodiesel: Optimization of the biodiesel production. *Journal of Molecular Catalysis B: Enzymatic*, 43, (1-4), 142-147.

Niesz K., Yang P. & Somorjai G.A. 2005, Sol-gel synthesis of ordered mesoporous alumina. *Chem Commun (Camb)*, (15), 1986-1987.

Noureddini H., Gao X. & Philkana R.S. 2005, Immobilized Pseudomonas cepacia lipase for biodiesel fuel production from soybean oil. *Bioresour Technol*, 96, (7), 769-777.

OJ Alamu M.W., SO Jekayinfa 2007, Biodiesel production from Nigerian palm kernel oil: effect of KOH concentration on yield. *Energy for Sustainable Development*, 11, (3), 77-82.

Pal N. & Bhaumik A. 2013, Soft templating strategies for the synthesis of mesoporous materials: Inorganic, organic–inorganic hybrid and purely organic solids. *Advances in colloid and interface science*, 189, 21-41.

Paul M., Pal N., Mondal J., Sasidharan M. & Bhaumik A. 2012, New mesoporous magnesium–aluminum mixed oxide and its catalytic activity in liquid phase Baeyer–Villiger oxidation reaction. *Chemical Engineering Science*, 71, 564-572.

Peng Bai P.W., Zifeng Yan, Jinkai Zhou, X. S Zhao 2007, Self-Assembly of Clewlike ZnO Superstructures in the Presence of Copolymer. *The Journal of Physical Chemistry C*, 111, (27), 9729–9733.

Pérez L.L., Perdriau S., Brink G.t., Kooi B.J., Heeres H.J. & Melián-Cabrera I. 2013, Stabilization of Self-Assembled Alumina Mesophases. *Chemistry of Materials*, 25, (6), 848-855.

Peters T., Benes N., Holmen A. & Keurentjes J. 2006, Comparison of commercial solid acid catalysts for the esterification of acetic acid with butanol. *Applied Catalysis A: General*, 297, (2), 182-188.

Petkar M., Lali A., Caimi P. & Daminati M. 2006, Immobilization of lipases for non-aqueous synthesis. *Journal of Molecular Catalysis B: Enzymatic*, 39, (1-4), 83-90.

Pugnet V.,Maury S.,Coupard V.,Dandeu A.,Quoineaud A.-A.,Bonneau J.-L. ,Tichit D. 2010, Stability, activity and selectivity study of a zinc aluminate heterogeneous catalyst for the transesterification of vegetable oil in batch reactor. *Applied Catalysis A: General*, 374, (1-2), 71-78.

Q Y.,AX Y.,C L.,LD S.,YW Z.,WT D.,HC L. ,CH Y. 2008, Facile Synthesis for Ordered Mesoporous ç-Aluminas with High Thermal Stability. *J. Am. Chem. Soc.*, 130, (11), 3465-3472.

Ramimoghadam D., Hussein M.Z. & Taufiq-Yap Y.H. 2012, The effect of sodium dodecyl sulfate (SDS) and cetyltrimethylammonium bromide (CTAB) on the Properties of ZnO synthesized by hydrothermal method. *International Journal of Molecular Sciences*, 13, (10), 13275-13293.

Rashid U. & Anwar F. 2008, Production of biodiesel through optimized alkaline-catalyzed transesterification of rapeseed oil. *Fuel*, 87, (3), 265-273.

Rashid U., Anwar F., Ashraf M., Saleem M. & Yusup S. 2011, Application of response surface methodology for optimizing transesterification of Moringa oleifera oil: Biodiesel production. *Energy Conversion and Management*, 52, (8-9), 3034-3042.

Salis A., Bhattacharyya M.S., Monduzzi M. & Solinas V. 2009, Role of the support surface on the loading and the activity of Pseudomonas fluorescens lipase used for biodiesel synthesis. *Journal of Molecular Catalysis B: Enzymatic*, 57, (1-4), 262-269.

Salis A., Casula M.F., Bhattacharyya M.S., Pinna M., Solinas V. & Monduzzi M. 2010, Physical and Chemical Lipase Adsorption on SBA-15: Effect of Different Interactions on Enzyme Loading and Catalytic Performance. *ChemCatChem*, 2, (3), 322-329.

Sanjib Kumar Karmee P.M., R. Ravi, Anju Chadha 2004, Kinetic study of the base-catalyzed transesterification of monoglycerides from pongamia oil. *Journal of the American Oil Chemists' Society*, 81, (5), 425–430.

Sarin A. (2012). Biodiesel: production and properties, Royal Society of Chemistry.

Sasidharan M. & Kumar R. 2004, Transesterification over various zeolites under liquid-phase conditions. *Journal of Molecular Catalysis A: Chemical*, 210, (1-2), 93-98.

SathyaSelvabala V., Selvaraj D.K., Kalimuthu J., Periyaraman P.M. & Subramanian S. 2011, Two-step biodiesel production from Calophyllum inophyllum oil: optimization of modified beta-zeolite catalyzed pre-treatment. *Bioresour Technol*, 102, (2), 1066-1072.

Scherer R., Oliveira J.V., Pergher S. & Oliveira D.d. 2011, Screening of supports for immobilization of commercial porcine pancreatic lipase. *Materials Research*, 14, (4), 483-492.

Semwal S., Arora A.K., Badoni R.P. & Tuli D.K. 2011, Biodiesel production using heterogeneous catalysts. *Bioresour Technol*, 102, (3), 2151-2161.

Serra E., Mayoral Á., Sakamoto Y., Blanco R.M. & Díaz I. 2008, Immobilization of lipase in ordered mesoporous materials: Effect of textural and structural parameters. *Microporous and Mesoporous Materials*, 114, (1-3), 201-213.

Shah S., Sharma S. & Gupta M. 2004, Biodiesel Preparation by Lipase-Catalyzed Transesterification of Jatropha Oil. *Energy & Fuels*, 18, (1), 154-159.

Sharma Y.C., Singh B. & Korstad J. 2011, Latest developments on application of heterogenous basic catalysts for an efficient and eco friendly synthesis of biodiesel: A review. *Fuel*, 90, (4), 1309-1324.

Sing K.S.W. 1985, Reporting physisorption data for gas/solid systems with special reference to the determination of surface area and porosity. *Pure and Applied Chemistry*, 57, (4), 603-619.

Singh A.K. & Fernando S.D. 2007, Reaction Kinetics of Soybean Oil Transesterification Using Heterogeneous Metal Oxide Catalysts. *Chemical Engineering & Technology*, 30, (12), 1716-1720.

Singh A.K. & Fernando S.D. 2009, Preparation and Reaction Kinetics Studies of Na-based Mixed Metal Oxide for Transesterification. *Energy & Fuels*, 23, (10), 5160-5164.

Sivasamy A., Cheah K.Y., Fornasiero P., Kemausuor F., Zinoviev S. & Miertus S. 2009, Catalytic applications in the production of biodiesel from vegetable oils. *ChemSusChem*, 2, (4), 278-300.

SK Karmee P.M., R Ravi, A Chadha 2004, Kinetic Study of the Base-Catalyzed Transesterification of Monoglycerides from Pongamia Oil. *Journal of the American Oil Chemists' Society*, 81, (5), 425-430.

Stacy M. Morris, Pasquale F. Fulvio & Jaroniec M. 2008, Ordered Mesoporous Alumina-Supported Metal Oxides. *J. Am. Chem. Soc.*, 130, (45), 15210-15216.

Suzuki N., Kimura T. & Yamauchi* Y. 2010, General synthesis of fibrous mesoporous metal oxides in polycarbonate membrane. *Journal of Materials Chemistry,* 20, (25), 5294-5300.

Taher H., Al-Zuhair S., Al-Marzouqi A.H., Haik Y. & Farid M.M. 2011, A review of enzymatic transesterification of microalgal oil-based biodiesel using supercritical technology. *Enzyme Res,* 2011, 468292-468302.

Tan T., Lu J., Nie K., Deng L. & Wang F. 2010, Biodiesel production with immobilized lipase: A review. *Biotechnol Adv,* 28, (5), 628-634.

Teng G., Gao L., Xiao G. & Liu H. 2009, Transesterification of Soybean Oil to Biodiesel over Heterogeneous Solid Base Catalyst. *Energy & Fuels,* 23, (9), 4630-4634.

Tian Z. & Snyder M.A. 2014, Hard templating of symmetric and asymmetric carbon thin films with three-dimensionally ordered mesoporosity. *Langmuir,* 30, (32), 9828-9837.

Tian Z. & Snyder M.A. 2014, Nanocasting of carbon films with interdigitated bimodal three-dimensionally ordered mesopores by template-replica coassembly. *Langmuir,* 30, (41), 12411-12420.

Tomin A.,Weiser D.,Hellner G.,Bata Z.,Corici L.,Péter F.,Koczka B. ,Poppe L. 2011, Fine-tuning the second generation sol–gel lipase immobilization with ternary alkoxysilane precursor systems. *Process Biochemistry,* 46, (1), 52-58.

Umdu E.S., Tuncer M. & Seker E. 2009, Transesterification of Nannochloropsis oculata microalga's lipid to biodiesel on Al2O3 supported CaO and MgO catalysts. *Bioresour Technol,* 100, (11), 2828-2831.

Valange S., Guth J.L., Kolenda F., Lacombe S. & Gabelica Z. 2000, Synthesis strategies leading to surfactant-assisted aluminas with controlled mesoporosity in aqueous media. *Microporous and Mesoporous Materials,* 35, 597-607.

Vujicic D., Comic D., Zarubica A., Micic R. & Boskovic G. 2010, Kinetics of biodiesel synthesis from sunflower oil over CaO heterogeneous catalyst. *Fuel,* 89, (8), 2054-2061.

Vyas A.P., Subrahmanyam N. & Patel P.A. 2009, Production of biodiesel through transesterification of Jatropha oil using KNO3/Al2O3 solid catalyst. *Fuel,* 88, (4), 625-628.

Wang C.-f., Zhou G.-w., Li Y.-J., Lu N., Song H.-b. & Zhang L. 2012, Biocatalytic esterification of caprylic acid with caprylic alcohol by immobilized lipase on amino-functionalized mesoporous silica. *Colloids and Surfaces A: Physicochemical and Engineering Aspects,* 406, 75-83.

Wang X., Dou P., Zhao P., Zhao C., Ding Y. & Xu P. 2009, Immobilization of lipases onto magnetic Fe(3)O(4) nanoparticles for application in biodiesel production. *Chemsuschem,* 2, (10), 947-950.

Wang X., Liu X., Zhao C., Ding Y. & Xu P. 2011, Biodiesel production in packed-bed reactors using lipase-nanoparticle biocomposite. *Bioresour Technol,* 102, (10), 6352-6355.

Wilson K. & Lee A.F. 2012, Rational design of heterogeneous catalysts for biodiesel synthesis. *Catalysis Science & Technology,* 2, (5), 884-897.

Wu C., Zhou G., Jiang X., Ma J., Zhang H. & Song H. 2012, Active biocatalysts based on Candida rugosa lipase immobilized in vesicular silica. *Process Biochemistry,* 47, (6), 953-959.

Wu Z., Li Q., Feng D., Webley P.A. & Zhao D. 2010, Ordered mesoporous crystalline γ-Al2O3 with variable architecture and porosity from a single hard template. *Journal of the American Chemical Society,* 132, (34), 12042-12050.

X Liu X.P., Y Wang, S Zhu 2010, Model Study on Transesterification of Soybean Oil to Biodiesel with Methanol Using Solid Base Catalyst. *Journal of Physical Chemistry A,* 114, (11), 3750–3755.

Xiao Y., Gao L., Xiao G. & Lv J. 2010, Kinetics of the Transesterification Reaction Catalyzed by Solid Base in a Fixed-Bed Reactor. *Energy & Fuels,* 24, (11), 5829-5833.

Xie W. & Li H. 2006, Alumina-supported potassium iodide as a heterogeneous catalyst for biodiesel production from soybean oil. *Journal of Molecular Catalysis A: Chemical,* 255, (1-2), 1-9.

Xie W., Peng H. & Chen L. 2006, Transesterification of soybean oil catalyzed by potassium loaded on alumina as a solid-base catalyst. *Applied Catalysis A: General*, 300, (1), 67-74.

Xie X., Li Y., Liu Z.Q., Haruta M. & Shen W. 2009, Low-temperature oxidation of CO catalysed by Co(3)O(4) nanorods. *Nature*, 458, (7239), 746-749.

Xu B.,Xiao T.,Yan Z.,Sun X.,Sloan J.,González-Cortés S.L.,Alshahrani F. ,Green M.L.H. 2006, Synthesis of mesoporous alumina with highly thermal stability using glucose template in aqueous system. *Microporous and Mesoporous Materials*, 91, (1-3), 293-295.

Xuejun Liu X.P., Yujun Wang, Shenlin Zhu 2008, Calcium ethoxide as a solid base catalyst for the transesterification of soybean oil to biodiesel. *Energy & Fuels*, 22, (2), 1313–1317.

Xuejun Liu X.P., Yujun Wang, Shenlin Zhu 2010, Model Study on Transesterification of Soybean Oil to Biodiesel with Methanol Using Solid Base Catalyst. *J. Phys. Chem. A*, 114, (11), 3750–3755.

Xuejun Liu X.P., Yujun Wang, Shenlin Zhu 2010, Model Study on Transesterification of Soybean Oil to Biodiesel with Methanol Using Solid Base Catalyst. *J. Phys. Chem. A*, 114 (11), 3750–3755.

Yagiz F., Kazan D. & Akin A.N. 2007, Biodiesel production from waste oils by using lipase immobilized on hydrotalcite and zeolites. *Chemical Engineering Journal,* 134, (1-3), 262-267.

Yan J.-Y., Yan Y.-J., Yang J.-K., Xu L. & Liu Y. 2009, Combined strategy for preparation of a bioimprinted Geotrichum sp. lipase biocatalyst effective in non-aqueous media. *Process Biochemistry,* 44, (10), 1128-1132.

Yan J., Liu S., Hu J., Gui X., Wang G. & Yan Y. 2011, Enzymatic enrichment of polyunsaturated fatty acids using novel lipase preparations modified by combination of immobilization and fish oil treatment. *Bioresour Technol,* 102, (14), 7154-7158.

Yang J., Hu Y., Jiang L., Zou B., Jia R. & Huang H. 2013, Enhancing the catalytic properties of porcine pancreatic lipase by immobilization on SBA-15 modified by functionalized ionic liquid. *Biochemical Engineering Journal,* 70, 46-54.

Yuji Shimada Y.W., Taichi Samukawa, Akio Sugihara, Hideo Noda, Hideki Fukuda, Yoshio Tominaga 1999, Conversion of vegetable oil to biodiesel using immobilized Candida antarctica lipase. *Journal of the American Oil Chemists' Society,* 76, (7), 789-793.

Yusuf N.N.A.N., Kamarudin S.K. & Yaakub Z. 2011, Overview on the current trends in biodiesel production. *Energy Conversion and Management,* 52, (7), 2741-2751.

Zabeti M., Daud W.M.A.W. & Aroua M.K. 2010, Biodiesel production using alumina-supported calcium oxide: An optimization study. *Fuel Processing Technology,* 91, (2), 243-248.

Zabeti M., Wan Daud W.M.A. & Aroua M.K. 2009, Activity of solid catalysts for biodiesel production: A review. *Fuel Processing Technology,* 90, (6), 770-777.

Zeng H.-y., Liao K.-b., Deng X., Jiang H. & Zhang F. 2009, Characterization of the lipase immobilized on Mg–Al hydrotalcite for biodiesel. *Process Biochemistry,* 44, (8), 791-798.

Zhang L., Sheng B., Xin Z., Liu Q. & Sun S. 2010, Kinetics of transesterification of palm oil and dimethyl carbonate for biodiesel production at the catalysis of heterogeneous base catalyst. *Bioresour Technol,* 101, (21), 8144-8150.

Zhang X., Zhang F. & Chan K.-Y. 2004, The synthesis of large mesopores alumina by microemulsion templating, their characterization and properties as catalyst support. *Materials Letters,* 58, (22-23), 2872-2877.

Zhangxiong Wu Q.L., Dan Feng, Paul A. Webley and Dongyuan Zhao 2010, Ordered Mesoporous Crystalline γ-Al2O3 with Variable Architecture and Porosity from a Single Hard Template. *J. Am. Chem. Soc.,* 132, (34), 12042–12050.

Zhao S. & Zhang D. 2013, A parametric study of supercritical carbon dioxide extraction of oil from Moringa oleifera seeds using a response surface methodology. *Separation and Purification Technology,* 113, 9-17.

Zhao S. & Zhang D. 2013, Supercritical fluid extraction and characterisation of Moringa oleifera leaves oil. *Separation and Purification Technology*, 118, 497-502.

Zhao S. & Zhang D. 2014, An experimental investigation into the solubility of Moringa oleifera oil in supercritical carbon dioxide. *Journal of Food Engineering*, 138, 1-10.

Zhao X., El-Zahab B., Brosnahan R., Perry J. & Wang P. 2007, An Organic Soluble Lipase for Water-Free Synthesis of Biodiesel. *Applied Biochemistry and Biotechnology*, 143, (3), 236-243.

Zheng M.M.,Lu Y.,Dong L.,Guo P.M.,Deng Q.C.,Li W.L.,Feng Y.Q. ,Huang F.H. 2012, Immobilization of Candida rugosa lipase on hydrophobic/strong cation-exchange functional silica particles for biocatalytic synthesis of phytosterol esters. *Bioresour Technol*, 115, 141-146.

Zou B.,Hu Y.,Yu D.,Xia J.,Tang S.,Liu W. ,Huang H. 2010, Immobilization of porcine pancreatic lipase onto ionic liquid modified mesoporous silica SBA-15. *Biochemical Engineering Journal*, 53, (1), 150-153.